AD-A182 395 MULTILAYER CAPACITOR DIELECTRICS PRODUCED FROM METALLO-ORGANIC PRECURSORS(U) PURDUE UNIV LAFAYETTE IN R W VEST ET AL 15 MAY 87 N00014-83-K-0321 1/2

UNCLASSIFIED F/G 9/1 NL

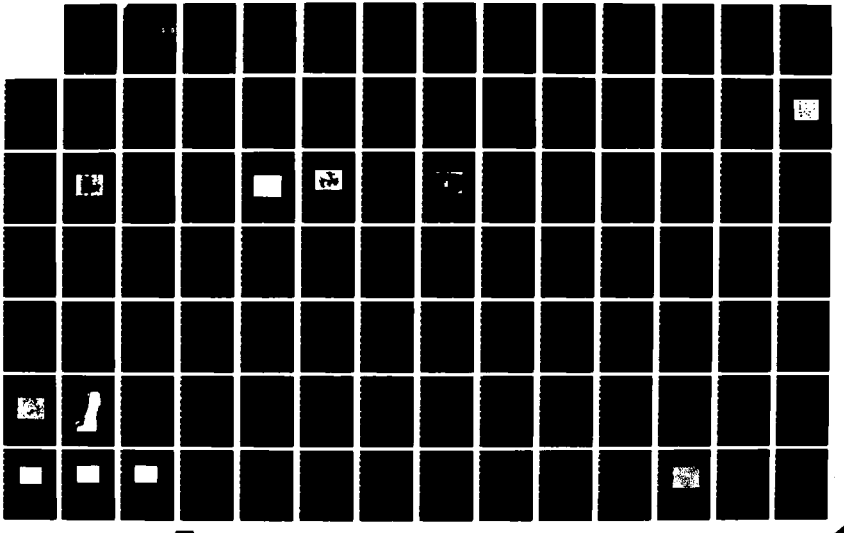

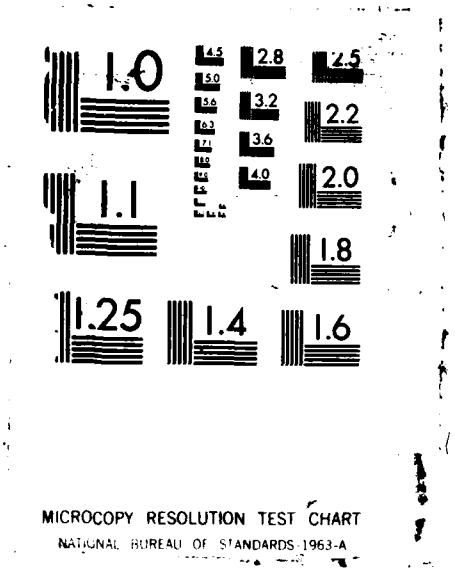

# MULTILAYER CAPACITOR DIELECTRICS PRODUCED FROM METALLO-ORGANIC PRECURSORS

R.W. Vest, G.M. Vest, A.S. Shaikh and G.L. Liedl
Purdue University
W. Lafayette, IN

15 May 1987



Annual Report

For the Period 4/1/86 - 3/31/87
Contract No. N00014-83-K-0321

Prepared for: Office of Naval Research

TABLE OF CONTENTS


1. INTRODUCTION . . . . . 3

2. BACKGROUND . . . . . 3

2.1 Substrate Materials . . . . . 3

2.2 Electrode Films . . . . . 4

2.3 Electro-Optical Films . . . . . 4

2.4 Dielectric Films . . . . . 5

2.4.1 Barium Titanate Films . . . . . 5

2.4.2 Relaxor Dielectrics . . . . . 6

2.4.2.1 PMN . . . . . 9

3. EXPERIMENTAL PROCEDURE . . . . . 11

3.1 Synthesis of Metallo-organic Compounds . . . . . 11

3.1.1 Tin -2-Ethylhexanoate . . . . . 14

3.1.2 Indium 2-ethylhexanoate . . . . . 15

3.1.3 Synthesis of Iron Neodecanoate . . . . . 15




A-1

3.1.4 Synthesis of Nickel Neodecanoate . . . . . 16

3.1.5 Synthesis of Magnesium Neodecanoate . . . . . 16

3.2 Compound Characterization . . . . . 17

3.2.1 Thermogravimetric Analysis . . . . . 17

3.2.2 Bulk Decomposition of MO Compounds . . . . . 18

3.3 Preparation of the Metallo-Organic Formulation . . . . . 18

3.4 Wet Film Formation . . . . . 20

3.5 Firing . . . . . 20

3.5.1 Electrode Films . . . . . 20

3.5.1.1 ITO Films . . . . . 20

3.5.2 PLZT Films . . . . . 23

3.5.3 Dielectric Films . . . . . 29

3.5.3.1 Barium Titanate Films . . . . . 29

3.5.3.2 Relaxor Dielectrics . . . . . 29

3.5.3.2.1 Relaxor Powders . . . . . 29

3.5.3.2.2 Relaxor Films . . . . . 32

3.6 Property Measurements . . . . . 32

4. RESULTS AND DISCUSSION . . . . . 39

4.1 ITO Films . . . . . 39

4.1.1 Thermal Decomposition Behavior . . . . . 39

4.1.2 Film Characterization . . . . . 39

4.1.3 Electrical Properties . . . . . 47

4.1.4 Optical Properties . . . . . 54

4.2 PLZT Films . . . . . 54

4.2.1 Thermal Decomposition . . . . . 54

4.2.2 Crystal Structure . . . . . 57

4.3 Barium Titanate Films . . . . . 57

4.3.1 Microstructure . . . . . 63

4.3.2 Dielectric Properties . . . . . 67

4.3.2.1 Temperature Dependence . . . . . 67

4.3.2.2 Frequency Dependence . . . . . 70

4.3.2.3 D.C. Bias Field Dependence . . . . . 70

4.3.2.4 Spontaneous Polarisation . . . . . 78

4.3.2.5 Dielectric Breakdown . . . . . 78

4.4 Relaxor Film . . . . . 78

4.4.1 Thermogravimetric Analysis of MOD Compounds . . . . . 78

4.4.2 Bulk Decomposition of MOD Relaxor Solutions . . . . . 84

4.4.3 Film Formation . . . . . 86

4.4.4 Formation of the Perovskite Phase in PMN . . . . . 86

4.4.5 Formation of the Perovskite Phase in PNN and PFN . . . . . 93

4.4.6 Electrical Properties of PMN . . . . . 94

5. SUMMARY . . . . . 97

6. REFERENCES . . . . . 103

# FOREWORD

The research described in this report was conducted under Contract No. N00014-83-K-0321 with the Office of Naval Research under the technical cognisance of Dr. R.C. Pohanka. Research was conducted in the Turner Laboratory for Electroceramics, School of Materials Engineering and School of Electrical Engineering, Purdue University, West Lafayette, Indiana under the direction of R.W. Vest, G.M. Vest, A. S. Shaikh and G. L. Liedl. Contributing to the project were Messers. D.A. Binford, J.J. Xu and Ms. L.C. Veitch.

# 1. INTRODUCTION

The metallo-organic decomposition (MOD) process is an alternate to expensive methods of preparing thin films. The process involves: dissolving the metallo-organic compounds in an appropriate solvent; mixing the solutions to achieve desired stoichiometry; after adjusting the rheology, depositing these formulations on an appropriate substrate to make a film and then firing these wet films to obtain the desired conductor, resistor or dielectric thin/thick films. Since the mixing of the starting materials is on the molecular level, the inorganic species exist as atoms or molecules in intimate contact immediately after decomposition. This leads to much more rapid formation of compounds and sintering of films, which translates to lower temperature processing of equilibrium phases and more dense films.

The metallo-organic compounds used in the present study had oxygen as the hetero atom to bond a metal atom to an organic ligand. In this study, a low viscosity solution of metallo-organic compounds was deposited on a spinning substrate to obtain wet films.

The object of this project is to prepare multilayer dielectric films using the MOD technique. Studies of the formation of dielectric and electrode films using the MOD technique are the focus of this report. For Multilayer Capacitors.

# 2. BACKGROUND

## 2.1 Substrate Materials

The major considerations in the choice of the substrate materials were; 1) there should be thermal expansion coefficient match between the substrate and the film; 2) since MOD films are very thin, the surface of the substrate should be as smooth as possible; 3) the films should adhere to the substrate; and 4) the substrate should be chemically inert towards the film. In case of PLZT film, in addition to the above mentioned requirements, the transparency of

substrate was also required. Since the single layer thickness of the MOD films is very small (500A - 3000A) as compared to the thickness of the substrate the thermal stresses are small. Hence, the major criterion are the surface roughness and the chemical inertness. Previously [1], silicon wafer was used as a substrate for $PbTiO_3$ films. The firing temperatures for $PbTiO_3$ films were less than 700°C. Since at a higher firing temperature, silicon can be very reactive, the inert substrates such as Pt-foil, sapphire and quarts were considered. The interaction between the electrode and the substrate does not seriously affect the electrical properties of the electrode. However, any type of interaction between the dielectric and other materials, seriously degrade the properties of the dielectric. Hence, some times, a stable electrode layer was also used as a buffer layer to avoid substrate-dielectric interaction.

## 2.2 Electrode Films

The previous years report [1] describes the formation of platinum electrode films using MOD technique. These films were used as the bottom electrode for $PbTiO_3$ dielectric films, which were prepared at a lower temperatures using MOD technique. Since metallic electrode materials interact severely at higher temperatures, it was decided to use $In_{1.92}Sn_{0.08}O_{3-y}$ (ITO) for high temperature firing. These ITO films have some interesting and useful electro-optical applications. Since ITO films are transparent they were also chosen as electrodes for PLZT films. Previously, ITO films have been produced by methods such as RF sputtering, dc diode sputtering [2], dc magnetron sputtering [3] and spray pyrolysis [4]. This report discusses the effect of some processing variables, annealing atmosphere and temperature, on the electrical and optical properties of the ITO films produced by the MOD technique.

## 2.3 Electro-Optical Films

The quaternary solid solution of $Pb_{1-x/100}La_{x/100}(Zr_{y/100}Ti_{z/100})_{1-x/400}O_3$, is described in a short notation as PLZT (x/y/z). The PLZT is a very good transparent ferroelectric ceramic

material, which also exhibits interesting properties such as piesoelectricity, pyroelectricity, and linear, and quadratic elec' o-optic effect that depend upon the composition [5]. Since the electro-optic effects of this material are very large, many optoelectronics applications have been proposed [6] and thin films of PLZT are excellent candidates for optoelectronic applications. Thin films of PLZT have been prepared by r.f. sputtering [7-9], ion bean sputtering [10] and electron beam evaporation [11]. Large scale and complicated apparatus for the preparation of the thin films were needed in these methods. Further, the PbO loss during deposition is a major problem in these processes. Here, the fabrication of PLZT (8/65/35) thin films by metallo-organic decomposition technique is discussed. The main advantages of this process are easy control of stoichiometry of the films, low cost, low temperature processing and fairly high quality of the films.

## 2.4 Dielectric Films

Since the objective of this project is to produce high 'k' dielectric films, ferroelectric and relaxor materials were selected as the dielectric materials. Previous years report describes the preparation of $PbTiO_3$ films using the MOD technique and their properties, and the preliminary studies on relaxor dielectric materials. This year, films of $BaTiO_3$ and PLZT relaxor dielectrics such as $Pb(Mg_{1/3}, Nb_{2/3})O_3$, [PMN], $Pb(Ni_{1/3}, Nb_{2/3})O_3$ [PNN] and $Pb(Fe_{1/3}, Nb_{2/3})O_3$ [PFN] were prepared and characterised.

### *2.4.1 Barium Titanate Films*

$BaTiO_3$ films have been fabricated by sputtering [12-15] and vacuum evaporation [16-18]. However, the stoichiometry is very difficult to achieve in vacuum deposition of these films and the substrate temperature must be kept above 1000°C to obtain ferroelectric $BaTiO_3$ films in most sputtering methods. The dielectric properties, especially the dielectric constant, at room temperature for these films were reported to be about 200 - 500, depending on the procedures used. High dielectric constants have been reported in $BaTiO_3$ films for thicknesses greater than 1 $\mu$ [19]. However, the films exhibited very little evidence of ferroelectricity. J. Park [20]

reported the dielectric constant versus film thickness of films prepared by RF sputtering in pure oxygen. Also G. Arlt [21] studied very fine grained $BaTiO_3$ film and suggested that the low dielectric constant is due to the existence of a stable orthorhombic phase at room temperature or higher. More recently, Shaikh [22] reported dielectric constants of $BaTiO_3$ as a function of grain size and explained the dependence of the dielectric constant on grain size using a model which considers grain boundaries to be amorphous with a very low dielectric constant and the grains to be ferroelectric. The internal stress and domain wall contributions increase the dielectric constant of the ferroelectric grains with a decrease in grain size; whereas, grain boundary contributions decrease the dielectric constant with a decrease in grain size. Thus, a maximum room temperature dielectric constant is observed at an intermediate grain size of about 0.4-0.7 $\mu$m. Accordingly, the goal of this study was to prepare crack free and dense films of $BaTiO_3$, using MOD technique, which will have a grain size of 0.4-0.7 $\mu$m and hence a high dielectric constant.

### *2.4.2 Relaxor Dielectrics*

Since the onset of electronic circuit miniaturization, the development of multilayer ceramic capacitors has been increasing rapidly. Most of the effort has been focused on reducing the cost of the materials, particularly that of the internal electrodes, and, yet, maintaining a large capacitance.

One group of materials that can be fired at lower temperatures in order to make it possible to use silver electrodes and have high dielectric constants are the perovskite relaxor ferroelectrics [23]. These relaxor dielectrics have broad dielectric maxima. Of particular interest are the lead based perovskite ferroelectrics. Table I [24] lists some of the more popular lead-based perovskites and their corresponding dielectric properties. The perovskite structure can be described as a network of corner-linked oxygen with smaller cations such as $Ti^{+4}$, $Mg^{+2}$ filling the octahederal holes and larger cations such as $Pb^{+2}$ filling the dodecahedral holes. This structure is shown in Fig. 1 [24] and plays a significant role in the dielectric properties of the

Table I. Physical Properties of Some Perovskite Based Relaxors.

| Compound | $T_c$ (°K) | $K_{max}$ | Lattice Parameters | $P_s$ C/m$^2$ |
|---|---|---|---|---|
| $Pb(Mg_{1/3}Nb_{2/3})O_3$ | 265 | 15000 | a=4.04 | 0.24 |
| $Pb(Zn_{1/3}Nb_{2/3})O_3$ | 413 | 50000 | a=4.061, $\alpha$=89.91° | 0.28 |
| $Pb(Cd_{1/3}Nb_{2/3})O_3$ | 543 | 1500 | a=4.135 | 0.01 |
| $Pb(Co_{1/3}Nb_{2/3})O_3$ | 175 | 6000 | a=4.04 | |
| $Pb(Ni_{1/3}Nb_{2/3})O_3$ | 120 | 4000 | a=4.03 | |
| $Pb(Mg_{1/3}Ta_{2/3})O_3$ | 175 | 7000 | a=4.02 | |
| $Pb(Co_{1/3}Ta_{2/3})O_e$ | 133 | 4000 | a=4.01 | |
| $Pb(Ni_{1/3}Ta_{2/3})O_3$ | 93 | 2300 | a=4.01 | |
| $Pb(Fe_{1/2}Nb_{1/2})O_3$ | 387 | 12000 | a=4.014A, $\alpha$=89.92° | |
| $Pb(Fe_{1/2}Ta_{1/2})O_3$ | 238 | 3700 | a=4.006, $\alpha$=89.89° | 0.28 |
| $Pb(Sc_{1/2}Nb_{1/2})O_3$ | 363 | 5000 | a=4.073, $\alpha$=89.89° | 0.25 |
| $K_{1/2}Bi_{1/2}TiO_3$ | 668 | 3000 | a=3.913, c=3.993 | |
| $Na_{1/2}Bi_{1/2}TiO_3$ | 593 | 2300 | a=3.891, $\alpha$=89.60° | 0.08 |

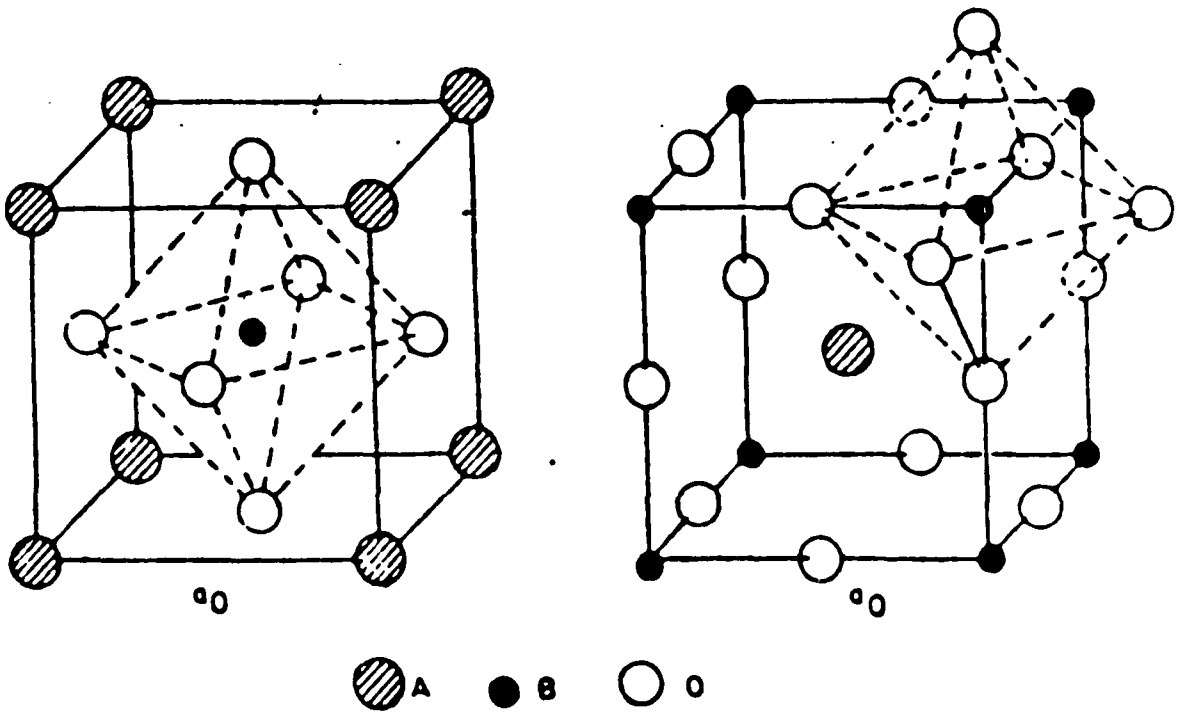


Figure 1. Ideal Perovskite Structure ($ABO_3$).

relaxor ferroelectrics.

The disadvantages of using these materials are: dielectric properties depend on frequency, high dielectric losses (also a function of frequency), difficult to reproduce, lead oxide, which is the major component of the relaxor formulations, is both volatile and toxic. The lead losses coupled with several other factors lead to the formation of a stable parasitic pyrochlore phase, which degrades the dielectric properties of the relaxor ferroelectric. Thus, various studies have been made on the kinetics of the formation of the pyrochlore phase in relaxor materials. Lead magnesium niobate (PMN) has been studied the most extensively. This particular relaxor has a large dielectric constant just below room temperature, making it a strong candidate for the multilayer capacitor industry. Consequently, this study is focused upon PMN.

*2.4.2.1 PMN*

It was over 25 years ago that PMN was first fabricated and studied by Smolenskii and Agranovskaya [25]. Other studies followed by Bokov and Myl'nikova [26] on single crystal PMN. In the latter article, it was briefly mentioned that additional lines in the x-ray diffraction pattern of polycrystalline samples studied by Ismailzad [27] corresponded to a pyrochlore structure; however, in their study of single crystal PMN, they did not observe these same lines.

Inada [28] was one of the first to propose a mechanism for the formation of the pyrochlore phase:

$$3PbO + 2Nb_2O_5 \xrightarrow{530-650^\circ C} 3PbO \cdot 2Nb_2O_5 \ (pyrochlore)$$

$$3PbO \cdot 2Nb_2O_5 + PbO \xrightarrow{600-700^\circ C} 2(2PbO \cdot Nb_2O_5) \ (pyrochlore)$$

$$2PbO \cdot Nb_2O_5 + 1/3MgO \xrightarrow{700-800^\circ C} Pb(Mg_{1/3}Nb_{2/3})O_3 + 1/3(3PbO \cdot 2Nb_2O_5) \ (perovskite \text{ and } pyrochlore)$$

Inada concluded that to bypass the pyrochlore phase it was necessary to prevent the

evaporation of PbO and possibly necessary to add excess MgO and PbO. A slightly different reaction sequence was found by Swarts and Shrout [29]. From their investigation, the following sequence was proposed:

$$PbO + Nb_2O_5 + MgO \xrightarrow{25-650^\circ C} NO\ RXN$$

$$PbO + Nb_2O_5 + (MgO) \xrightarrow{700-800^\circ C} cubic\ pyrochlore$$

$$pyrochlore + PbO + (MgO) \xrightarrow{850-900^\circ C} perovskite\ \text{and}\ pyrochlore$$

They also noted that the processing parameters (particle size, heating rate, etc.) would influence the sequence of reactions.

Another reaction sequence has been reported by Lejuene and Boilot [30]. They reported that three types of pyrochlore phases formed between 650 and 700°C, while two other pyrochlore phases formed between 700°C and 800°C. Finally, at 830°C, one of the pyrochlore phases reacted with MgO to form perovskite PMN while the other pyrochlore phase from the 700-800°C range was left unaltered above 800°C. From their study, they concluded that the formation of perovskite was dependent on the reactivity of MgO relative to the pyrochlore phases. Lead loss was also found to increase the amount of the parasitic phase forming. It was suggested that an increase in the partial pressure of $O_2$ would increase the amount of perovskite phase, because the pyrochlore phases that were observed have an oxygen deficient structures.

A variety of variations in processing techniques have been studied in order to form the stoichiometric perovskite PMN. Lowering the sintering temperatures and decreasing the sintering times and processing in $O_2$ decreased the amount of pyrochlore phase. Lejuene and Boilot [31] reported that an addition of 6 wt% excess PbO to PMN avoided the formation of pyrochlore phase. However, adding excess PbO has several undesired effects. If PbO is present in the grain boundaries, this will tend to influence aging and lower the dielectric constant as reported by Swartz, et.al. [32]. An addition of excess MgO also avoided the formation of pyrochlore phase [33]. An excess of MgO tends to promote grain growth. From a study on the

microstructure of PMN, Goo [33] observed that MgO is essentially surrounded by the perovskite phase as shown in Fig. 2. It is therefore difficult for the MgO to react with the pyrochlore phase since the perovskite phase acts as a barrier. Excess MgO tends to increase the grain size. Thus, decreasing the number of grain boundaries and enhancing the reaction of MgO with the pyrochlore phase [33]. Finer particle size and enhanced degree of mixing and milling of the oxide powders have also been reported to increase the amount of perovskite formed.

One fabrication technique that has been successful in obtaining stoichiometric PMN pre-reacts the MgO and $Nb_2O_5$ oxide powders to form an intermediate structure, $MgNb_2O_6$. This intermediate structure is then reacted with PbO to form PMN [29]. By forming $MgNb_2O_6$, it was more difficult for PbO to react with $Nb_2O_5$ to form a pyrochlore structure. Also, the structure of $MgNb_2O_6$ is a oxygen octahedra structure, similar to the perovskite structure and, thereby, would promote the formation of this particular structure. A similar study has been made by pre-reacting PbO with $Nb_2O_5$ and then, reacting this intermediate compound with an excess of MgO [34]. Lead loss for this reaction sequence was eliminated and the excess MgO enhanced the reaction rate.

The objective of this study was to prepare crack free, dense and pyrochlore free relaxor dielectric films using MOD technique. The relaxor materials under consideration were, PMN, PNN and PFN. The development of the perovskite and pyrochlore phases for both single layer and multilayer samples, the effect of firing conditions and electrode and substrate material on the phases formed were studied. The electrical properties of PMN films were studied.

# 3. EXPERIMENTAL PROCEDURE

## 3.1 Synthesis of Metallo-organic Compounds

The metallo-organic compounds required for this study were selected using the previously discussed selection criteria [35]. Table II lists the metallo-organic compounds used in the present

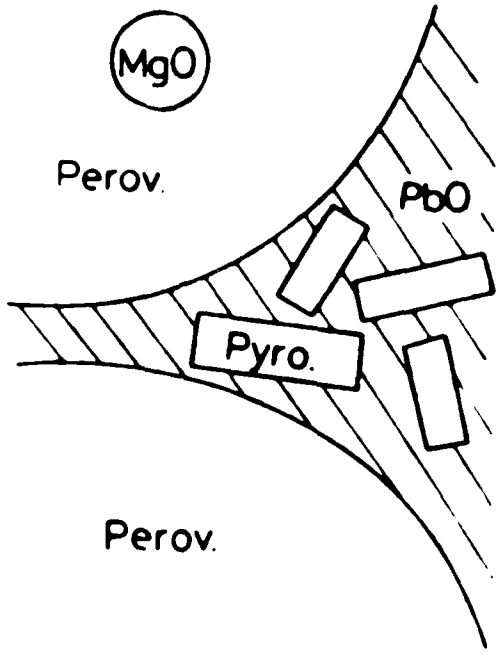


Figure 2. Schematic Illustration of Microstructure in PMN.

Table II. Metallo-Organic Compounds used in the Studies.

| Formulation | Metallo-Organic Compound | Solvent | Inorganic Thermal Decomposition Product |
|---|---|---|---|
| ITO | In neodecanoate | xylene | $In_2O_3$ |
| | Sn 2-ethylhexanoate | xylene | $SnO_2$ |
| $BaTiO_3$ | Barium neodecanoate | xylene | $BaCO_3$ |
| | Ti dimethoxy dineodecanoate | xylene | $TrO_2$ |
| PMN | Pb neodecanoate | xylene | PbO |
| | Mg neodecanoate | xylene | MgO |
| | Nb triethoxy-dineodecanoate | xylene | $Nb_2O_5$ |
| PNN | Pb neodecanoate | xylene | PbO |
| | Ni neodecanoate | xylene | NiO |
| | Nb triethoxy-dineodecanoate | xylene | $Nb_2O_5$ |
| PFN | Pb neodecanoate | xylene | PbO |
| | Fe neodecanoate | xylene | $Fe_2O_3$ |
| | Nb triethoxy-dineodecanoate | xylene | $Nb_2O_5$ |
| PLZT | Pb neodecanoate | xylene | PbO |
| | $La(C_{11}H_{19}O_2)_3 \cdot H_2O$ | | $La_2O_3$ |
| | $Zr(C_{11}H_{19}O_2)_4$ | xylene | $ZrO_2$ |
| | Ti-dimethoxy dineodecanoate | xylene | $TiO_2$ |

studies.

he general principles of synthesis of metallo-organic compounds have been discussed elsewhere [35,36] and the specific details of the synthesis of the compounds used for this work are given in the reports [1]. The synthesis of the compounds which were not reported in the previous annual reports are described below.

### *3.1.1 Tin -2-Ethylhexanoate*

Stannous chloride hydrolyses, if added to distilled water. Thus, the stannous chloride solution was prepared in a highly acidic medium. Twenty eight grams (0.124 moles) of $SnCl_2.2H_2O$* were dissolved in 21.6 ml of concentrated hydrochloric acid (~37%). Fourty ml (0.249 moles) of 2-ethyl hexanoic acid** were neutralised by 16.7 ml $NH_4OH$*** (conc. ~58 %). The solution was stirred vigorously to form the ammonium soap. An additional 17.2 ml of $NH_4OH$ was added to this solution to neutralise the hydrochloric acid. The stannous chloride solution in hydrochloric acid was added dropwise to the above mixture. A pale viscous substance settled to the bottom as white fumes of $NH_4Cl$ escaped.

The supernatent clear solution was decanted. The viscous tin soap was washed several times with hot water, then extracted with xylene. The solution was washed with water and then dried two times over molecular sieves.

Reactions

$$C_7H_{15}COOH + NH_4OH \rightarrow C_7H_{15}COONH_4 + H_2O$$

* No. 8176 Mallinckrodt Inc. Paris KY 40361

** No. 32,914-1 Aldrich Chemicals Co. Inc. Milwaukee WI

*** No. A 669 S Fisher Scientific Co.

$$2(C_7H_{15}COO)NH_4 + SnCl_2 \longrightarrow (C_7H_{15}COO)_2Sn + 2NH_4Cl$$

*3.1.2 Indium 2-ethylhexanoate*

Twenty three ml (0.142 moles) 2-ethylhexanoic acid was reacted with 10 ml 58% ammonium hydroxide in a 100 ml beaker. The reaction mixture was stirred with a bar magnet for about one hour. Ten and half grams of $InCl_3^+$ was dissolved in 50 ml water containing a few drops of HCl acid. The $InCl_3$ water solution was then added slowly to the ammonium soap. A white oily precipitate appeared on the top of the aqueous solution. The reaction mixture was further stirred for one hour. The oily precipitate was separated, washed several times by deionised water and then dissolved in xylene. Traces of water were removed by distillation. A clear yellow colored solution of $In(C_7H_{15}COO)_3$ in xylene was obtained.

Reactions:

$$C_7H_{15}COOH + NH_4OH \longrightarrow C_7H_{15}COONH_4 + H_2O$$

$$InCl_3 + 3C_7H_{15}COONH_4 \longrightarrow In(C_7H_{15}COO)_3 + 3NH_4Cl$$

*3.1.3 Synthesis of Iron Neodecanoate*

Ten grams (0.04 moles) of neodecanoic acid was reacted with 15.5 m. (0.111 moles) of triethylamine to form a soap. This soap was added dropwise to a solution of $FeCl_3 \cdot 6H_2O$ (10 grams) in 200 proof ethanol. The solution was stirred constantly while the amine soap additions were made and for 30 minutes afterwards. The solution was then heated and stirred on a water bath at ~80 $^0$C for another 30 minutes. A red oil and a white precipitate of amine chloride formed. The white precipitate was dissolved in water and the red oil was separated and dissolved in xylene. The organic solution was vacuum distilled in a rotavac system for 2 hours to remove the remaining water.

**Reactions:**

$$C_9H_{19}COOH + N(C_2H_5)_3 \rightarrow C_9H_{19}COO^-(C_2H_5)_3NH^+$$

$$FeCl_3 \cdot 6H_2O + 3(C_9H_{10}COO^-(C_2H_5)_3NH^+ \rightarrow$$

$$Fe(C_9H_{19}COO)_3 + 3(C_2H_5)_3N \cdot HCl + 6H_2O$$

*9.1.4 Synthesis of Nickel Neodecanoate*

Ten grams (0.4 moles) of nickel acetate, 15.08 ml (0.08 moles) of neodecanoate acid and ~100 ml of 200 proof ethyl alcohol were added to a large evaporating dish on top of a steam bath. A clear green solution was obtained as the solution was heated. Most of the ethanol and acetic acid was evaporated off, leaving an oily green residue. This residue was placed in a 600 ml beaker and about 500 ml of $H_2O$ was added to the oil to remove the remaining acetic acid. The oil was then extracted in xylene. The final solution was vacuumed distilled in a rotavac system to remove any remaining $H_2O$ and some of the solvent.

**Reactions:**

$$Ni(OOCCH_3)_2 \cdot 2(C_9H_{19}COOH) \rightarrow Ni(C_9H_{19}COO)_2 + 2CH_3COOH$$

*9.1.5 Synthesis of Magnesium Neodecanoate*

Ten grams of magnesium turnings (0.4113 moles) and 125 ml of absolute methanol were placed in a 500 ml round bottom flask. Approximately 0.01 grams of iodine crystals were added and the mixture was heated very slowly and with extreme caution because of the large amount of $H_2$ that forms. A white gummy powder was formed. Fifty more milliliters of methanol was added after the reaction was completed. One hundred fifty seven milliliters (0.8228 moles) of neodecanoic acid was then added to this flask. This mixture was stirred and refluxed for 5

hours. The final reaction mixture was filtered to remove unreacted alkoxide. The solution was further vacuum distilled to remove methanol. The final product was dissolved in xylene.

Reactions:

$$Mg + 2CH_3OH \xrightarrow[I_2 \text{ crystals}]{\text{exothermic}} Mg(OCH_3)_2 + H_2$$

$$Mg(OCH_3)_2 + 2C_9H_{19}COOH \xrightarrow{CH_3OH} Mg(C_9H_{19}COO)_2 + 2CH_3OH$$

## 3.2 Compound Characterisation

### *3.2.1 Thermogravimetric Analysis*

Thermogravimetric analysis (TGA) was used to study the decomposition behavior of the metallo-organic compounds. This analysis gave information concerning the temperature ranges of the thermal decomposition of the various compounds. Although weight loss can also be determined by TGA, bulk firings of the MO compounds were performed. This method involved less error and there was sufficient decomposition product left for characterisation. This method is described in the next section. It should be noted that the temperature ranges of the thermal decomposition of compounds vary with heating rate. In particular, the thermal decomposition takes place at a relatively lower temperature range with a lower heating rate. Also, the lower the surface to volume ratio, the longer is the time required for the completion of decomposition. In this study it is worthy to note that the surface to volume ratios involved in thin metallo-organic films are very high compared to the surface to volume ratios of the samples used for the TGA studies. Thus, kinetics of thermal decomposition of metallo-organic compounds are expected to be faster in the film form than observed in the TGA studies. Hence, TGA results can be used as a safe guideline in deciding firing temperatures for thin films.

*3.2.2 Bulk Decomposition of MO Compounds*

A small amount of a MO compound was weighed in a platinum crucible and placed in a small quarts lined Blue M box furnace[#] at room temperature. The furnace temperature was controlled by a 570 Model Barbara Coleman controller[+]. The sample was heated to 600°C in air at 1°C/minute. After a ten minute stabilisation period at 600°C, the sample was removed and re-weighed at room temperature. The inorganic thermal decomposition residues were characterised using a powder X-ray diffractometer[*] with copper radiation.

## 3.3 Preparation of the Metallo-Organic Formulation

The among and the formula of the inorganic decomposition products obtained by thermal decomposition of the solutions of the MO compounds listed in Table II were determined using the procedure described in the Section 3.2.2. The stoichiometric calculations were performed. The exact stoichiometric amounts of the organic solutions were mixed to form the dielectric and the electrode formulations. The metallo-organic formulations in all the cases were clear and stable organic solutions. A sample calculation is given for PMN formulation in Table III.

The preparation of PLZT formulation required a special procedure. The compounds were mixed in the following order. First, the solutions of $Ti(CH_3O)_2$ $(C_9H_{19}COO)_2$ and $Zr(OC_3H_7)_4$ in xylene were mixed to obtain a true solution. Then, to this true solution, the $La(C_2H_3O_2)_3 \cdot 1.5\ H_2O$ solid was added. The mixture was stirred for 30-60 minutes until the dissolution was complete. Finally, $Pb(C_9H_{19}COO)_2$ was added to the solution to yield a very stable solution that was a yellow color and had a low viscosity. The concentration of the solution was 22 wt% of PLZT (8/65/35) and the viscosity was 3-4 cp.

# Blue M Company, Blue Island, IL
+ Barber Coleman Company, Indianapolis, IN
* Kristalloflex4, Siemens Inc., Cherry Hill, NJ

Table III. Sample Stoichiometry Calculation for the Preparation of PMN Formulation from Metallo-Organic Compounds.

| | wt% | Moles |
|---|---|---|
| Amount of PbO in Solution | 19.175 | .086 |
| Amount of MgO in solution | 6.46 | .160 |
| Amount of $Nb_2O_5$ in solution | 18.05 | .068 |

Molecular wt. of PMN: 975.77 g/mole

Molecular formula of PMN: $Pb_3MgNb_2O_9$

From stoichiometry of PMN, the percentage of the oxides are determined:

$$3\frac{(223 \text{ g/mole PbO})}{975.77 \text{ g/mole PMN}} \times 100 = 68.62\%$$

$$\frac{40.32 \text{ g/mole MgO}}{975.77 \text{ g/mole PMN}} \times 100 = 4.13\%$$

$$\frac{265.8 \text{ g/mole } Nb_2O_5}{975.77 \text{ g/mole PMN}} \times 100 = 27.24\%$$

To calculate the amount of metallo-organic solutions needed to make PMN, the following relationships were used:

$$\frac{\text{moles of PbO per 100 g PMN}}{\text{Xg of MO solution}} = \frac{\text{moles of PbO in MO soln.}}{\text{100 g soln.}}$$

$$\frac{68.62 \text{ g PbO} \times \frac{\text{mole PbO}}{223 \text{ g}}}{\text{Xg of MO soln.}} = \frac{.086 \text{ moles PbO}}{100 \text{ g solution}} = 353.4 \text{ g Pb neodecanoate needed}$$

$$\frac{4.13 \text{ g MgO} \times \frac{\text{mole MgO}}{40.32 \text{ g}}}{\text{Xg of MO soln.}} = \frac{.160 \text{ moles MgO}}{100 \text{ g solution}} = 63.88 \text{ g Mg neodecanoate needed}$$

$$\frac{27.24 \text{ g } Mb_2O_5 \times \frac{\text{mole } Nb_2O_5}{265.82 \text{ g}}}{\text{Xg of MO soln.}} = \frac{.068 \text{ moles } Nb_2O_5 \text{ in soln.}}{100 \text{ g solution}}$$

= 148.52 g Nb trimethoxy dineodecanoate needed

## 3.4 Wet Film Formation

The conventional spinning technique was used to form uniform wet films on the substrate. The metallo-organic formulations of the electrode and the dielectric were deposited on a spinning substrate. Table IV lists the substrate used for various dielectric and electrode film studies. The spinning was carried out in a Class 100 hood to minimize dust particle streaks in the film. The film thickness was established by controlling the spinning speed, the spinning time, the viscosity and the concentration of the solution of metallo-organic compounds. In this study substrates were spun at 1200-1500 rpm for 10 seconds.

## 3.5 Firing

### *3.5.1 Electrode Films*

The firing of Pt film has been described previously [1]. Here, processing of ITO is discussed.

#### *3.5.1.1 ITO Films*

To obtain continuous ITO films after firing, a special firing profile was needed. Due to the tendency of the indium compound to gel, it was difficult to obtain a continuous film of ITO. In general, the viscosity of metallo-organic compounds of III A and IV A elements (containing 7-9 C atoms) is high and decreases with increasing atomic numbers. For example, the metallo-organic compounds of Al and Si gel even at room temperature. The $In(C_7H_{15}COO)_3$ and $Sn(C_7H_{15}COO)_4$ did not gel at room temperature, but at a temperature between room temperature and the decomposition temperature a semi-solid gel formed. This gel melted as the temperature was further raised. To obtain continuous ITO films, the gel formation should be avoided. It was observed that $In(C_7H_{15}COO)_3$ gel at about 150--200°C. The ITO wet films fired at slower heating rates underwent gelation and resulted in discontinuous film (Fig. 3). However, firing the films directly in a furnace at 550°C avoided the formation of gel and

Table IV. Substrates Used in the Various Film Formation Studies.

| Film | Substrates |
|---|---|
| ITO | Silicon, crystalline quartz, sapphire and Pt-foil |
| PLZT | Sapphire, fused and crystalline quartz |
| $BaTiO_3$ | Silicon, Pt-foil and fused and crystalline quartz |
| PMN | Silicon, fused quartz and Pt-foil |
| PNN | Silicon, fused quartz and Pt-foil |
| PFN | Pt-foil |

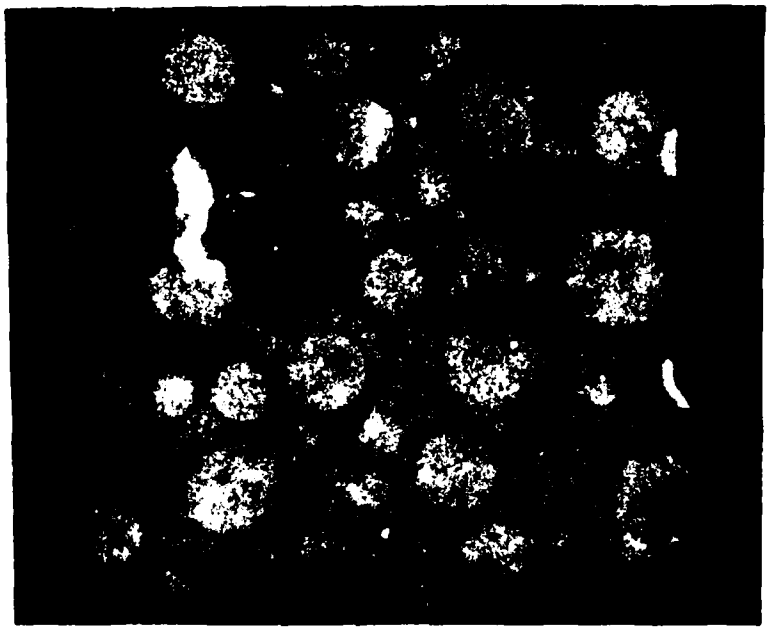

Figure 3. Microphotograph of an ITO film fired at 20°C/min to 550°C.

resulted in a continuous uniform and transparent ITO film on all the substrates used (Fig. 4). The metallo-organic formulation containing 9.53 wt% $In_{2-x}Sn_xO_{3-y}$ resulted in a single layer fired thickness of 0.12 $\mu$m. The procedure of deposition and firing was repeated three times to obtain 0.36 $\mu$m thick transparent ITO films. These films were further annealed at different temperatures for 1 hr. in air or argon atmospheres (Table V lists the firing conditions for various samples).

*3.5.2 PLZT Films*

The wet films were fired using the firing profile shown in Fig. 5 to form the crystalline PLZT film. The preparation of high quality PLZT thin films was found to be sensitive to processing parameters. The quality of fired PLZT film was controlled by: 1) the choice of metallo-organic precursors, 2) single layer thickness of PLZT films, 3) the rate of heating and cooling and 4) the firing temperature. The effects of different metallo-organic precursors on the quality of formed PLZT films are being studied.

The thermal expansion coefficient mismatch between sapphire and PLZT along with the phase transformation of PLZT (8/65/35) at 200°C make it more difficult to prepare crack free PLZT films on this substrate. Figure 6 shows a cracked PLZT film. The thermal expansion mismatch cracks were controlled by adjusting the firing temperature profile, especially the cooling rate. Cooling rates below 5°C/min. produced crack free PLZT films on sapphire substrates.

The second type of surface damage observed on the PLZT thin films is thermal etching which was reported [37-38] for pressure-sintered transparent PLZT ceramics. Figure 7 shows the thermal etching observed on a thin PLZT film made from metallo-organic precursors. It was found that this thermal etching can be controlled by reducing the firing temperature. At lower firing temperature, the thermal etching of the PLZT thin films was significantly reduced. However, a lowering of the firing temperature also reduces the crystallization of the PLZT film

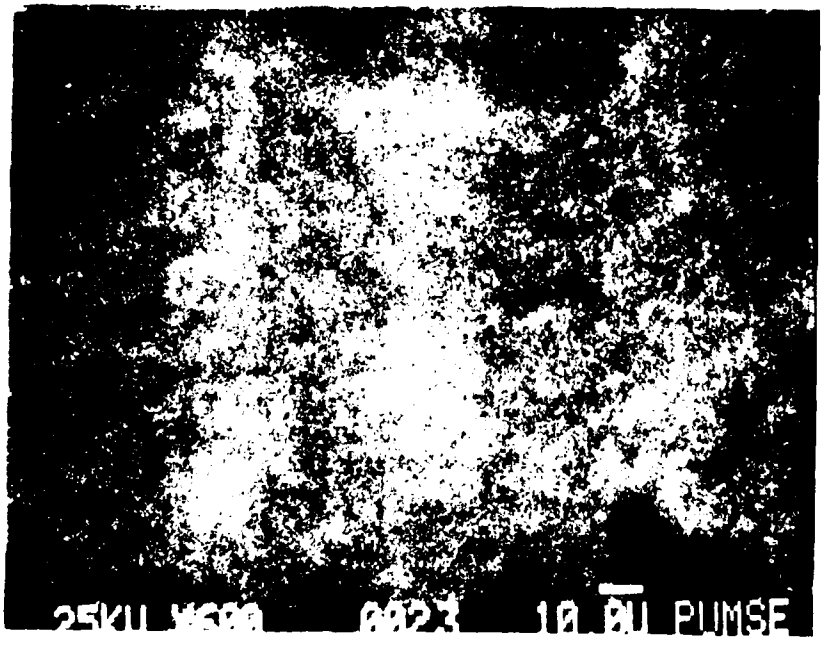

Figure 4. Microphotograph of an ITO film fired directly at 550°C.

Table V. The Processing Conditions of ITO Films.

| Sample | Firing T | Firing t | Atmosphere |
|---|---|---|---|
| ITO(a) | 550°C | 1 Hr. | air |
| ITO(b) | 650°C | 1 Hr. | air |
| ITO(c) | 750°C | 1 Hr. | air |
| ITO(d) | 800°C | 1 Hr. | air |
| ITO(e) | 550°C | 1 Hr. | Ar |
| ITO(f) | 650°C | 1 Hr. | Ar |
| ITO(g) | 750°C | 1 Hr. | Ar |
| ITO(h) | 800°C | 1 Hr. | Ar |

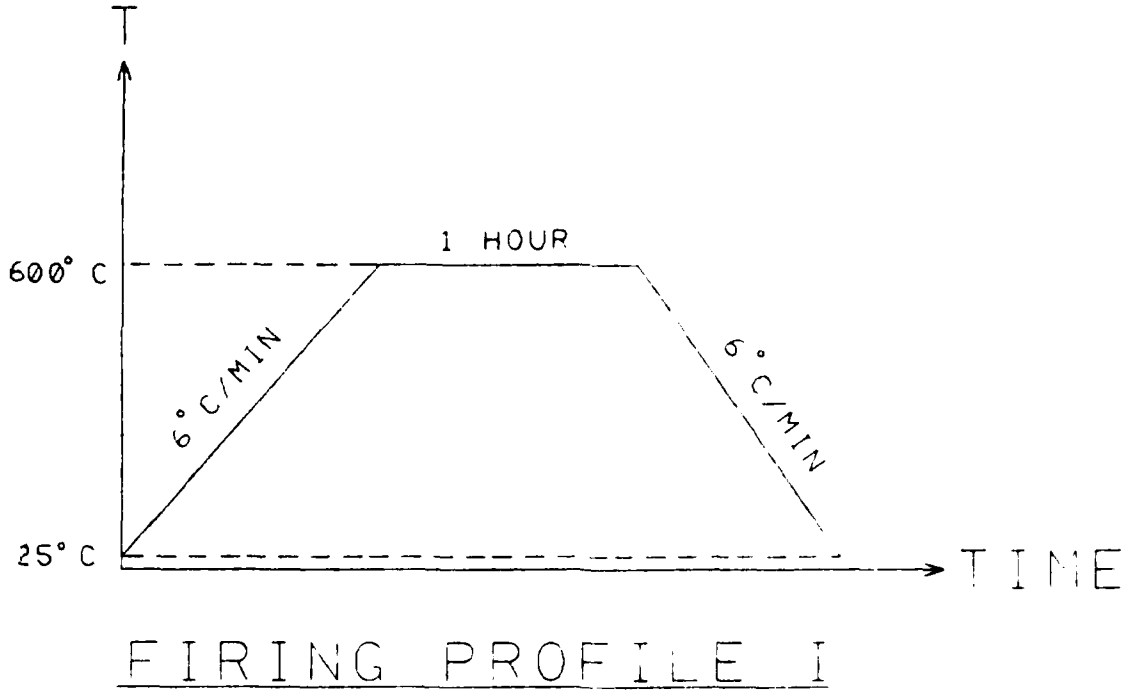


FIRING PROFILE I

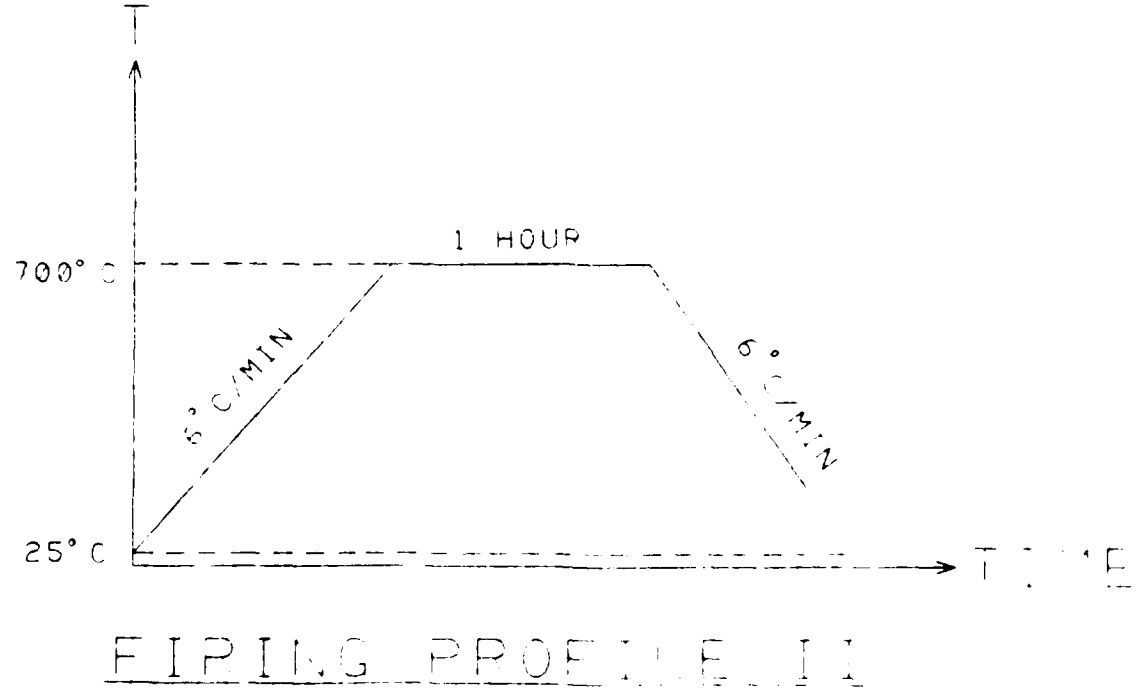


FIRING PROFILE II

Figure 5. The Firing Profile [illegible] on Sapphire Substrate.


Figure 9. Crazed Platinum.

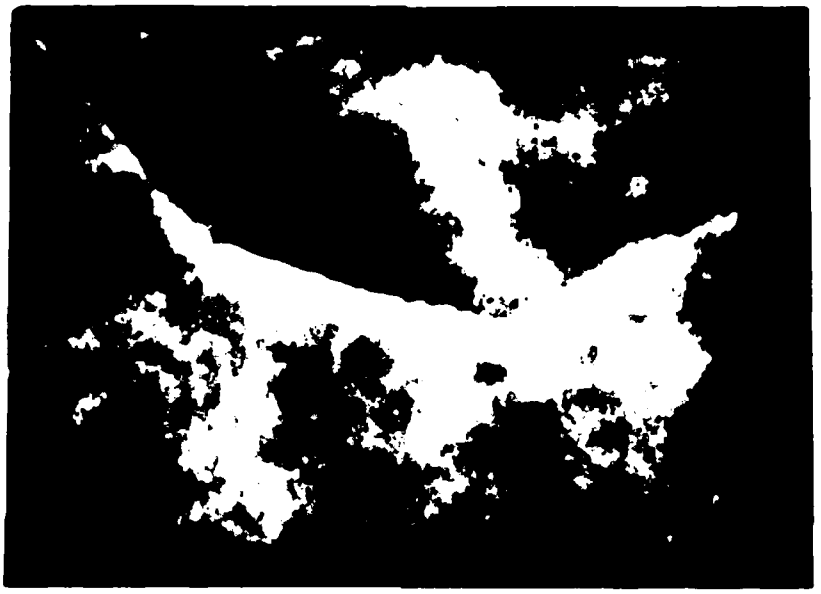

[illegible]

and leads to an incomplete reaction between $ZrO_2$,$TiO_2$,$La_2O_3$ and PbO. Thus, an optimum firing temperature of 570°C-600°C was selected. Figure 8 shows the PLZT thin film on a sapphire substrate obtained by firing the film according to the temperature profile II shown in Fig. 5.

*9.5.9 Dielectric Films*

*9.5.9.1 Barium Titanate Films*

Shaikh and G. Vest [39] reported that the formation of $BaTiO_3$ powder from metallo-organic precursors is completed by 700°C. However, the present study indicates that the formation of $BaTiO_3$ in metallo-organic films was completed at the temperatures as low as 500°C. This could be due to the surface to volume effect. The films prepared in this study had much higher surface to volume ratio than the solution of metallo-organic precursors fired in the crucible by Shaikh and G. Vest [39]. Thus, the wet metallo-organic films of $BaTiO_3$ prepared using the formulation containing 9.3 w% $BaTiO_3$ were fired. The fired single layer thickness of the films was 350 nm. The procedure of deposition and firing was repeated several times to obtain 5-8 $\mu$m thick film. The samples were then further annealed at 900°C - 1200°C in air for one hour to obtain different grain size $BaTiO_3$ films.

*9.5.9.2 Relaxor Dielectrics*

3.5.3.2.1 Relaxor Powders

The bulk decomposition studies were performed on the relaxor solutions. The heating cycle for the decomposition is shown in Fig. 9. The heating cycle includes a slow ramp to 450°C and, then a faster ramp to 875°C. Since, at higher heating rates lead neodecanoate evaporates before decomposition, a lower heating rate was maintained till decomposition of lead neodecanoate was completed.

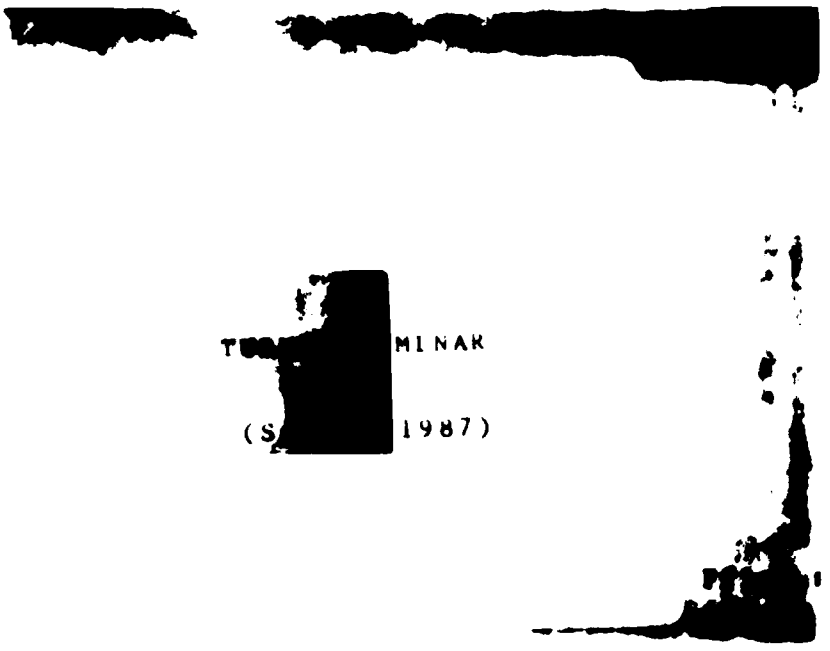
MINAR
1987)

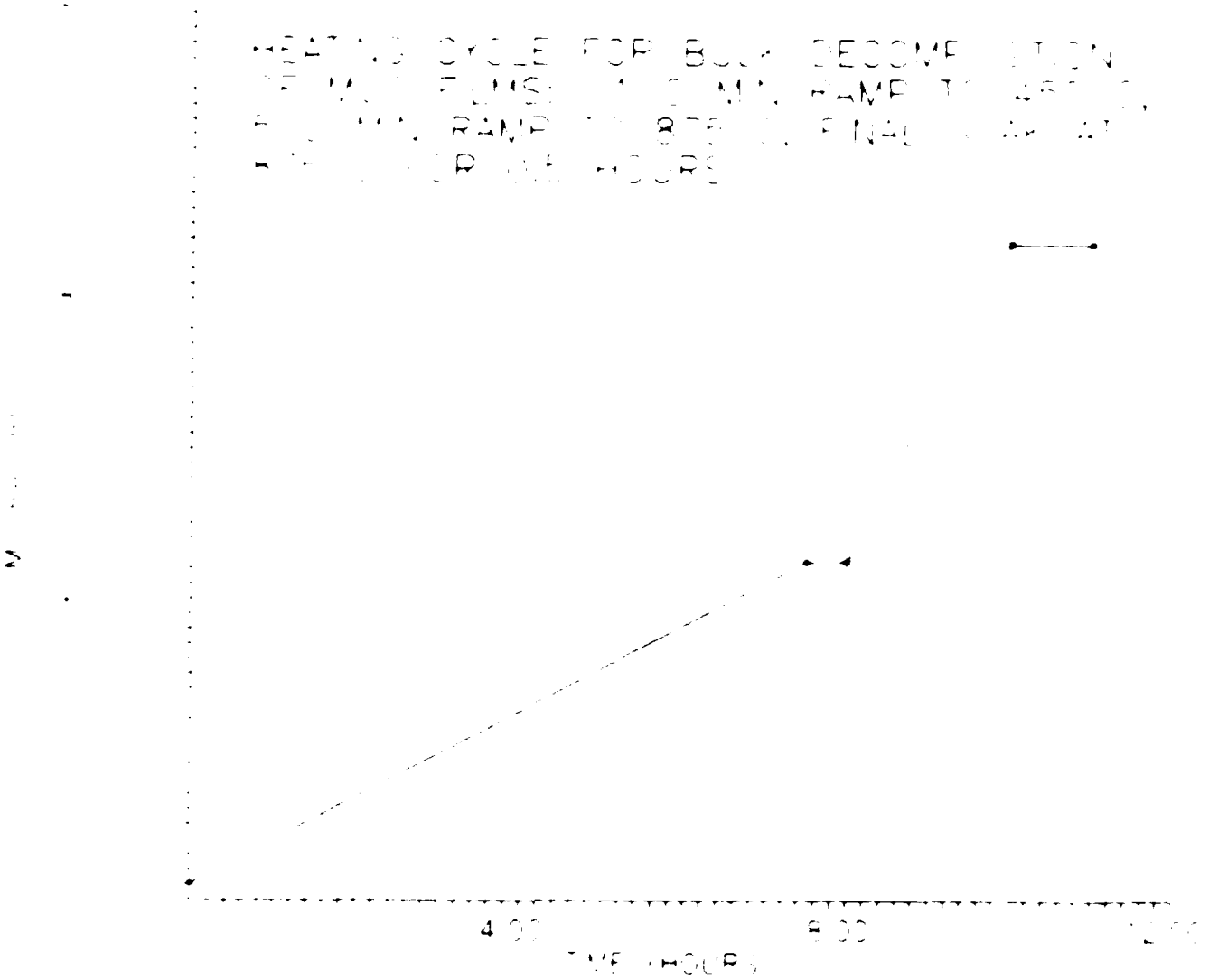

Figure 9. Heating Cycle for Bulk Decomposition of MOD Formulation.

3.5.3.2.2 Relaxor Films

All of the films were fired in the same quarts-lined furnace. Figure 10 is a schematic of the quarts process tube. The substrate on which films were deposited were laid on a quarts plate and placed in the center of the tube (the plate did not rest on the thermocouple). The end cap was packed in glass wool and aluminum foil to minimise heat losses. A 570 Barber Coleman programmable controller was used to regulate the temperature of the furnace. The heating cycles for the ferroelectric MOD films are shown in Figs. 11-14. A spotting problem was noted when the MOD films were placed in the furnace at room temperature and slowly ramped to higher temperatures for PMN and PNN. SEM/EDAX* demonstrated that the spots were richer in PbO than the areas that were not spotted. This observation was attributed to the heterogeneous decomposition of MOD films. By placing the substrate in the furnace at 500°C, the organics were immediately removed and no spotting was observed. All of the films were allowed to cool slowly to room temperature in order to prevent severe thermal stresses in the films.

## 3.6 Property Measurements

The microstructure of the thermally or chemically etched films was studied by x-ray, SEM and TEM. An acid mixture containing 2% (HF + $NHO_3$) was used to etch the $BaTiO_3$ films in order to study the grain size of films fired at different temperatures. The grain sizes of very fine grained films were estimated using x-ray line broadening method. Gold dots were evaporated on the top of the dielectric film and were used as the top electrode. The resultant capacitor geometry has been described in the previous report [1]. The dielectric properties of the films were measured in a evacuated bell jar ($10^{-3}$ torr) in order to avoid moisture effects. The experiment was also designed to control the temperature of the film from -50°C to 200°C. The

* CF35 JEOL Inc. Peabody MA

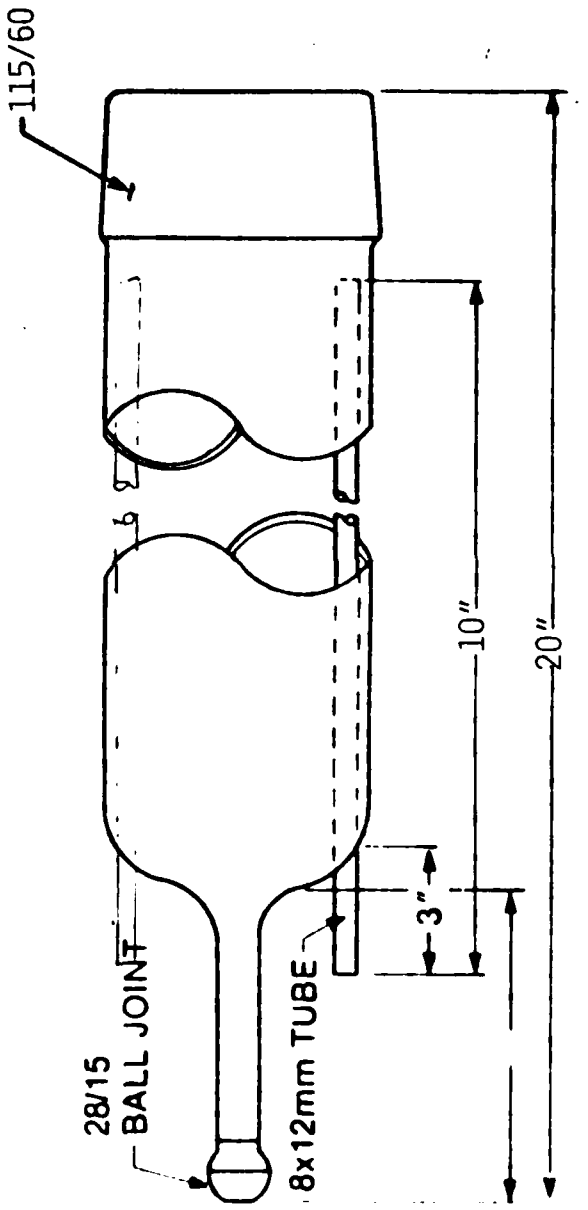


Figure 10. Quartz Diffusion Tube used in Lindberg Single Zone Tube Furnace.

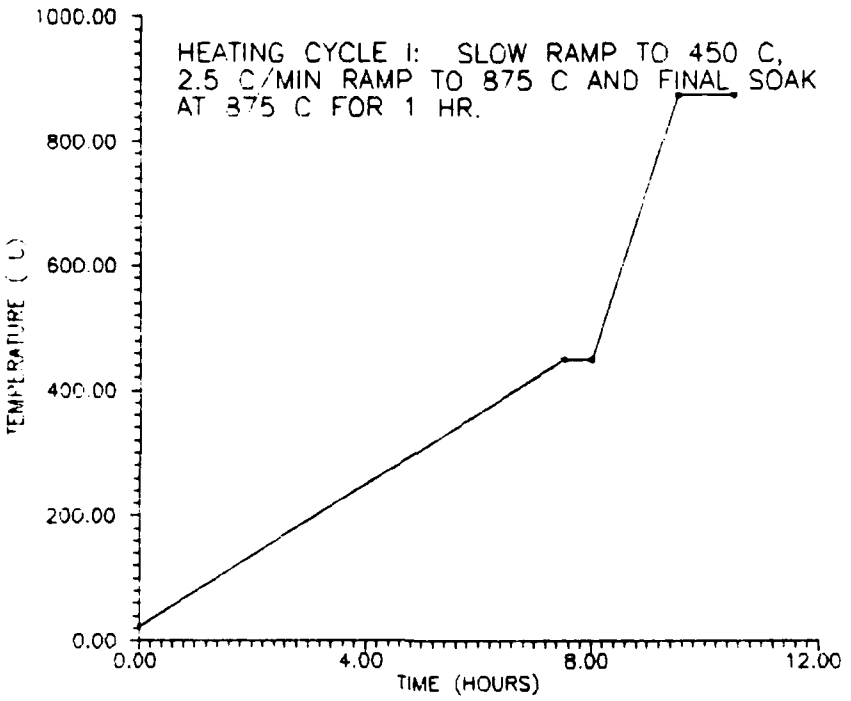


Figure 11. Heating Cycle I for MOD Relaxor Films.

A

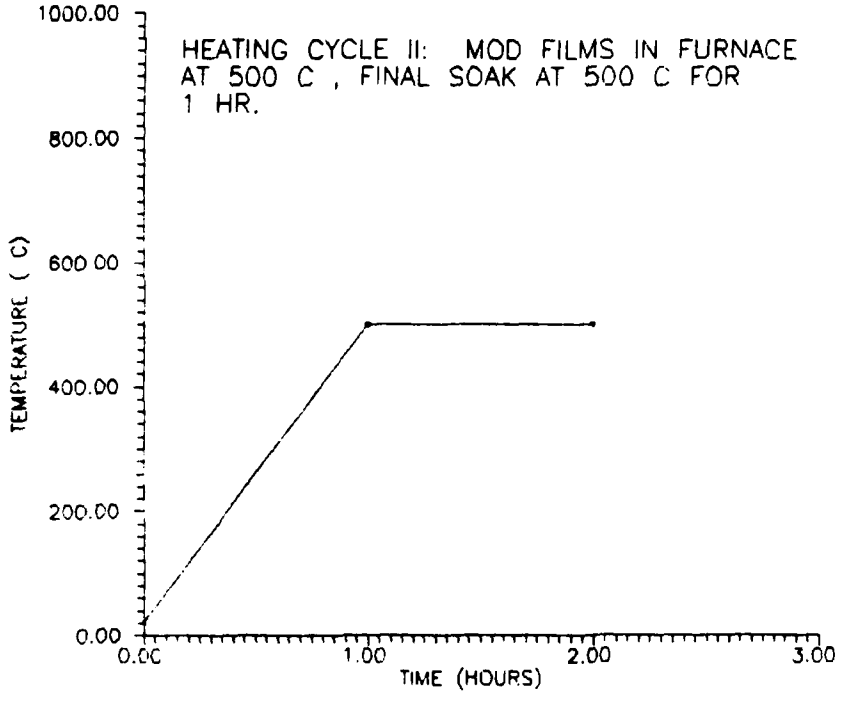


B

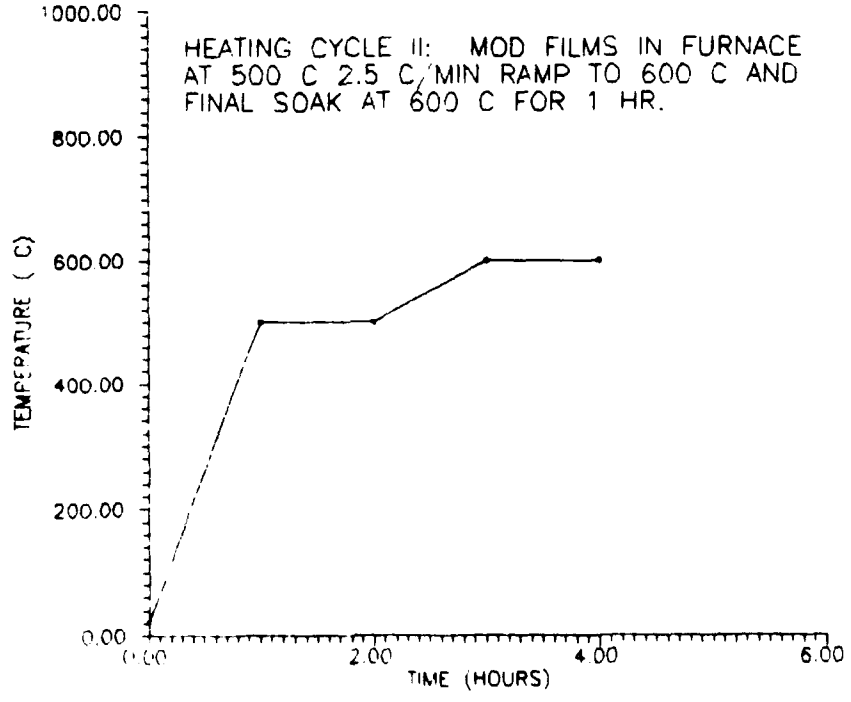


Figure 12. Heating Cycle II: a) 500°C, b) 600°C, c) 700°C and d) 800°C for MOD Films.

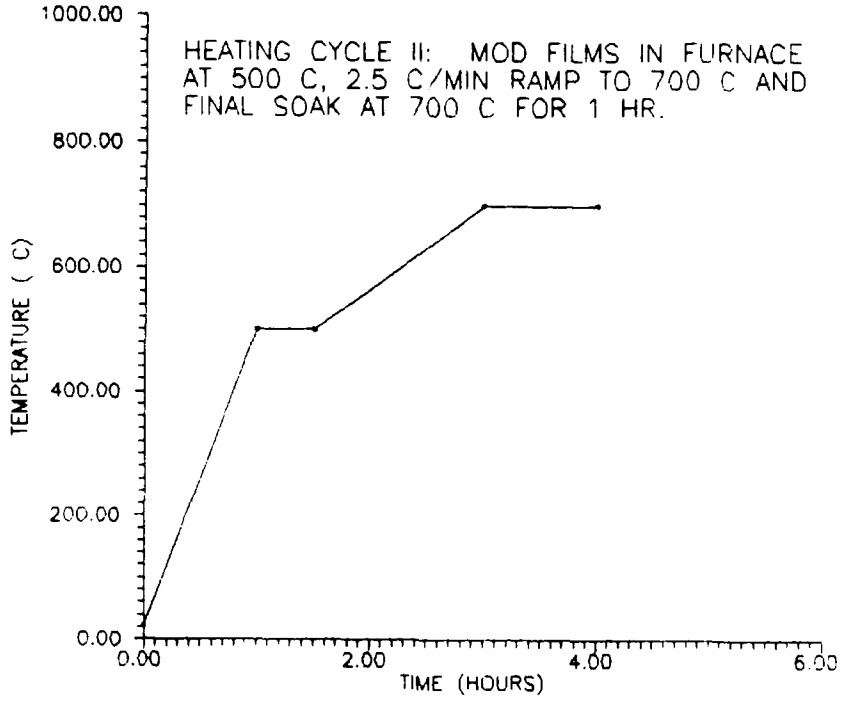
HEATING CYCLE II: MOD FILMS IN FURNACE AT 500 C, 2.5 C/MIN RAMP TO 700 C AND FINAL SOAK AT 700 C FOR 1 HR.
1000.00
800.00
600.00
400.00
200.00
0.00
TEMPERATURE ( C)
0.00
2.00
4.00
6.00
TIME (HOURS)

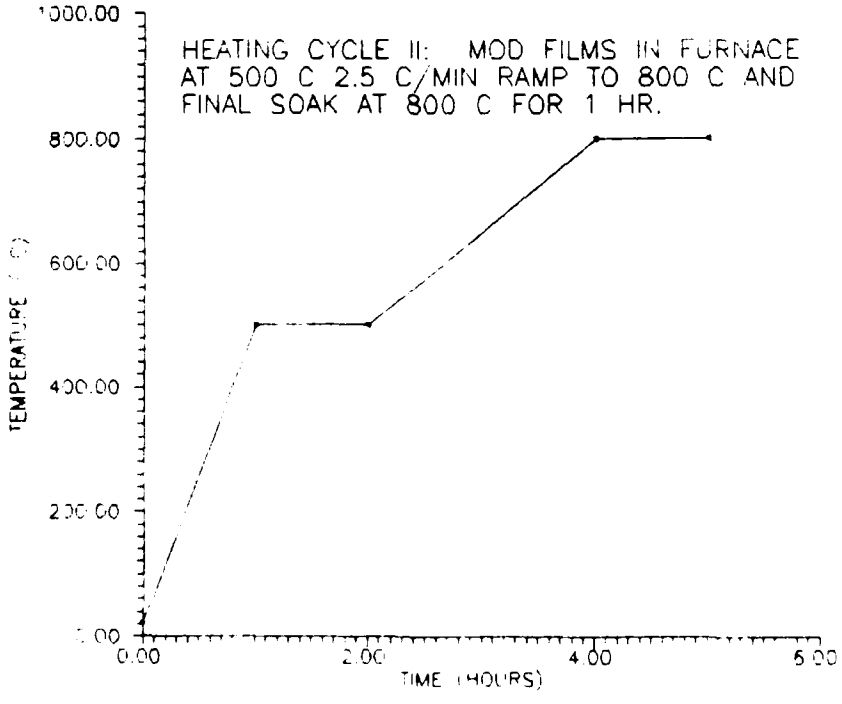
HEATING CYCLE II: MOD FILMS IN FURNACE AT 500 C 2.5 C/MIN RAMP TO 800 C AND FINAL SOAK AT 800 C FOR 1 HR.
1000.00
800.00
600.00
400.00
200.00
0.00
TEMPERATURE ( C)
0.00
2.00
4.00
5.00
TIME (HOURS)

A.

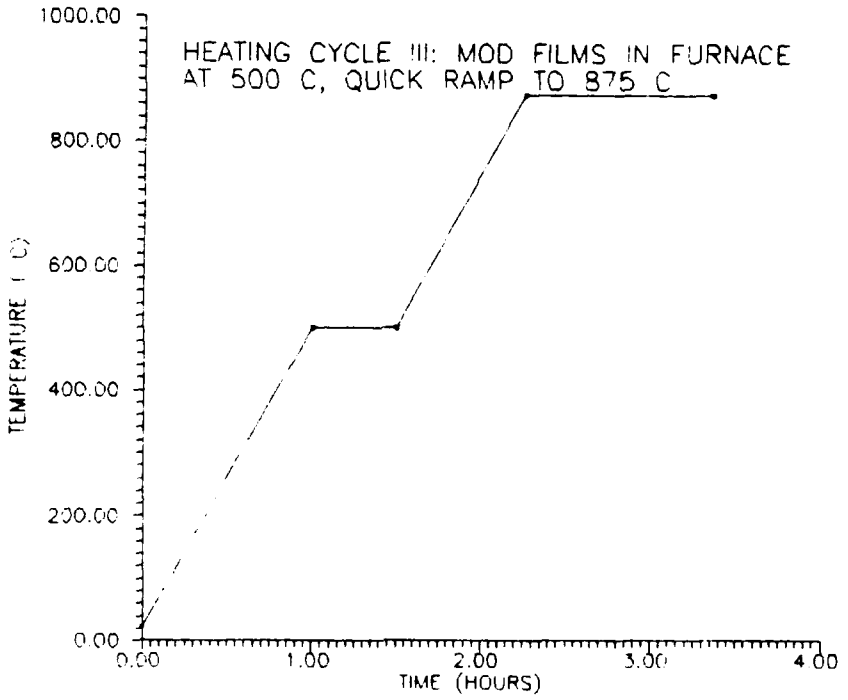


B.

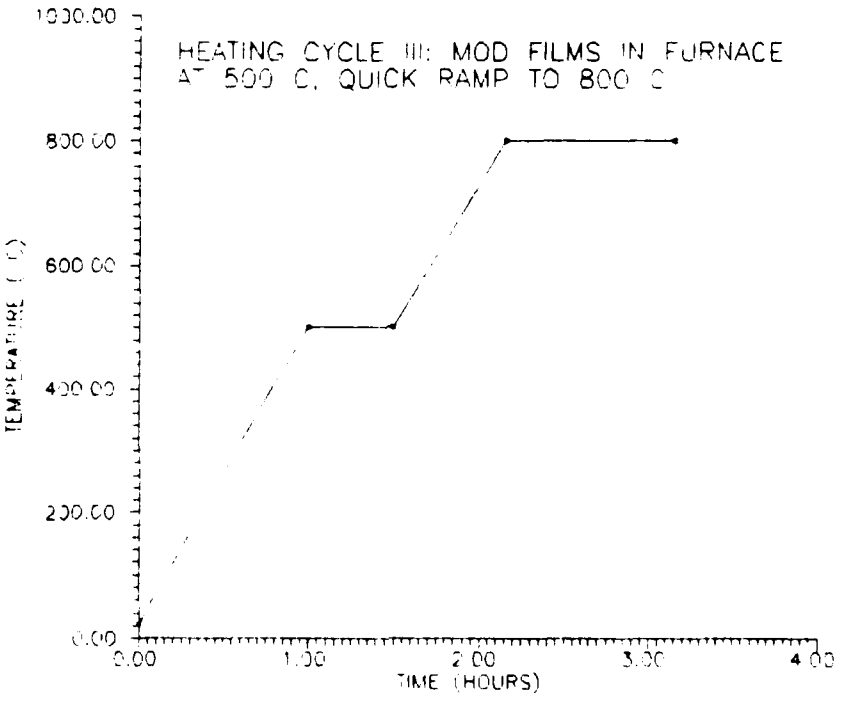


Figure 13. Heating Cycle III: a) 875$^{O}$C and b) 800$^{O}$C for MOD Films.

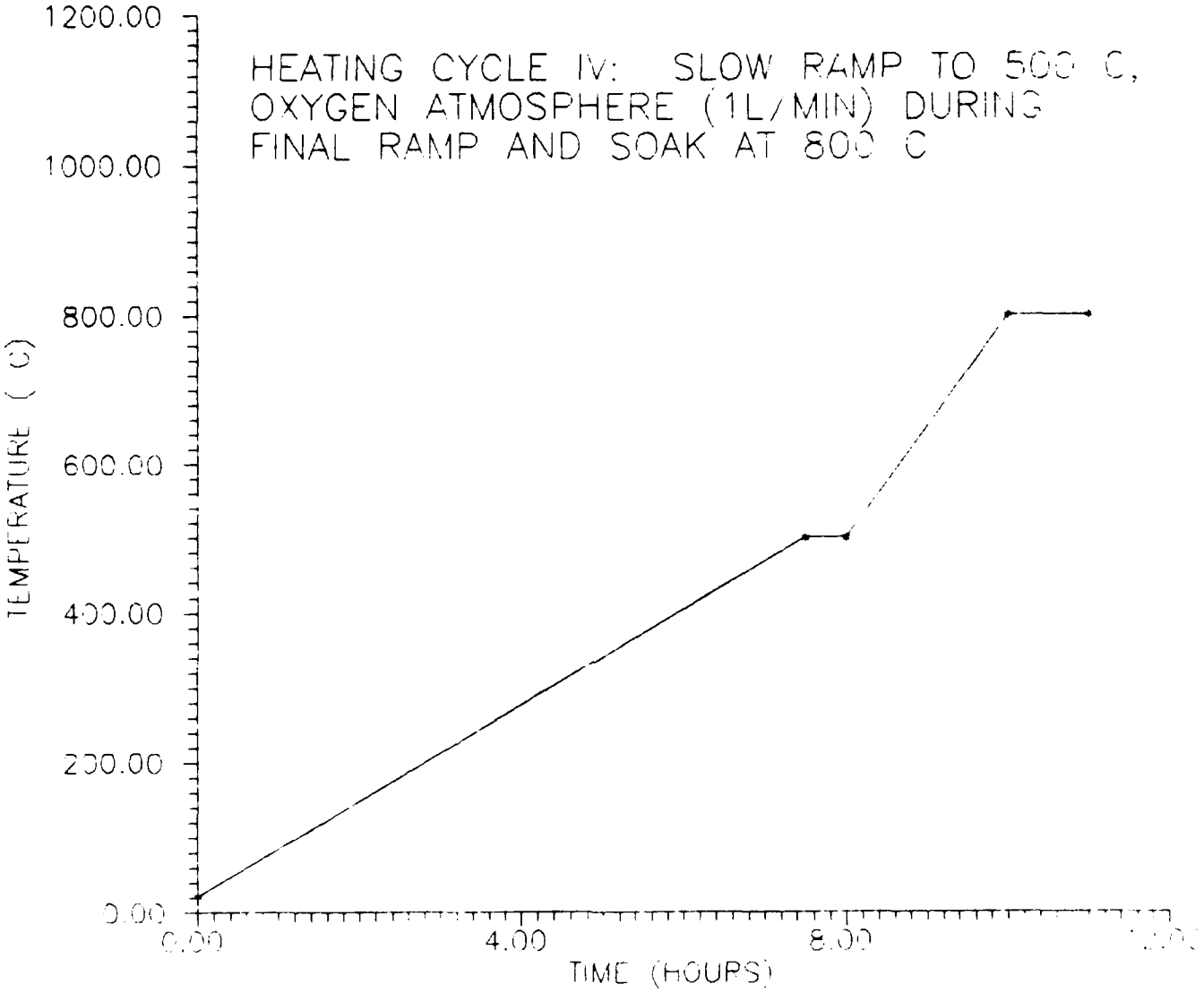


Figure 14. Heating Cycle IV for MOD Films.

dielectric constant and dissipation factor were measured by HP 4274A and 4275A multi LCR meters using 0.5 $V_{rms}$ signal. Together they were used to cover the frequency range of 100 Hz to 10 MHz. The D.C. bias electric field of 0 to 150 kV/cm was used to determine the D.C. bias dependence of the dielectric properties. The spontaneous polarization of the sample was measured from the ferroelectric hystersis loop at 60 Hz using a modified Sawyer and Tower circuit [40].

# 4. RESULTS AND DISCUSSION

## 4.1 ITO Films

### *4.1.1 Thermal Decomposition Behavior*

Figures 15 to 17 are the thermograms of the two xylene solutions of the metallo-organic compounds used in this study. and the ITO formulation. A summary of the results of the TGA studies is given in Table VI.

### *4.1.2 Film Characterization*

The x-ray diffraction pattern of an ITO film ($In_{2-x}Sn_xO_{3-y}$,x=0.09) deposited on a Si wafer and fired at 500°C in air showed no evidence of the presence of $SnO_2$ as shown in Fig. 18. The lattice parameter of the cubic structure of the ITO film (x=0.09) was found to be 0.987 nm. The grain size of the ITO films was determined by using Scherer formula. Table VII shows the variation of grain size with firing temperature and atmosphere. The activation energy for grain growth was obtained from an Arhenius plot (Fig. 19). The activation energy for grain growth of the ITO films was found to be dependent on the firing atmosphere. The activation energy for films fired in Ar atmosphere is about 35 kJ/mol, while for those fired in air is about 60 kJ/mol.

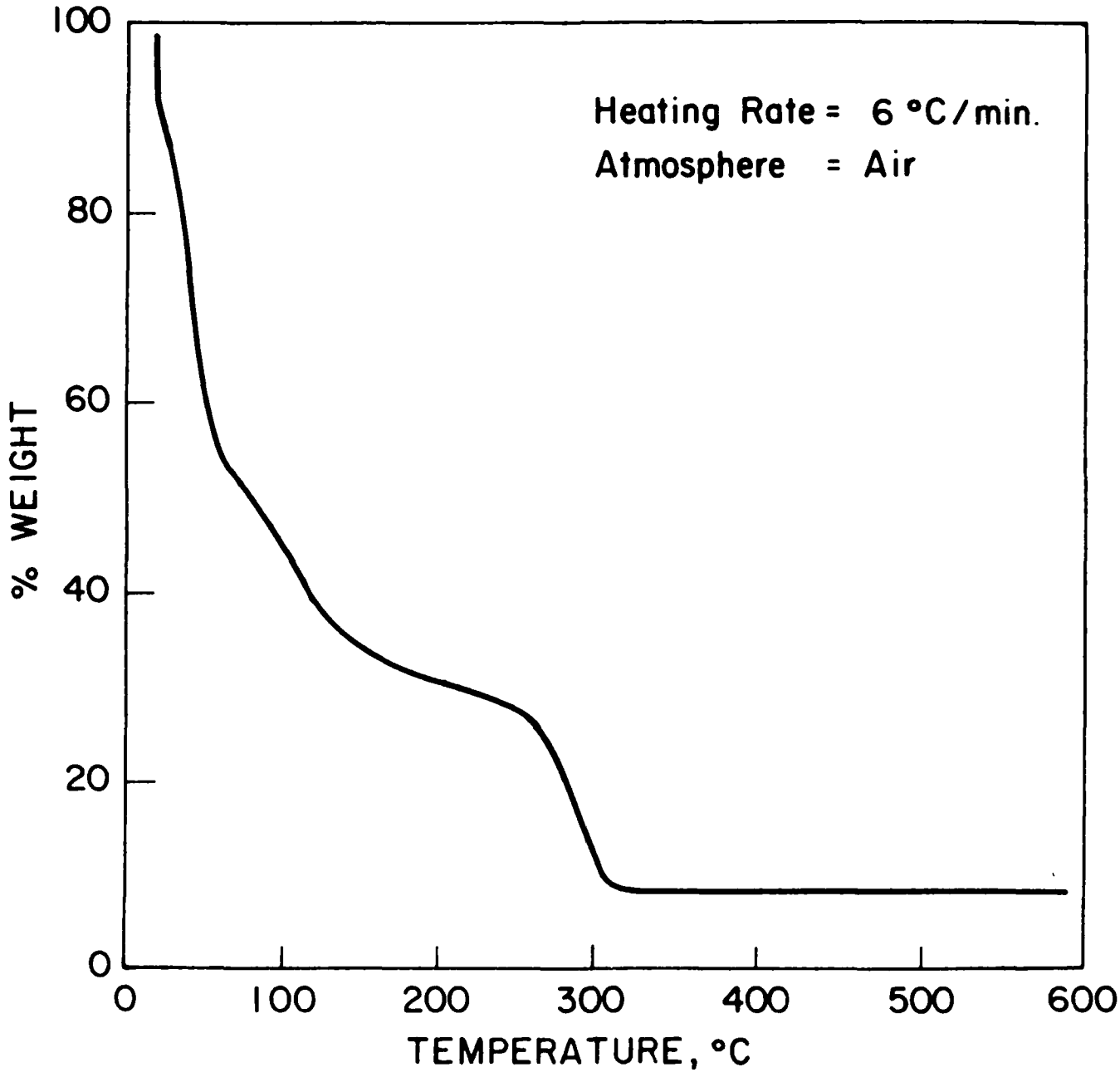


Figure 15. Thermogram of $In(C_7H_{15}COO)_3$ solution in xylene.

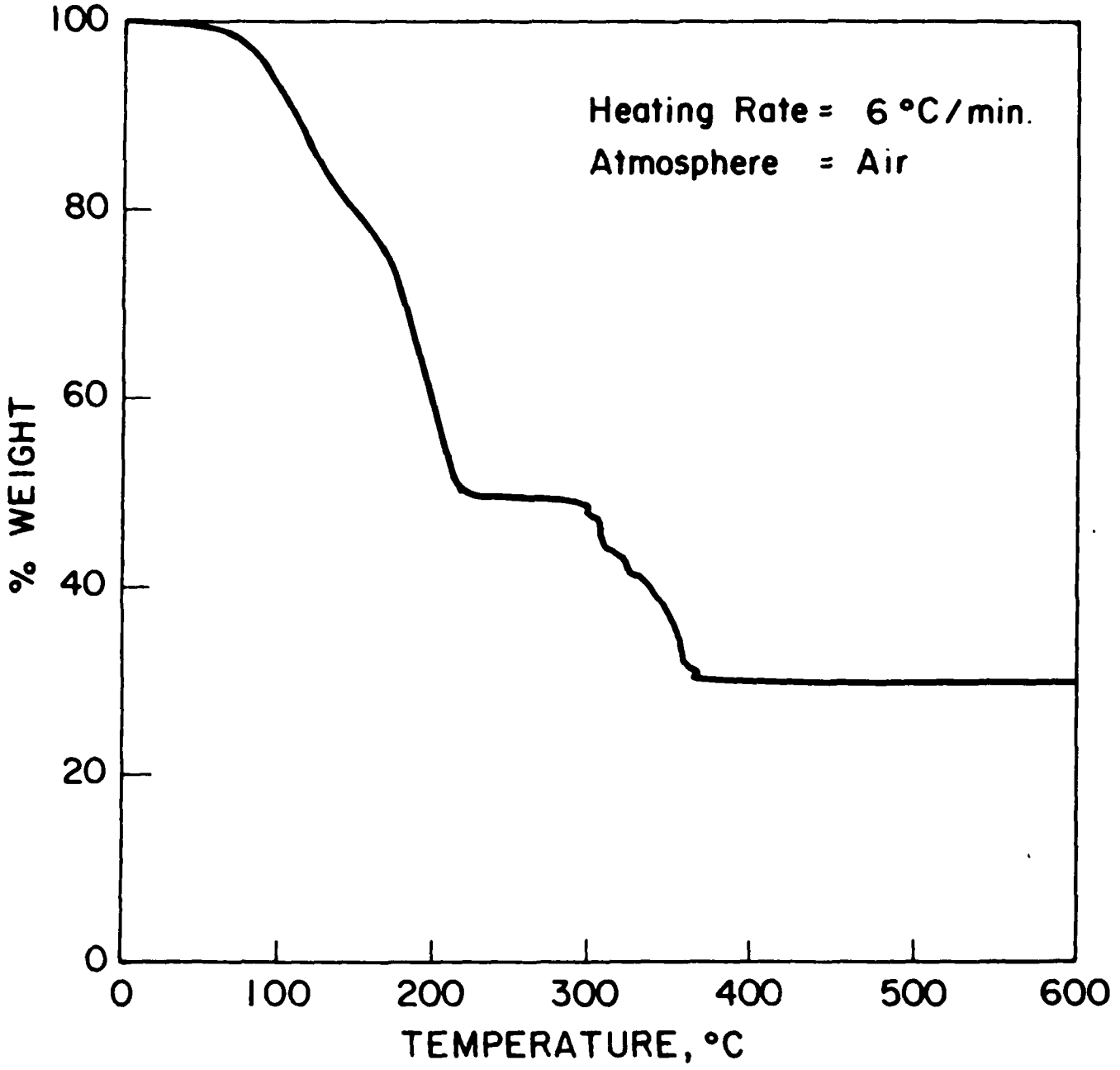


Figure 16. Thermogram of $Sn(C_7H_{15}COO)_2$ solution in xylene.

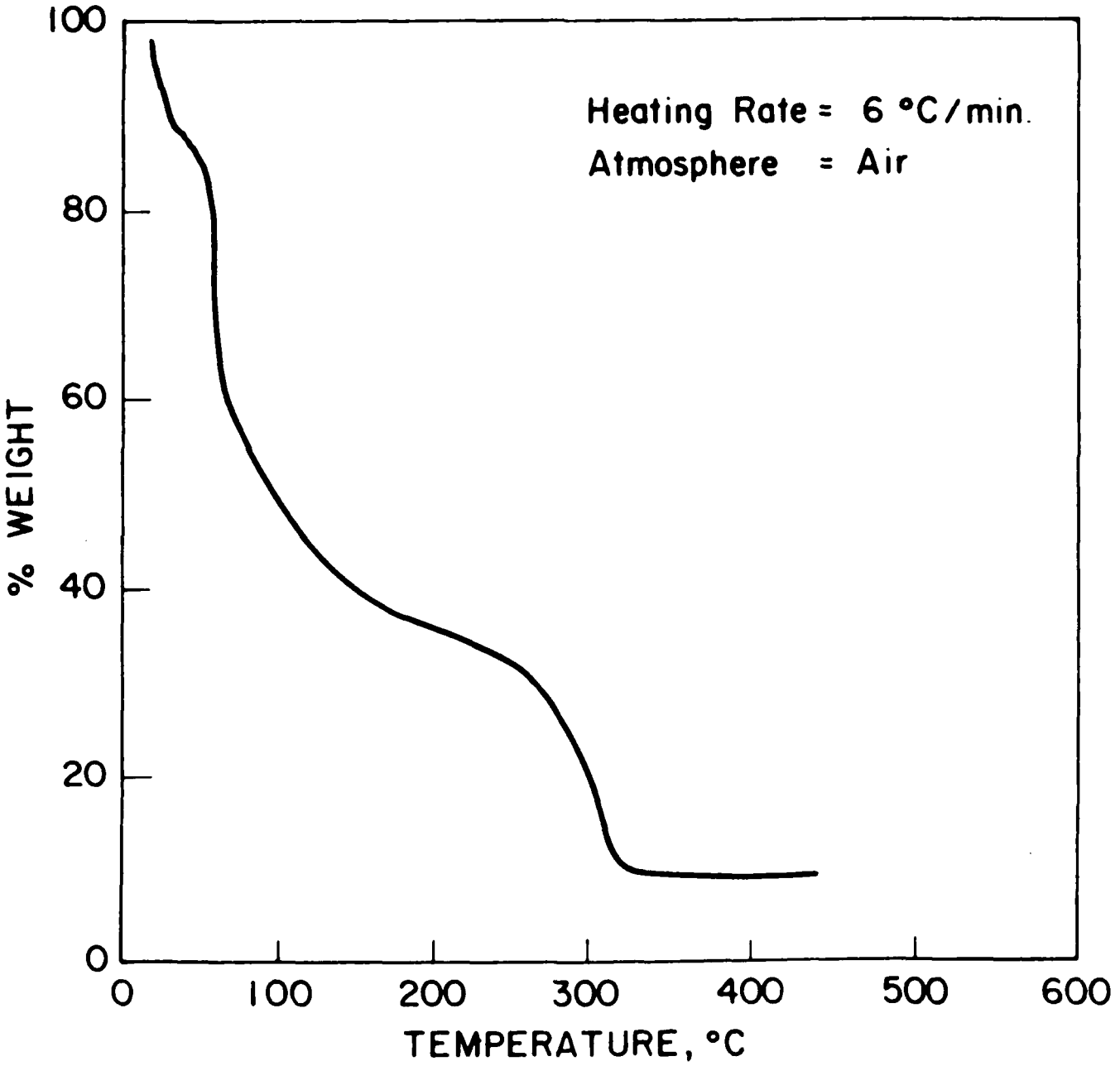


Figure 17. Thermogram of IIO formulation.

Table VI. Thermal Decomposition Behavior of Metallo-Organic Compounds.

| Compound | Stages | | | |
|---|---|---|---|---|
| | I | II | III | IV |
| $In(C_7H_{15}COO)_3$ in xylene | 25°C - 140°C xylene loss | 140°C - 260°C $In(C_7H_{15}COO)_3 \rightarrow In(C_7H_{15}COO)_2$ | 260°C - 340°C $In(C_7H_{15}COO)_2 \rightarrow In_2O_3$ | |
| $Sn(C_7H_{15}COO)_2$ in xylene | 25°C - 140°C xylene loss | 140°C - 225°C $Sn(C_7H_{15}COO)_2 \rightarrow Sn(C_7H_{15}COO)$ | 225°C - 390°C $Sn(C_7H_{15}COO) \rightarrow SnO_2$ | |
| $(CH_3O)_2Ti(C_9H_{19}COO)_2$ +0.37 X $Pb(C_9H_{19}COO)_2$ +0.63 X $Sr(C_9H_{19}COO)_2$ | 25°C - 140°C xylene loss | 225°C - 325°C $Ti(CH_3O)_2$ +0.37 X $Pb(C_9H_{19}COO)$ + 0.63 $Sr(C_9H_{19}COO)$ | 325°C - 360°C $Ti(CH_3O)_2$ +0.37 X PbO + 0.63 X $SrCO_3$ | 360°C - 460°C $TiO_2$ + 0.37 X PbO + 0.63 X SrO |

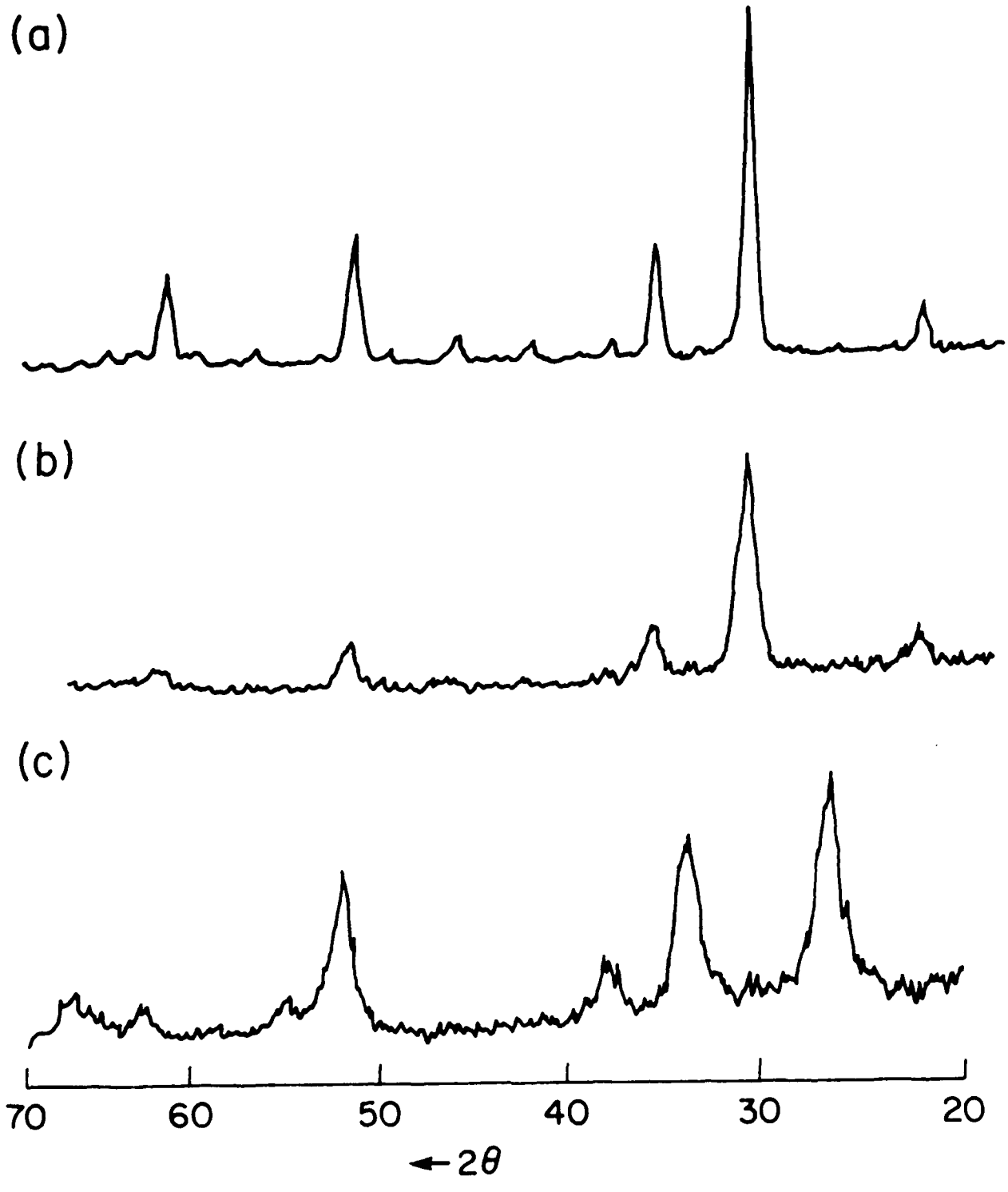


Figure 18. XRD of an ITO film. a) $In_2O_3$ powder with cubic bixbyite structure; b) two layer $In_{2-x}Sn_xO_{3-y}$, $x = 0.09$ on Si wafer; c) $SnO_2$ powder with tetragonal rutile structure.

Table VII. Grain Size of ITO Films (X-Ray Scherer Method).

| Sample | Grain Size |
|---|---|
| ITO(a) | 90 A |
| ITO(b) | 125 A |
| ITO(c) | 155 A |
| ITO(d) | 175 A |
| ITO(e) | 120 A |
| ITO(f) | 125 A |
| ITO(g) | 165 A |
| ITO(h) | 175 A |

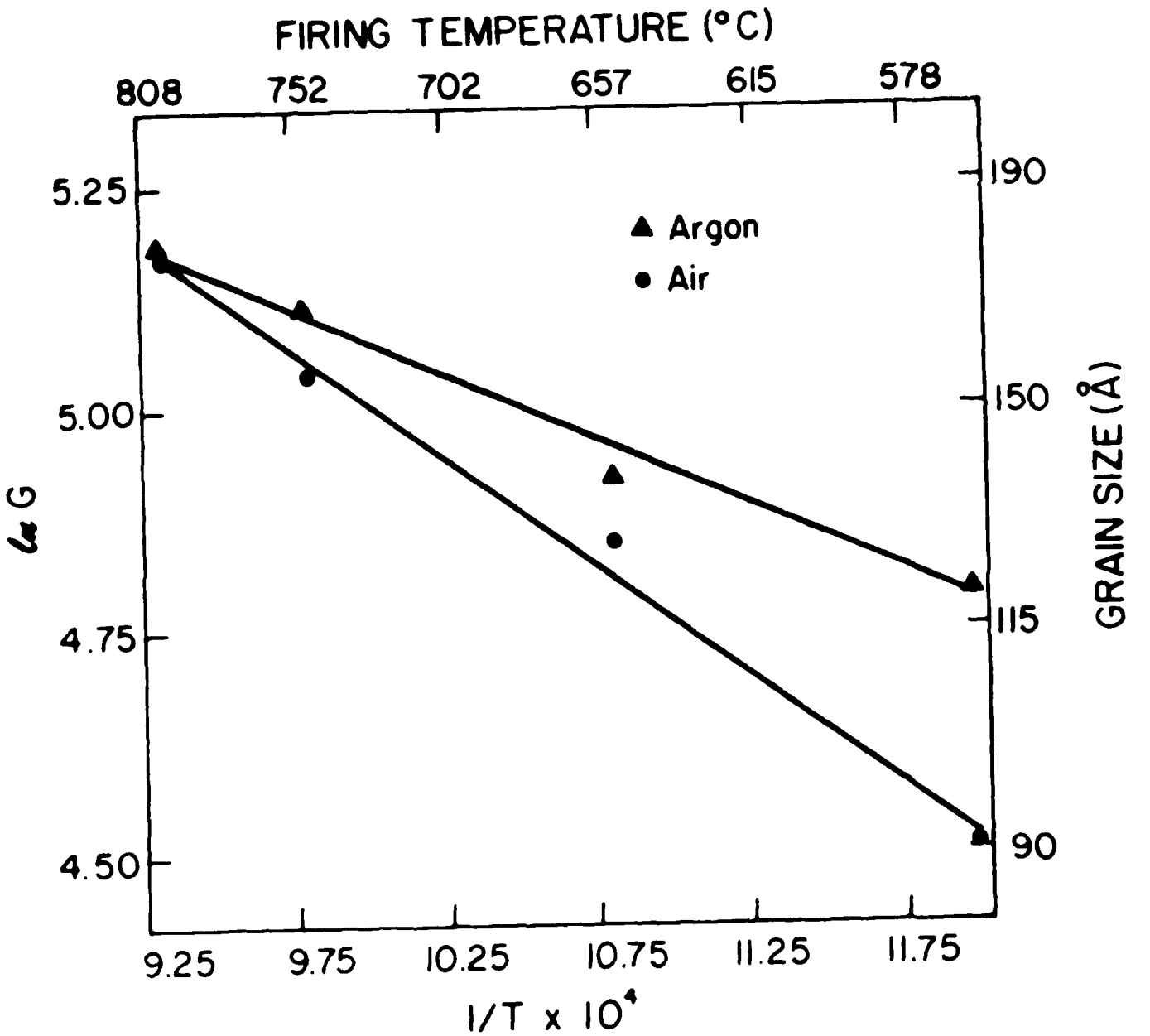


Figure 7. Variation of Grain Size of ITO Film with Firing Temperature

*4.1.3 Electrical Properties*

The sheet resistance of the ITO films was measured by Van der Pauw method and the resistivity was calculated by

$$\rho = R(sheet\ resistance)\ x\ t(thickness\ of\ the\ film)$$

Figure 20 shows the effect of firing conditions on the electrical properties. At fixed $SnO_2$ concentration, the resistivity changed with firing temperature and atmosphere. The resistivity decreased with an increase in firing temperature. The samples fired in an Ar atmosphere had a lower resistivity than than those fired in air at the same temperature. Figure 21 shows the change of resistivity with grain size for the films annealed in air. As seen in Fig. 21, the resistivity decreased with an increase in the grain size.

The Hall coefficient measurements were determined to characterize the charge carriers and their mobility in the ITO film. A Walker Scientific model HV4W electromagnet was used to generate the magnetic field. The Hall coefficient for all the samples was measured under a magnetic flux density of 5000 gauss at room temperature and liquid nitrogen temperature (77K). The relative uncertainty in the Hall coefficient measurements may be taken as a sum of the relative errors in the measured variable as:

$$\frac{\Delta R_h}{R_h} = \frac{\Delta I}{I} + \frac{\Delta B}{B} + \frac{\Delta t}{t} + \frac{\Delta V_h}{V_h}$$

where I is the measured electric current, B is the magnetic flux density, t is the thickness and $V_h$ is the measured voltage. The measurements were taken such that:

---

* Model HV4W, Walker Scientific, Inc , Worcester, MA 01606

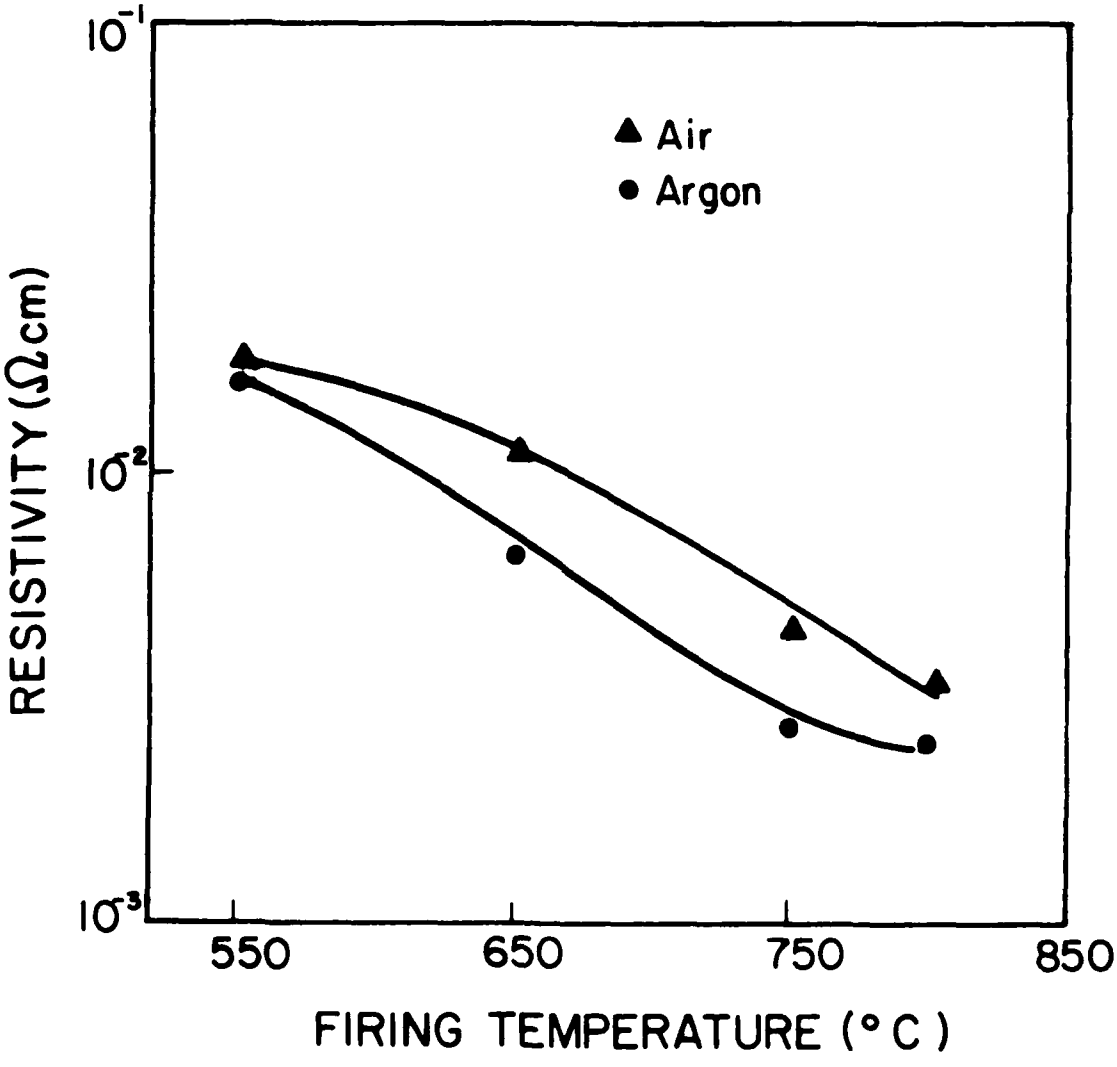


Figure 20. Variation of Resistivity of the ITO Film with Firing Temperature,

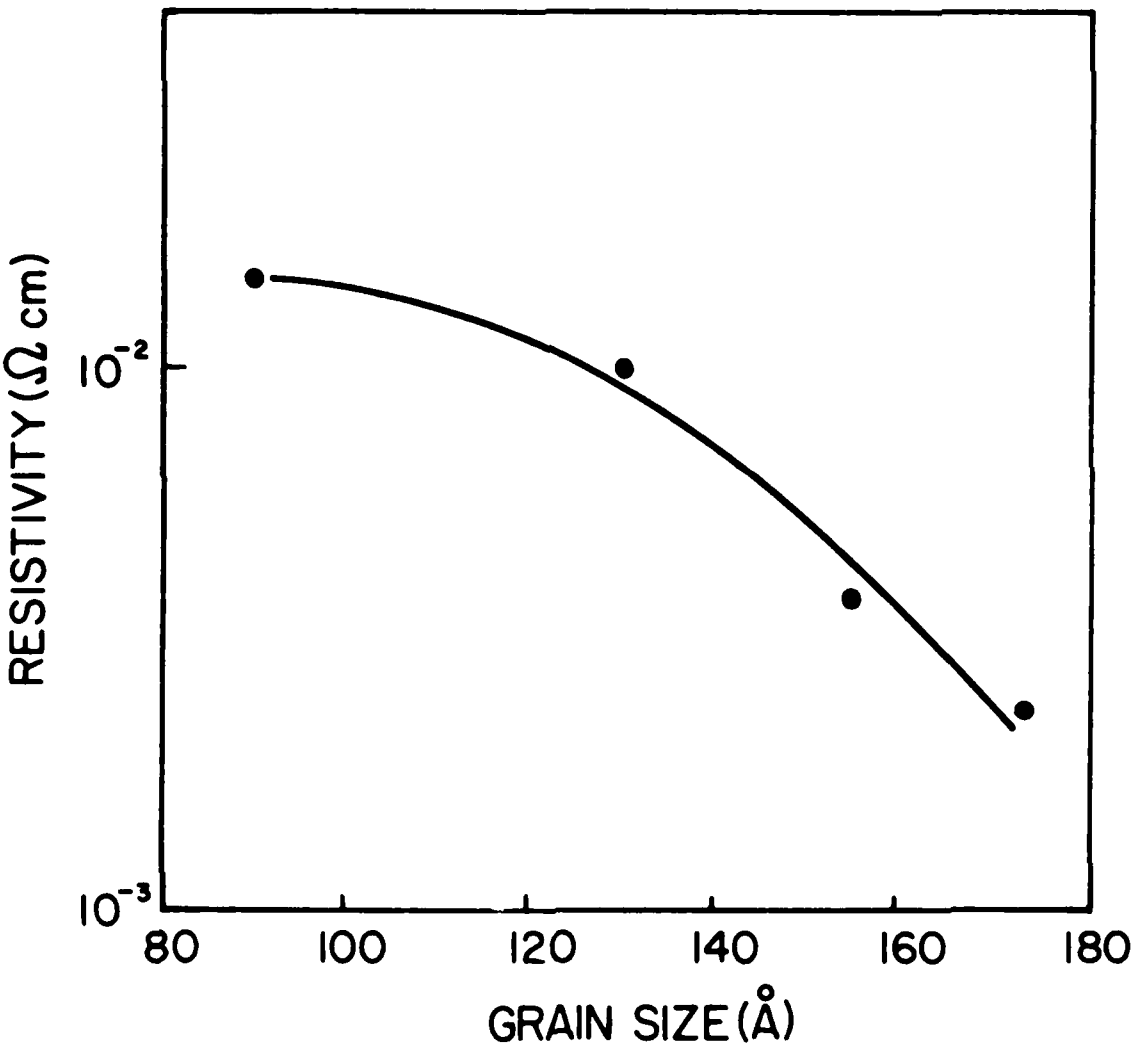


Figure 21. Variation of Resistivity of the ITO Film Fired in Air with Grain Size.

$$\frac{\Delta I}{I} < 0.005 \quad \frac{\Delta B}{B} < 0.01 \quad \frac{\Delta V_h}{V_h} < 0.005$$

Thus, for 5% error in the measurement of film thickness the uncertainty of the Hall coefficient was 7%. The measured Hall coefficient was used to determine the nature and the concentration of the charge carrier in ITO film (electrons or holes) by using the expressions: $n = \frac{1}{R_h e}$ and Hall mobility, $\mu_h = \frac{R_h}{\rho}$.

In this analysis the Hall factor $r_h = R_h e n$ was assumed to be equal to unity. The analysis of the Hall coefficients showed that the ITO films prepared by metallo-organic precursors is an n-type semiconductor. Similar observations were made on the films prepared by other techniques such as vapor deposition [41], RF sputtering [42], dc sputtering [2], spray pyrolysis [4] and magnetron sputtering [3]. The variations of Hall mobility and carrier concentration with firing temperature and atmosphere are shown in Table (VIII). These data are in good agreement with the reported data [43-47]. The high carrier concentration suggests that the film basically is an n-type degenerate semiconductor. The Hall mobility increased with an increase in the annealing temperature and for the same annealing temperature, it was higher for the films prepared in an Ar atmosphere compared to air. The carrier concentration did not vary significantly with either the annealing temperature or atmosphere. Figures 22 and 23 show the variation of the Hall mobility with carrier concentration and measurement temperature. At lower temperatures the carrier concentration was lower while the mobility was higher.

It is widely accepted that the $Sn^{+4}$ ion occupies the $In^{+3}$ site in ITO and the electrons are produced for charge compensation.

$$SnO_2 \longrightarrow Sn_{In}^{+1} + 3/2O_o + 1/2O_2 + e^{'}.$$

The experimental data shows, at the firing temperature and the firing atmosphere studied, the carrier concentration in the ITO films was almost unchanged. This may be due to very high doping of $SnO_2$. The very low carrier mobility in the ITO films may be due to the presence of

Table VIII. The Effect of Firing Conditions on the Electrical Properties of the Film.

| Sample | $R_h$ $cm^3/coulomb$ | $\mu_h$ | n $x10^{20}/cm^3$ |
|---|---|---|---|
| ITO(a) | -0.0238 | 1.80 | 2.62 |
| ITO(b) | -0.0229 | 2.12 | 2.73 |
| ITO(c) | -0.0262 | 5.20 | 2.38 |
| ITO(d) | -0.0385 | 9.14 | 1.62 |
| ITO(e) | -0.0418 | 3.27 | 1.49 |
| ITO(f) | -0.0421 | 5.50 | 1.48 |
| ITO(g) | -0.0396 | 11.22 | 1.58 |
| ITO(h) | -0.0281 | 7.71 | 2.22 |

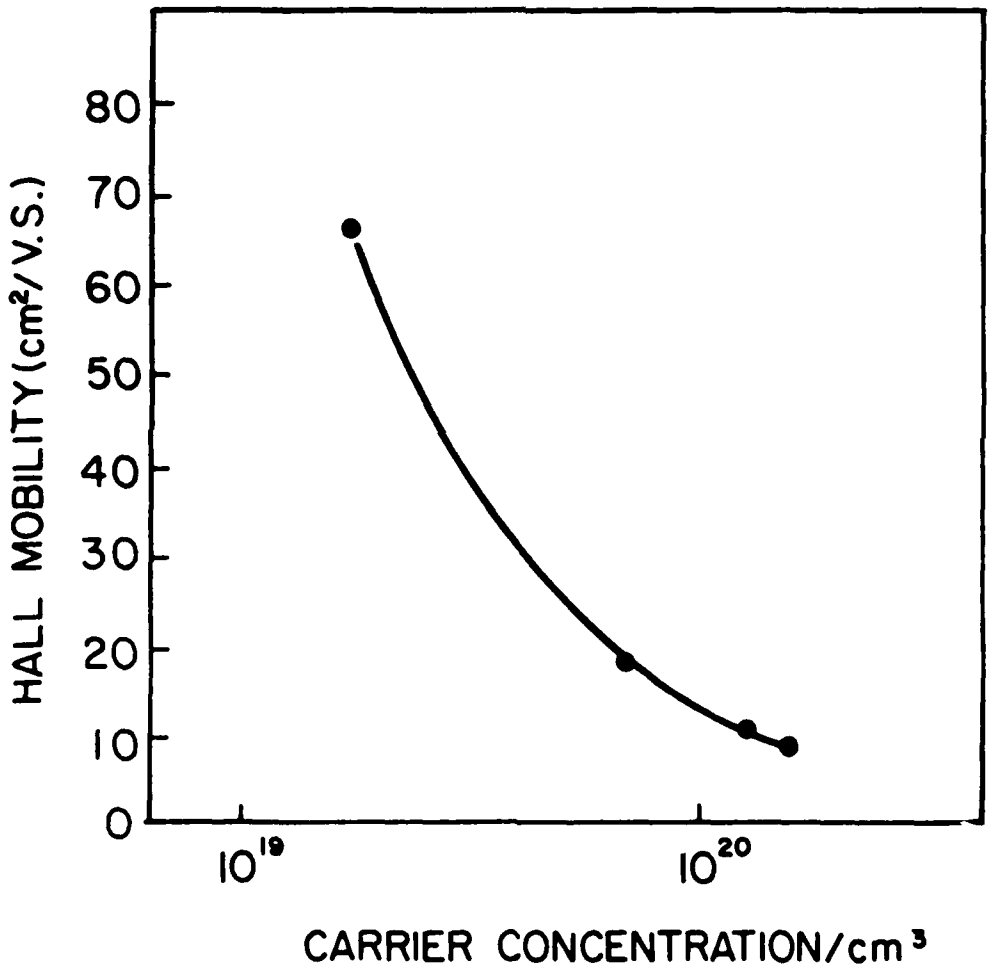


Figure 22. Variation of Hall Mobility of the Charge Carriers in the ITO Film with the Carrier Concentration.

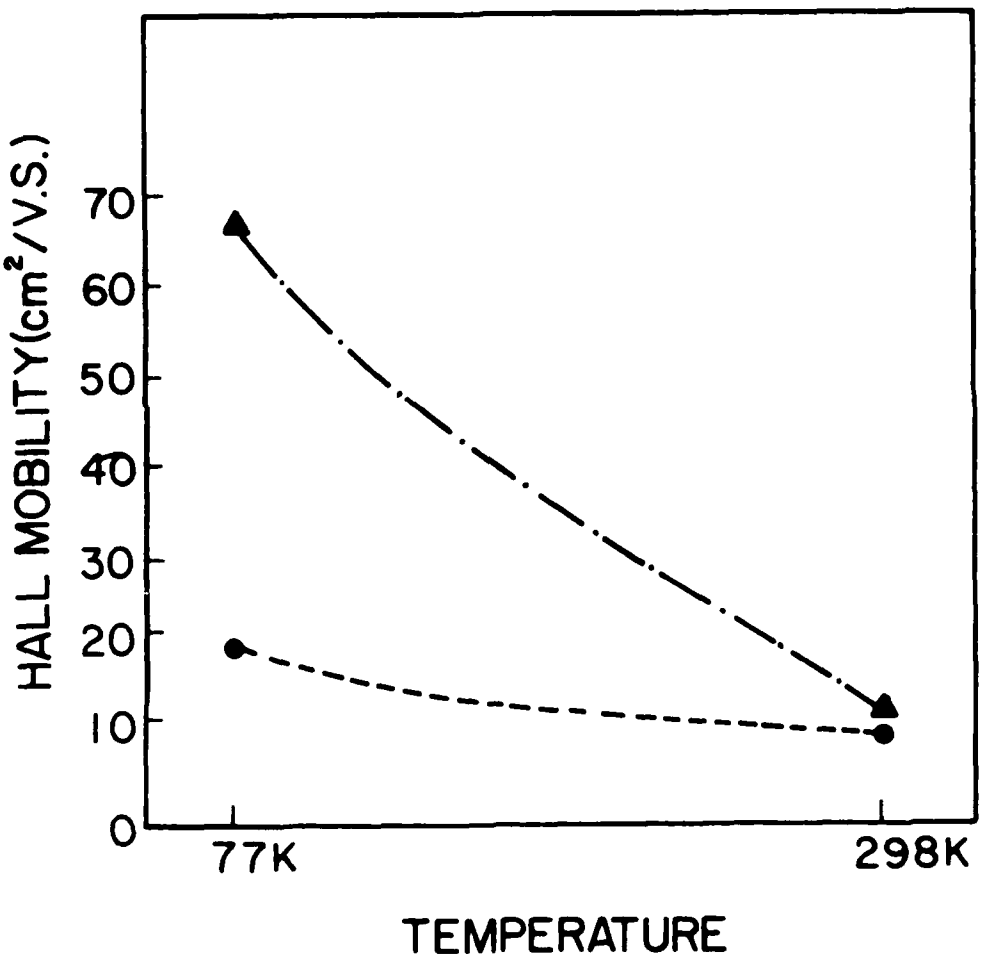


Figure 23. Variation of Hall Mobility with the Measurement Temperature, a) for Film Fired at 800°C in Air; b) for Film Fired at 800°C in Ar Atmosphere.

charge carrier traps. Based on the experimental data, $V_{In}^{-3}$ seems to be the charge trap. The charge traps might have been created by the following reaction

$$3SnO_2 \longrightarrow 3Sn^{+1}{}_{In} + 6O_o + V^{-3}{}_{In}$$

The reduction in the concentration of charge traps in a reducing atmosphere may be responsible for the increase in Hall mobility. The following chemical reaction may take place under the reducing atmosphere as well as at higher temperatures.

$$3Sn^{+1}{}_{In} + 6O_o + V^{-3}{}_{In} \longrightarrow 3Sn^{+1}{}_{In} + 5O_o + 1/2O_2 + 2/3\ V^{-3}{}_{In}$$

*4.1.4 Optical Properties*

A double beam uv-visible spectrophotometer[+] was used to measure the transmittance of the ITO films in the wavelength range of 190 nm to 900 nm at 15 nm/min scan speed. A bare substrate which was subjected to a similar firing condition was used as a reference. The transmittance of the ITO films fired at 650°C was greater than 95 % in the wavelength range of 350 nm to 850 nm (Fig. 24). The transmittance of the ITO films fired at temperatures greater than 650° C was slightly lower than 95 % but greater than 90 % in the same wavelength range.

## 4.2 PLZT Films

*4.2.1 Thermal Decomposition*

Figure 25 shows the thermogram of the PLZT (8/65/35) formulation in xylene at a heating rate of 6°C/minute. The small weight loss near 500°C is due to the reaction

$$La(C_2H_3O_2)_3 \longrightarrow La_2O_3$$

---

+ Model Lambda-3, Perkin Elmer Co, Oak Brook, Ill 60521

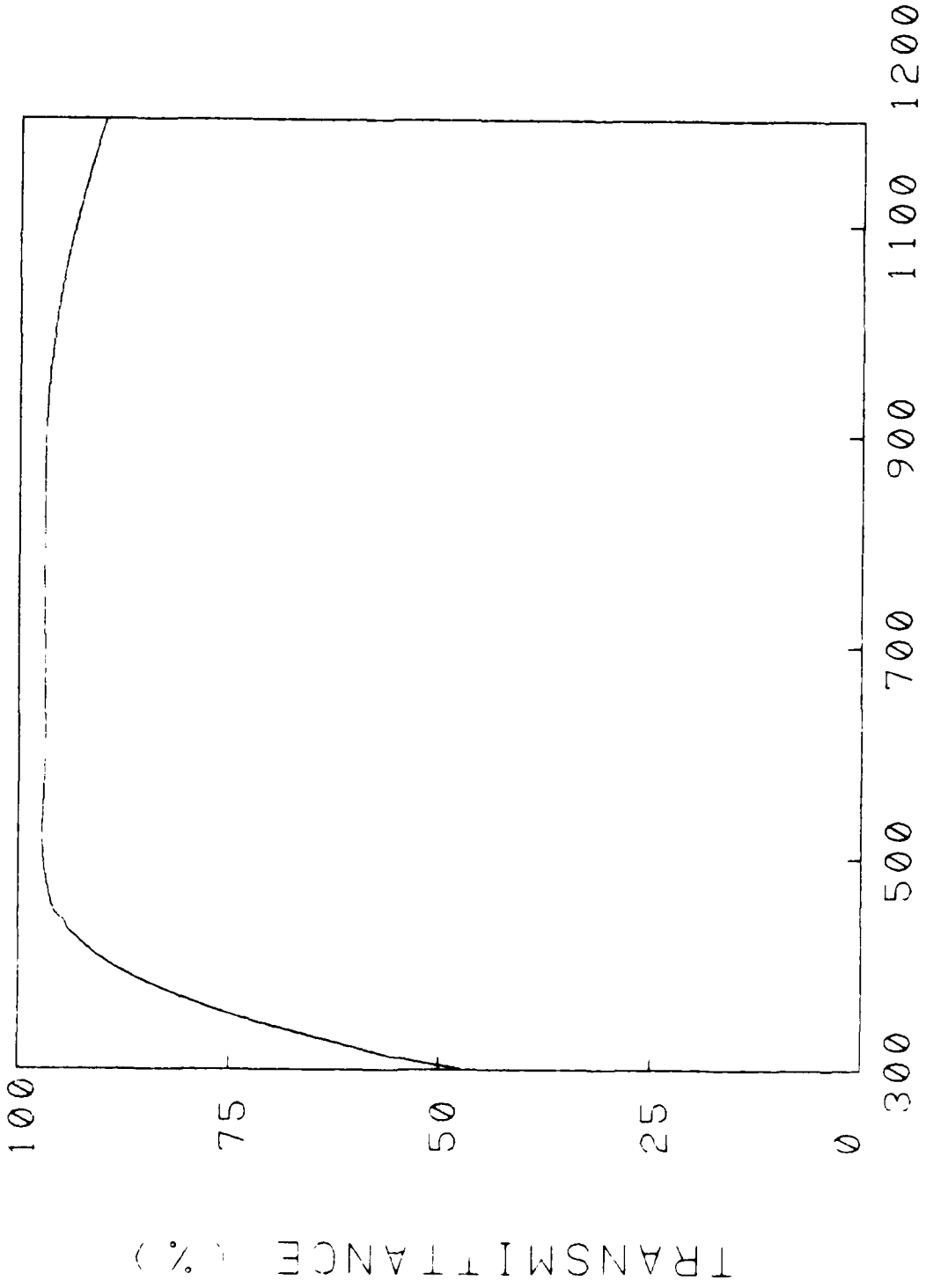


Figure 24. The Transmittance of the ITO Film

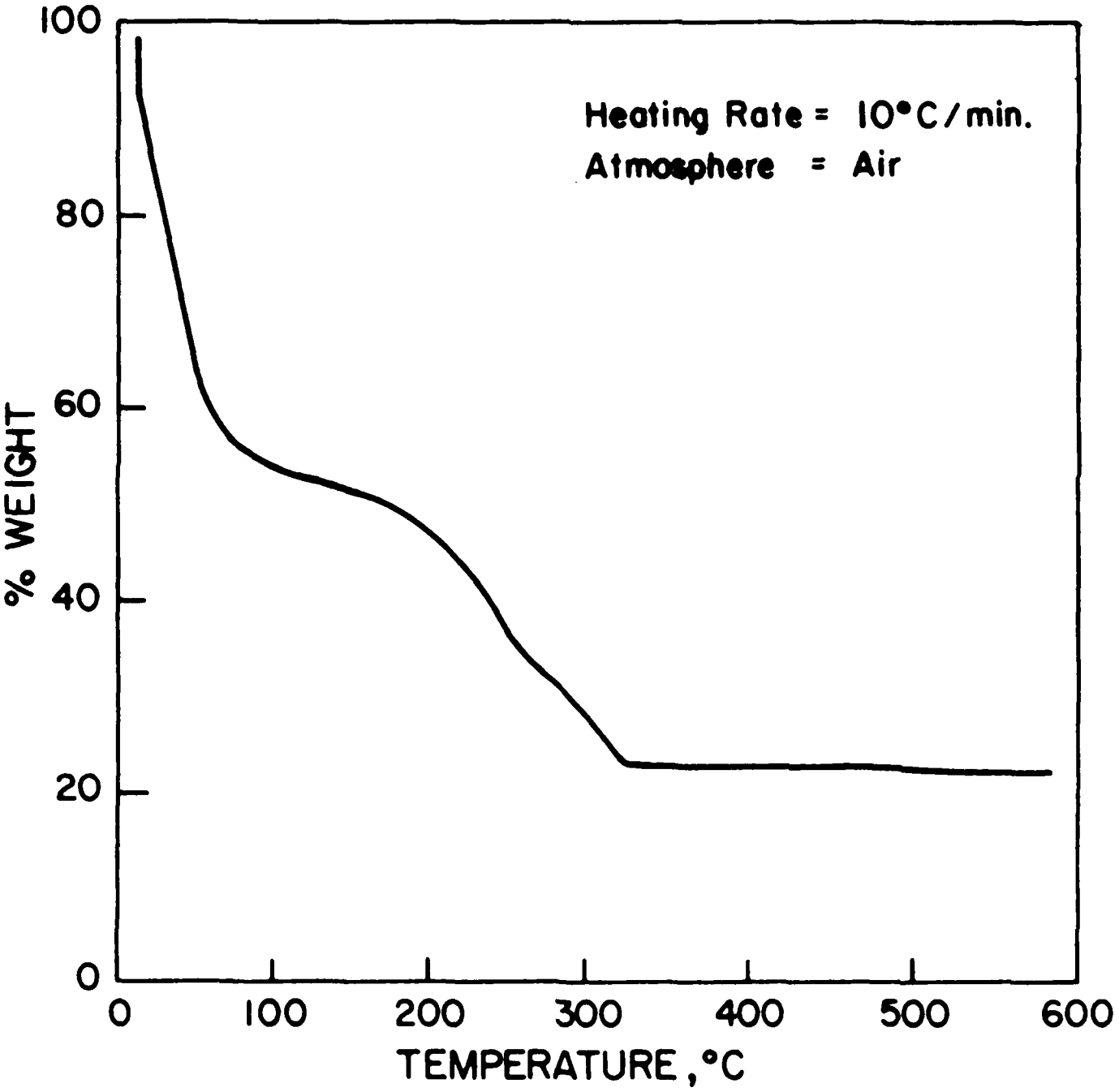


Figure 25. Thermogram of PLZT (8/65/35) Formulation.

Figures 26, 27 and 28 are the thermograms of lead titanate formulation, $Zr(O_3H_7)_4$ and $La(C_2H_3O_2)_3$ 1.5 $H_2O$, respectively. The result of the thermogravimetric analysis indicated that in order to form PLZT solid solution from the metallo-organic precursors it is necessary to fire the films above 500°C.

In order to test various electrical and optical properties of formed PLZT films, a thick ITO film layer (0.4 $\mu$m) was deposited on the substrate before the deposition of PLZT. The ITO film was used because of its good chemical stability, optical transparency, and its good electrical conductivity.

*4.2.2 Crystal Structure*

The x-ray diffraction patterns of PLZT 8/65/35 powder fired at various temperatures are shown in Fig. 29. Films fired at 550°C had a rhombohedral phase as a major phase along with a PbO-rich second phase as shown in Fig. 29a, which was present even at 650°C. However, when the samples were fired at 750°C, no PbO-rich phase was observed in the x-ray diffraction pattern. Figure 30 shows the x-ray pattern for a thin film PLZT (8/65/35) of 2.5 $\mu$ in thickness, deposited on 0.4 $\mu$ ITO coated sapphire and fired using the firing profile II shown in Fig. 5. No PbO-rich phase was found, which indicates that the chemical reaction rate in films is much faster than that in bulk form. All the peak locations in Fig. 30 are shifted along 2 $\theta$ axis as compared with those shown in Fig. 29. This may be due to different lattice parameters of PLZT film as compared to PLZT powder. The reason for this difference in lattice parameters of the film compared to the powders is still not known. The study of the effects of crystal structure modification of PLZT film on its electrical and optical properties is underway.

## 4.3 Barium Titanate Films

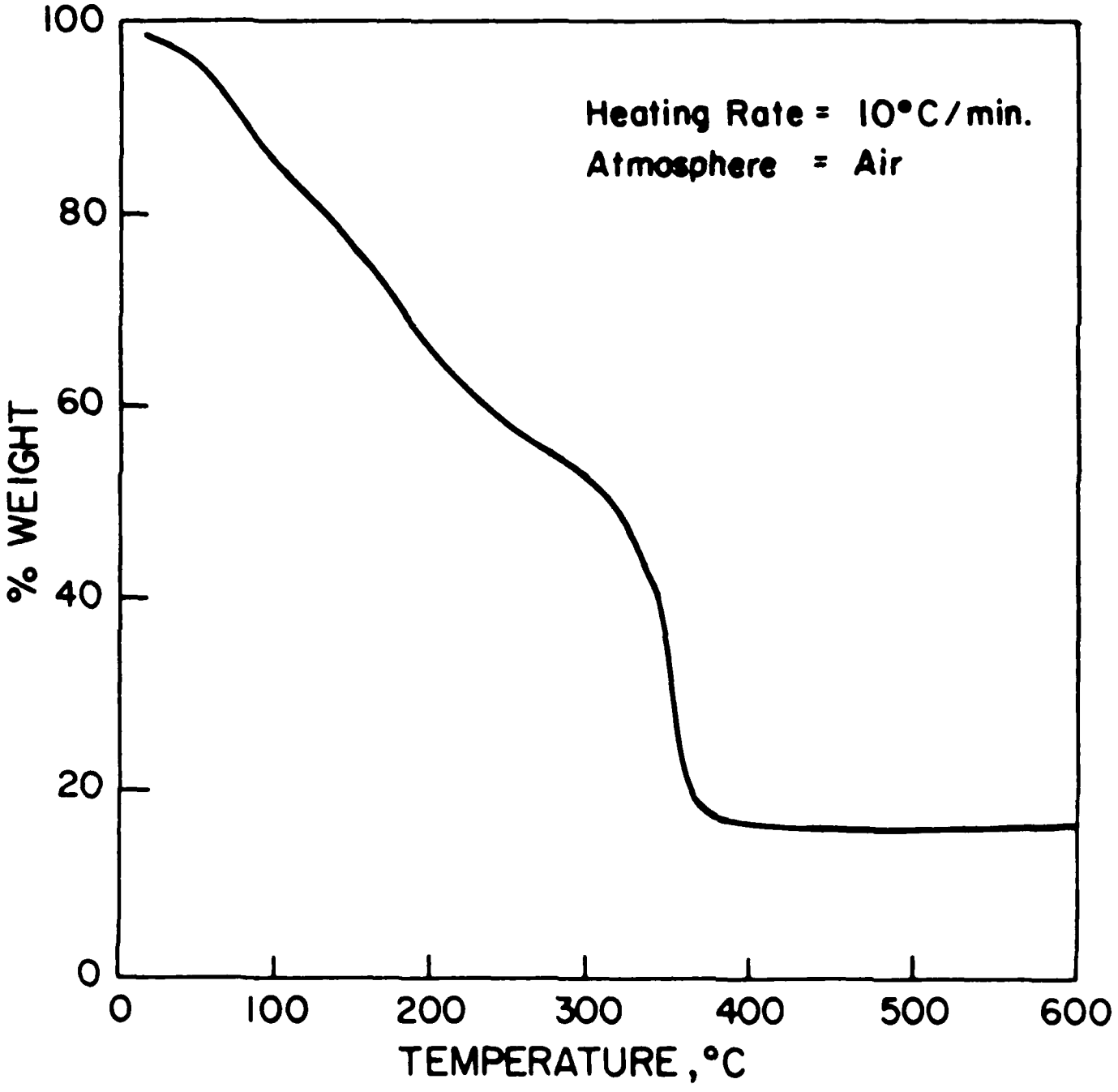


Figure 26. Thermogram of $PbTiO_3$ Formulation.

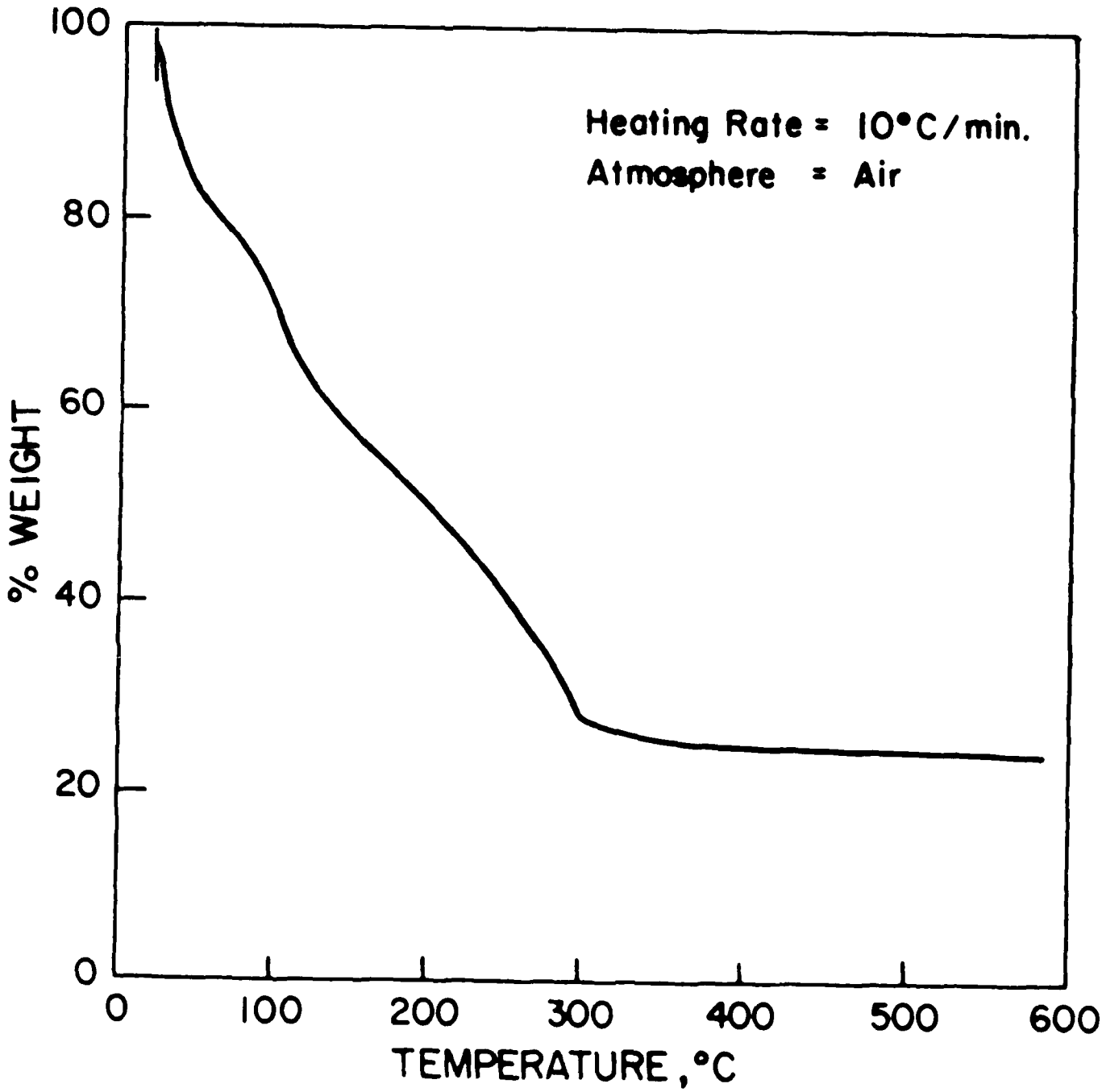


Figure 27. Thermogram of $Zr(OC_4H_9)_4$ Solution in Acetone.

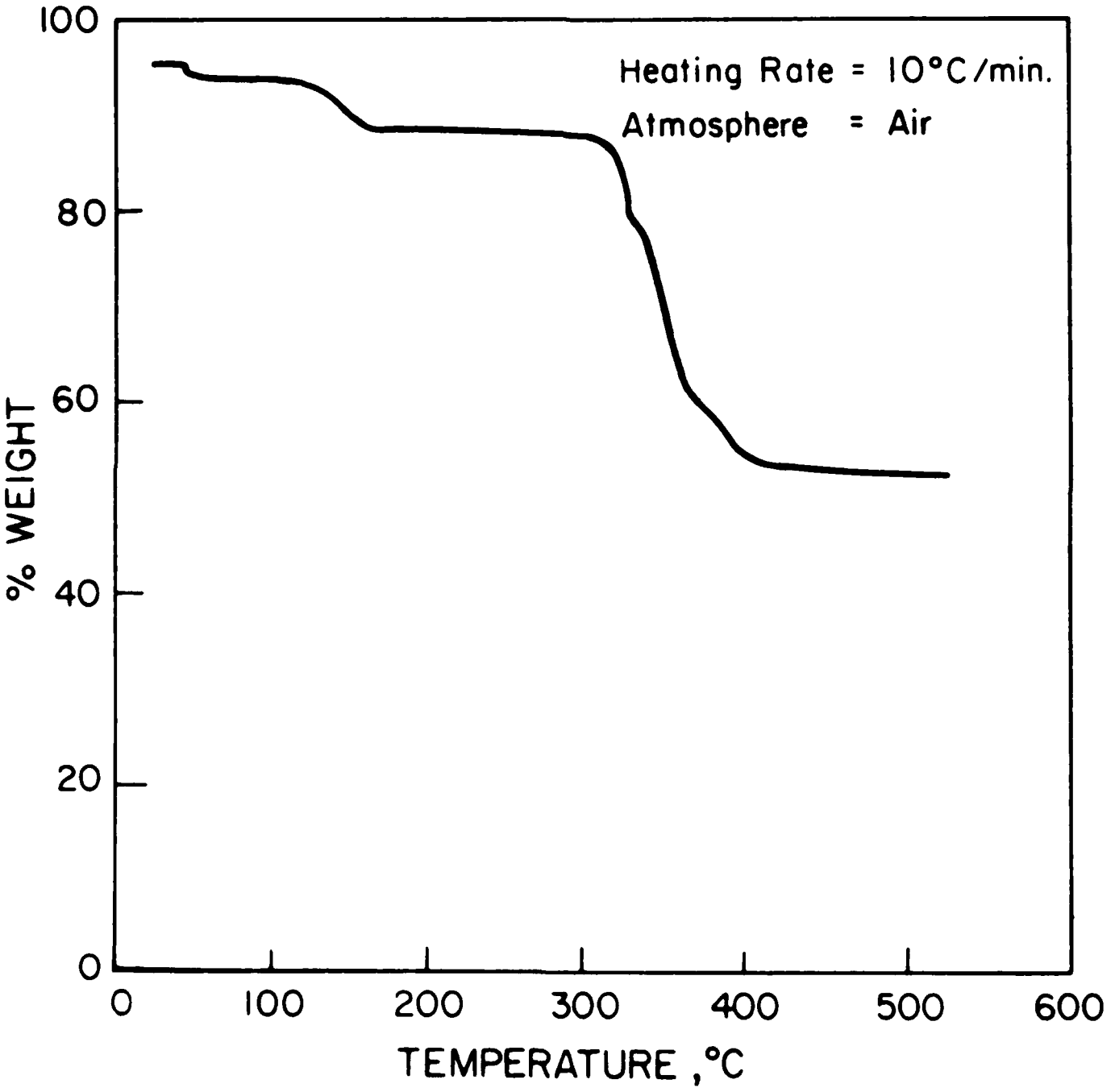
100
80
60
40
20
0
% WEIGHT
Heating Rate = 10°C/min.
Atmosphere = Air
0
100
200
300
400
500
600
TEMPERATURE ,°C

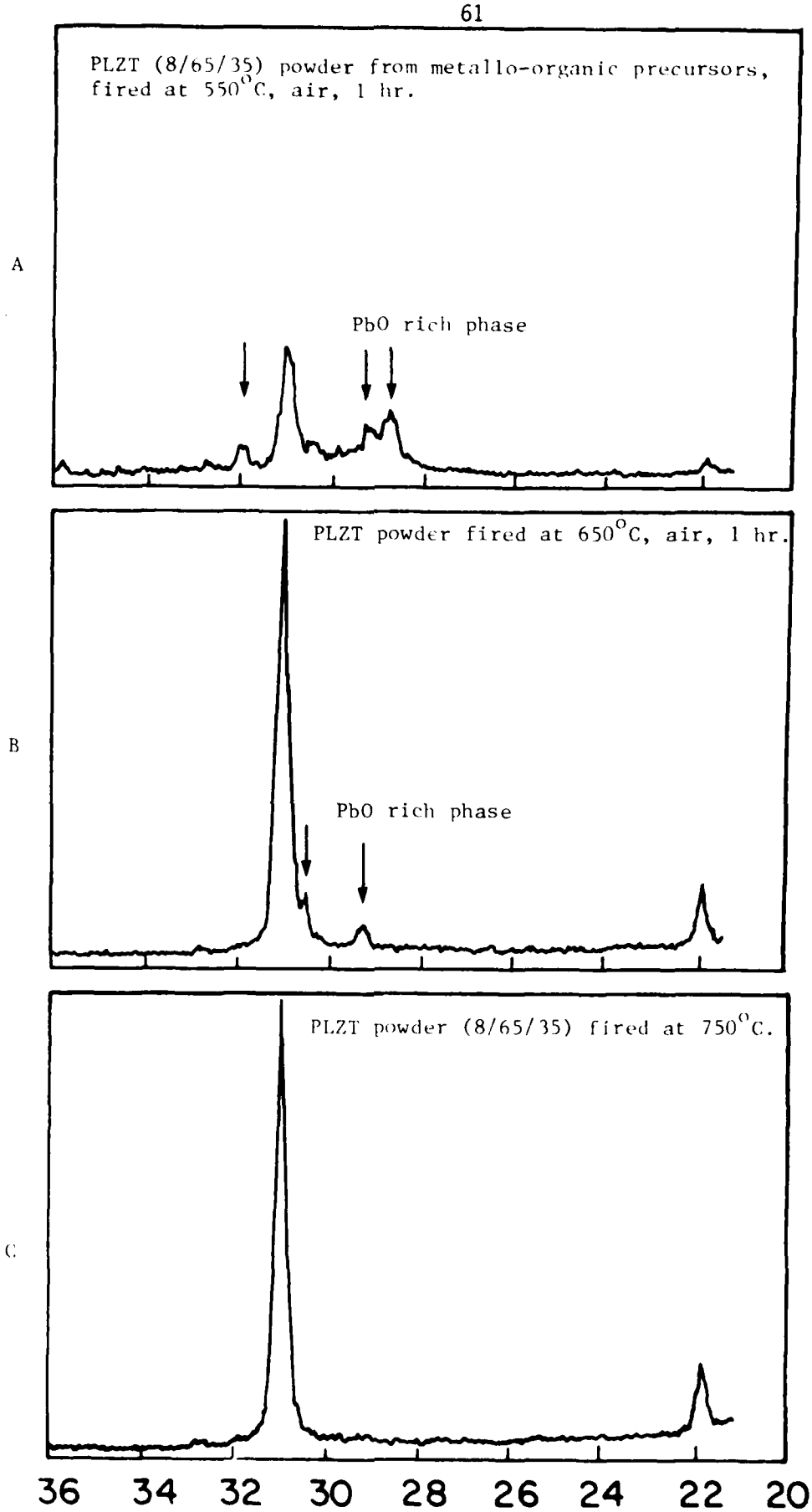


Figure 29. X-Ray Diffraction Patterns.

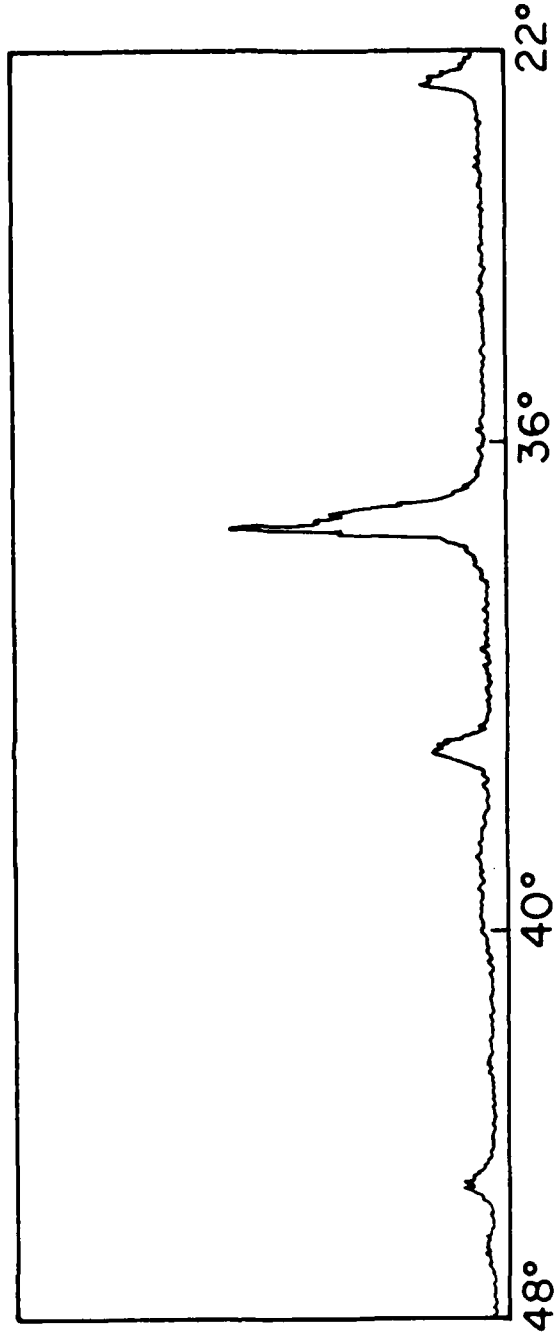


Figure 30. X-Ray Diffraction Patterns of PLZT (8/65/35) Film Fired at 600°C on Sapphire.

*4.3.1 Microstructure*

X-ray diffraction analysis was carried out for the $BaTiO_3$ films on various substrate-electrodes and fabricated at various firing temperatures. The $BaTiO_3$ films with the perovskite structure were obtained when the samples were fired above 550°C. However, when $BaTiO_3$ films deposited on ITO coated Si wafer were fired above 1100°C, the interaction between $BaTiO_3$-ITO-$SiO_2$-Si was serious enough to form additional phases. Table IX summerizes the interaction effects between substrate, electrode and dielectric.

The grain size was estimated from the half width of the diffraction peak using the Scherer Method. Figure 31 shows the grain size of $BaTiO_3$ film on ITO coated silicon substrate obtained from the (111) diffraction peak as a function of firing temperature. It was found that the grain size of $BaTiO_3$ deposited on the ITO coated Si wafer increases with an increase in firing temperature. Due to severe interactions between substrate, electrode and dielectric, ITO coated silicon wafer was not used to fire firing $BaTiO_3$ above 1000°C. A coarser grain sized $BaTiO_3$ was obtained by firing $BaTiO_3$ film at 1175°C on Pt-foil. Figure 32 is a SEM photogram of such $BaTiO_3$ film. A TEM photograph (Fig. 33) of $BaTiO_3$ film on ITO coated Si wafer fired at 1050°C for 1 hr in air showed a very dense $BaTiO_3$ film and also indicated the presence of amorphous $BaTiO_3$ in the film.

Very fine grained $BaTiO_3$ films can be obtained from metallo-organic precursors because of the fast reaction rates [39]. If it is assumed that the growth of grains is a diffusion controlled reaction in the $BaTiO_3$ films produced by MOD precursors, then the crystallized volume from an amorphous $BaTiO_3$ matrix will be proportional to $e^{-3E/2kT}$, where E represents the activation energy of diffusion. Thus, the grain size should be proportional to $e^{-E/2kT}$. Following this approach, the activation energy calculated from Fig. 31 is about 80.0 kJ/mole. This value is lower than that observed in the solid state reaction between $BaCO_3$ and $TiO_2$ powders to form $BaTiO_3$ [48] and the formation of $BaTiO_3$ powder from MOD precursors [39]. Both the reactions [48,39] were reported to be diffusion controlled. Thus, it appears that grain growth

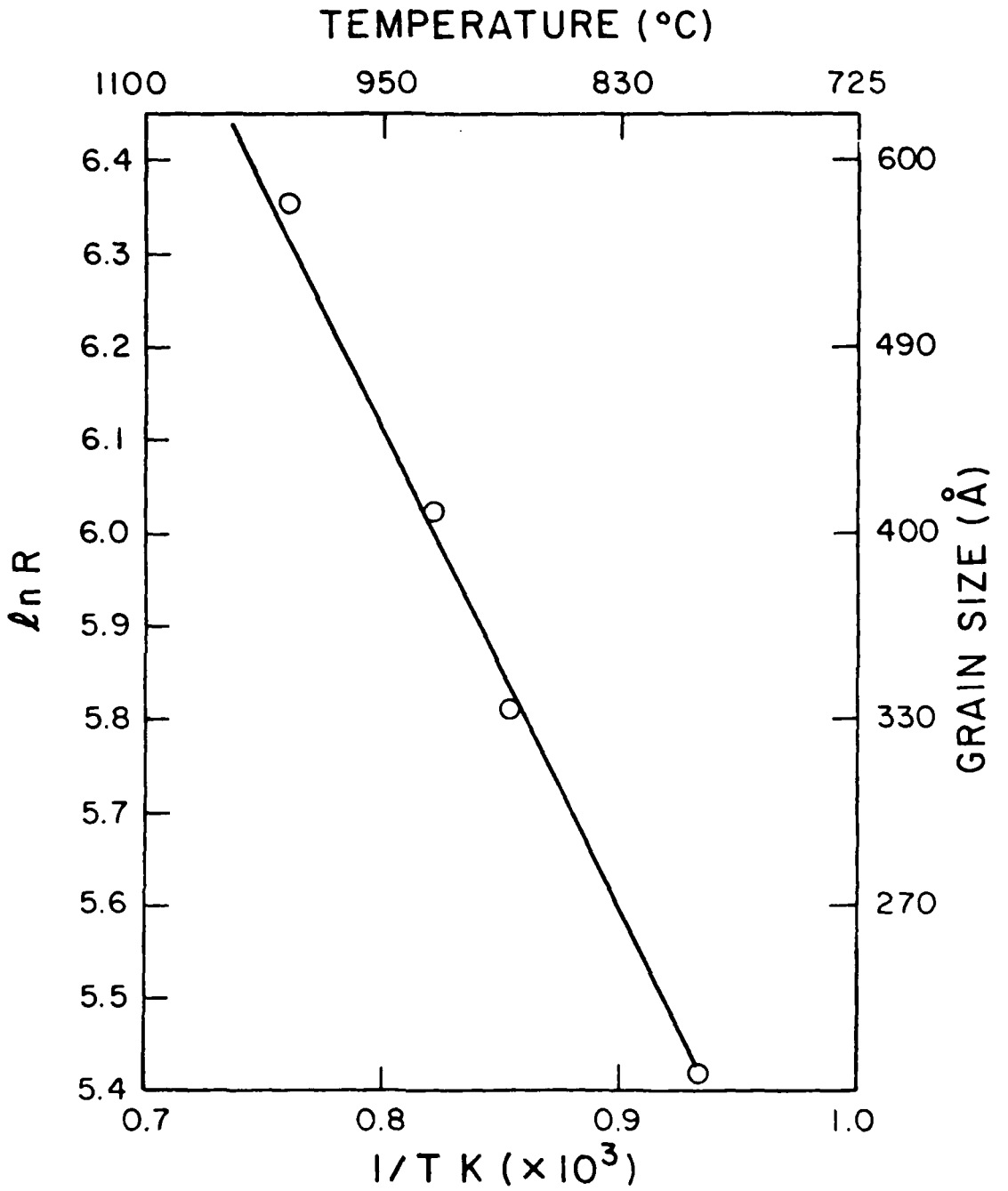


Figure 31. Grain Growth Kinetics of $BaTiO_3$ Film on the ITO Coated Silicon Substrate.

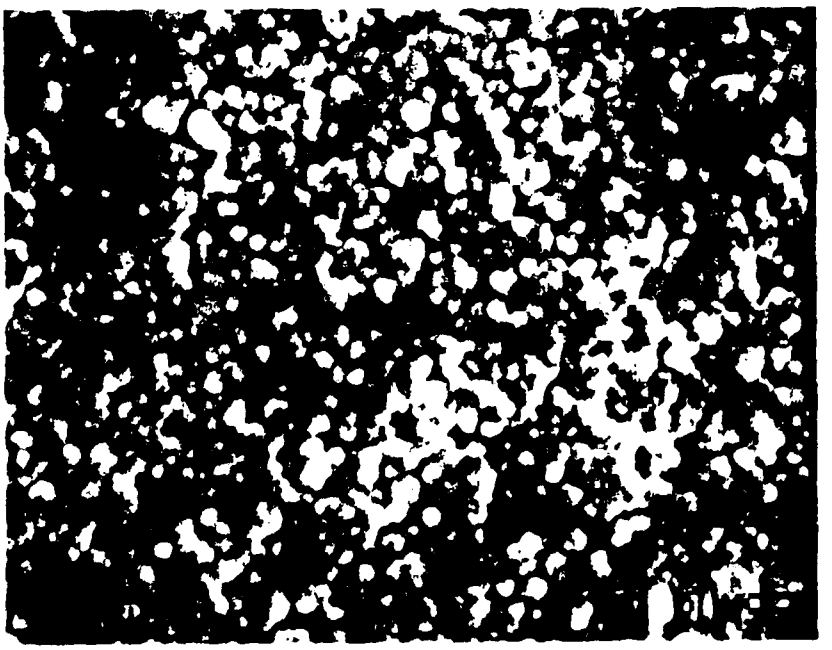

Figure 32. A SEM Microphotograph of $BaTiO_3$ Film Fired at 1175°C in Air for 1 hr. on Pt Foil Substrate. (.1 wt% $HF+HNO_3$ was used as etchent).


Figure 33. A TEM Photograph of $BaTiO_3$ Film on ITO Coated Si Wafer Fired at 1050°C for 1 hr.

kinetics are not diffusion controlled but interface controlled. This is consistent with the TEM observations which indicated that $BaTiO_3$ was crystallizing from amorphous regions. Also, the grain size of the MOD films made by the multilayer deposition technique is not only dependent on the activation energy but also upon the single layer thickness as discussed in the previous annual report [1]. If the grain growth is assumed to be interface controlled then the growth kinetics should follow the following relationship.

$$\frac{V}{V_o} = (Kt)^3 = (Ate^{\frac{-Q}{kT}})^3$$

where V is the volume crystallized, t is the annealing time, T is the annealing temperature, Q is the activation energy, A is a constant, K is the rate constant and $V_o$ is the total volume. The cube of the grain size is proportional to the volume crystallized and the grain size is inversely proportional to the number of nuclei per unit volume. The relationship may be given as $(GS)^3 N Vo = A't^3 e^{\frac{3Q}{kT}}$. where GS is grain size and N is the number of nuclei/unit volume. Using this approach, the value of the activation energy for grain growth was calculated to be 40 kJ/mole.

The c/a values for $BaTiO_3$ crystals were estimated from the (112) and (211) x-ray reflections. Figure 34 shows the dependence of c/a on grain size. For the films, of average grain size 0.2 $\mu$, c/a is about 1.018; this value is very close to the value reported for bulk $BaTiO_3$ [21]. For the very fine grained $BaTiO_3$ film (0.04 $\mu$), this value reduced to 1.004.

### *4.3.2 Dielectric Properties*

#### *4.3.2.1 Temperature Dependence*

Figure 35 shows the temperature dependence of the dielectric constant of the $BaTiO_3$ films as a function of grain size. At very fine grain size (0.034 $\mu$) the dielectric constant in the temperature range -20°C to 160°C was almost unchanged and was very low. With an increase

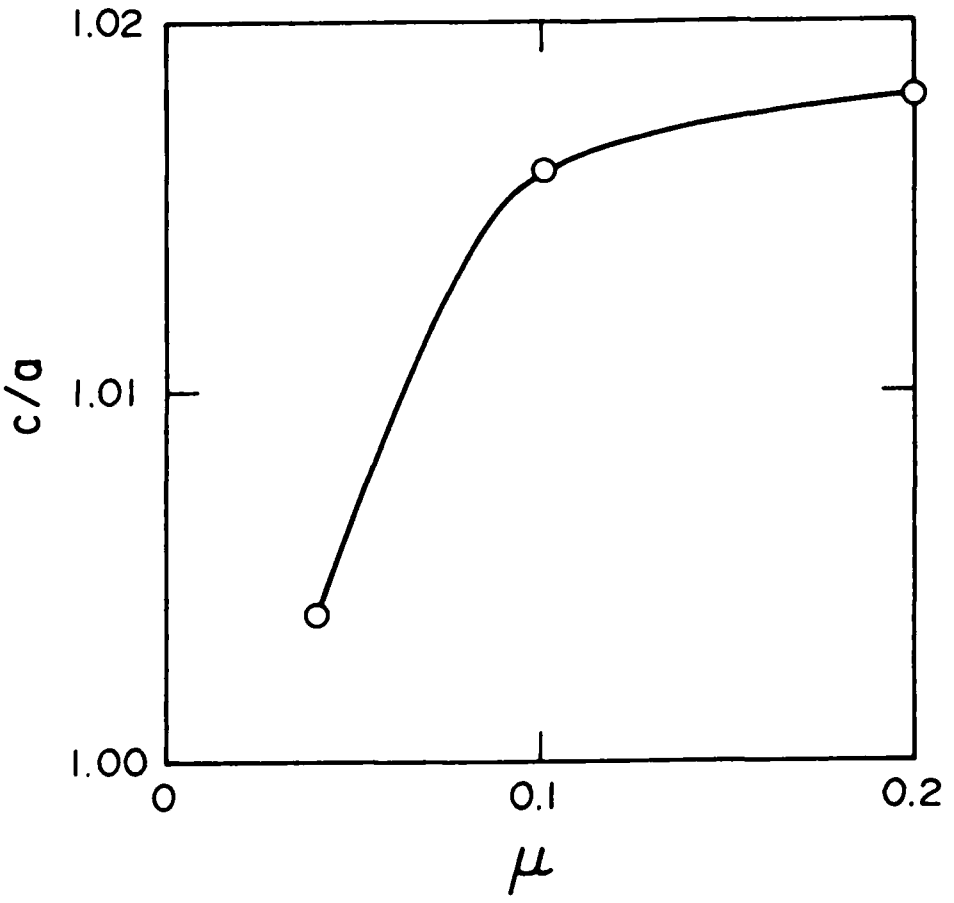


Figure 34. The Grain Size Dependence of c/a Ratio of $BaTiO_3$ in a Film Form.

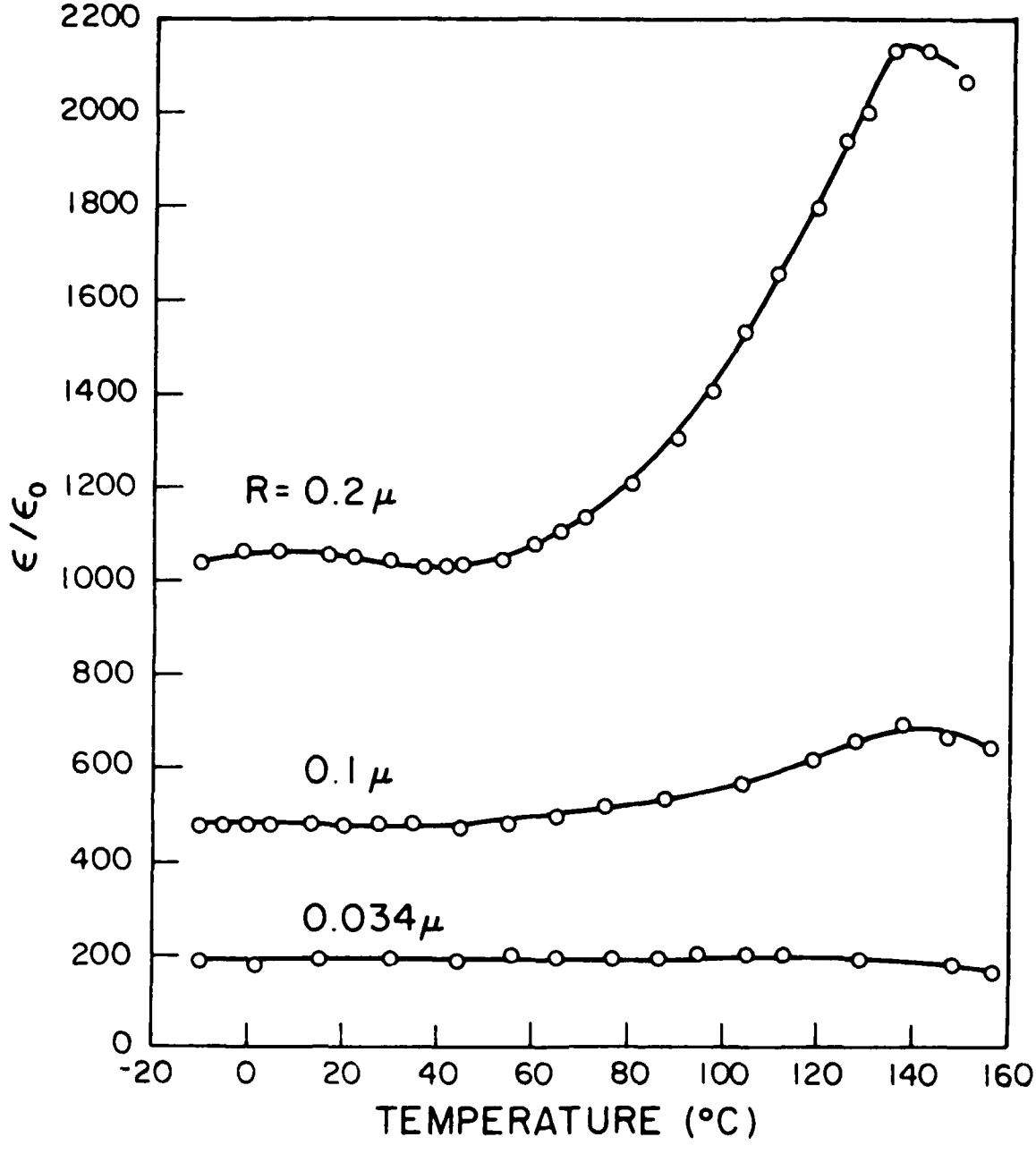


Figure 35. Variation of Dielectric Constant of $BaTiO_3$ Films of Varying Grain Sizes with Temperature.

in the grain size to 0.08 - 0.1 $\mu$, the dielectric constant increases and a broad maximum appears at the Curie point. For the samples with an average grain size of 0.2 $\mu$, the dielectric constant at room temperature was above 1000 and the Curie point $T_c$ was observed around 136°C. However, the Curie temperature peak was still broad as compared with that of bulk $BaTiO_3$. A lower dielectric constant for very fine grained $BaTiO_3$ (<1 $\mu$) is in good agreement with that reported by G. Arlt and his co-workers [21]. Figure 36 shows the temperature dependence of the dissipation factor for the same samples indicated in Fig. 35. The dissipation factor of very fine grained samples (0.034 $\mu$) was almost unchanged with temperature. However, at higher grain sizes the temperature dependence of tan $\delta$ was observed.

*4.3.2.2 Frequency Dependence*

Figure 37 shows the frequency dependence of the room temperature dielectric constant of $BaTiO_3$ films of varying grain sizes. For the very fine grain samples (0.034 $\mu$), the dielectric constant decreased continuously with increasing frequency, 100 Hz to 10 MHz. For a larger grained sample (0.1 - 0.2 $\mu$), the dielectric constant decreased with increasing frequency up to 1 MHz and then increased.

Figure 38 shows a frequency dependence of room temperature dissipation factors of various $BaTiO_3$ films. At lower frequencies, (< 100 kHz), the values of tan $\delta$ were almost constant. At frequencies greater than 100 KHz, the values of tan $\delta$ increased very rapidly with frequency for fine grained sample (0.034 $\mu$). However, for larger grained samples ( >0.1 $\mu$), this increase was very small. The increase in the dielectric constant and the dissipation factor of the $BaTiO_3$ films at higher frequency could be due to a resonance effect.

*4.3.2.3 D.C. Bias Field Dependence*

The dependences of dielectric constant and tan $\delta$ on D.C. bias electric field were measured at

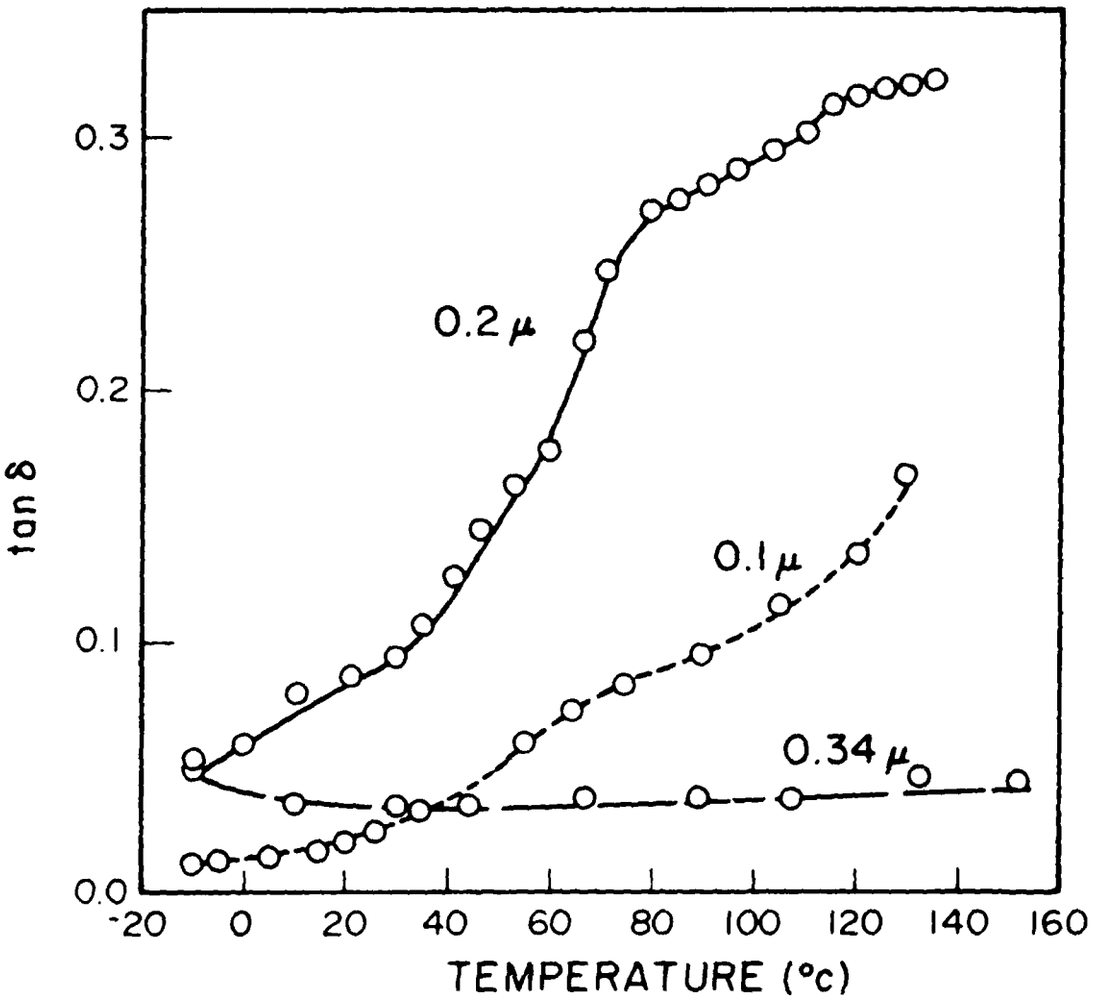


Figure 36. Variation of Dissipation Factor of $BaTiO_3$ Films of Varying Grain Size with Temperature.

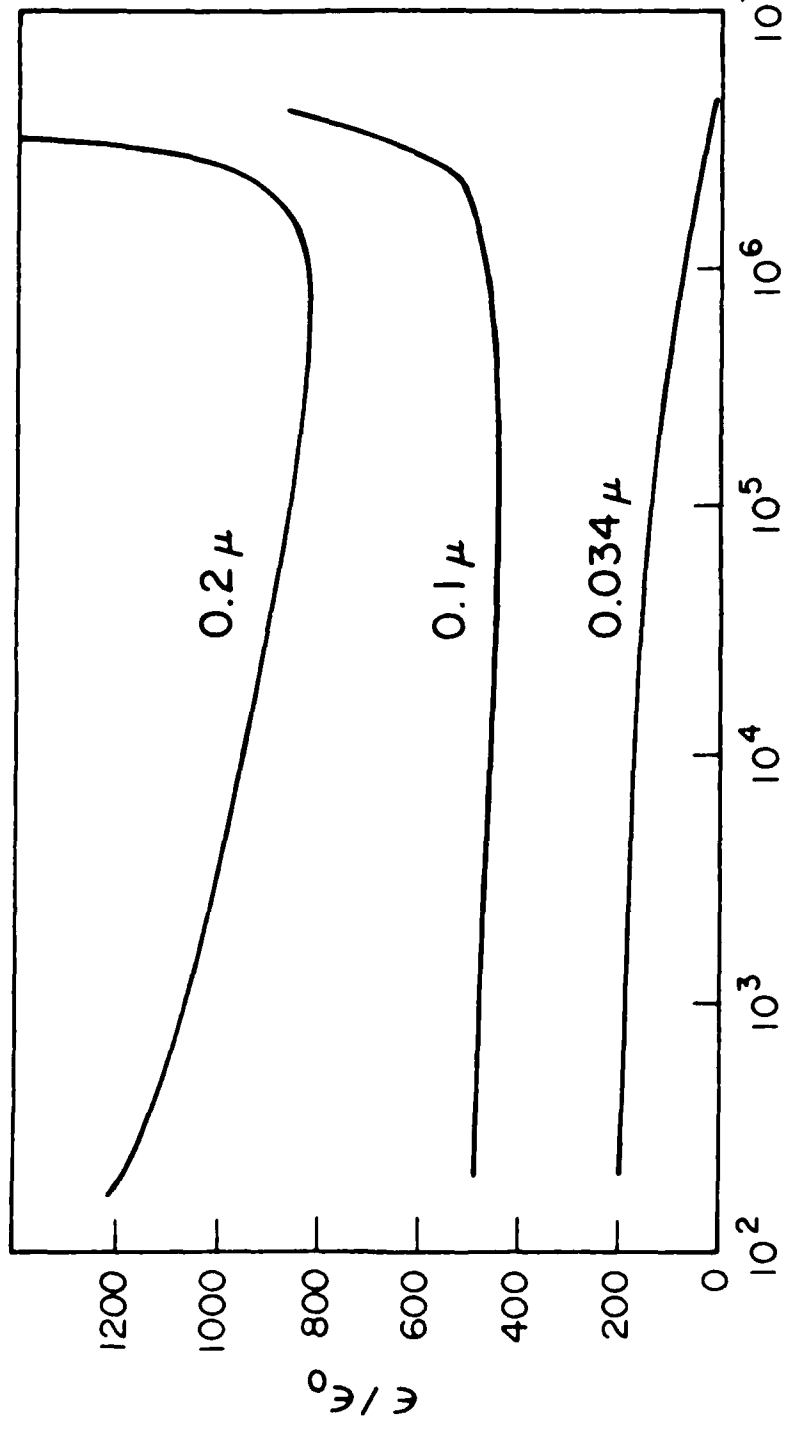


Figure 47. Variation of Dielectric Constant of $BaTiO_3$ Films of Various Grain Sizes with Frequency.

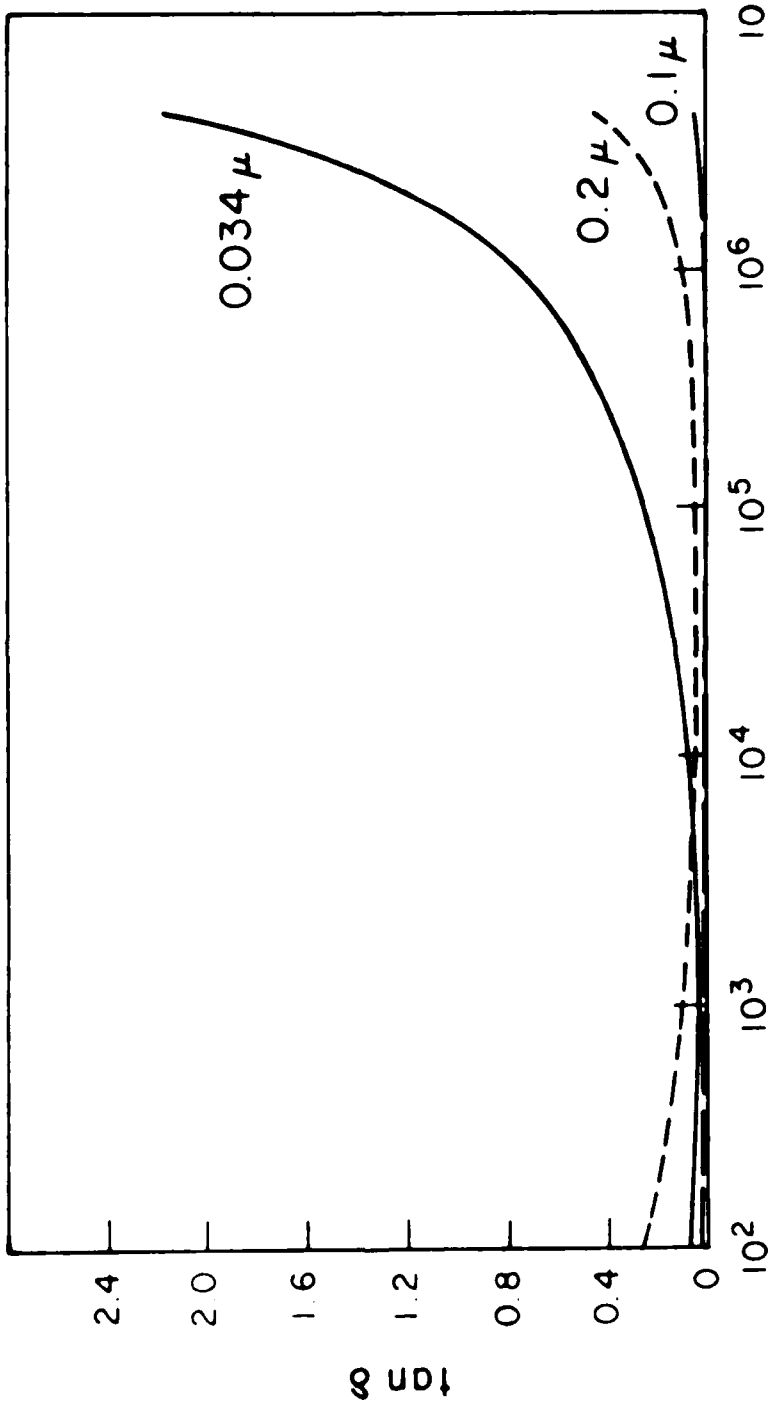


Figure [illegible]. Variation of Dissipation Factor of BaTiO$_3$ Films of Various Grain Sizes with Frequency.

room temperature using an the A.C. signal of 1 kV/cm. Figures 39 and 40 show the experimental results for 0.034 and 0.2 $\mu$ grain size $BaTiO_3$ films. In both cases, the dielectric constants decreased with D.C. bias field. However, more significant D.C. bias field dependence of dielectric constant was observed for the sample which had the larger grain size. The dielectric constant of the $BaTiO_3$ films of 0.2 $\mu$m grain size measured at 1 KHz and 1 MHz reduced by 1/4 by applying a D.C. bias field of 80 kV/cm. Figure 40 shows the D.C. bias field dependence of tan $\delta$. At higher measurement frequency (1 MHz), both the samples (0.034 $\mu$ and 0.2 $\mu$ grain size) show a decrease of tan $\delta$ with D.C. bias field. However, at lower frequency, (1 KHz), the value of tan $\delta$ increased with the D.C. bias field for the 0.2 $\mu$ grain size sample. Figure 41 shows the variation of the dielectric constant with frequency at various D.C. bias electric fields for the $BaTiO_3$ film of 0.034 grain size. These curves indicate that at a frequency higher than 4 MHz, no D.C. bias field dependence of k was observed.

The dielectric loss of $BaTiO_3$ at low frequencies, < 1kHz mainly is due to electrical conductivity. It is known that oxygen deficient defects in $BaTiO_3$ films serves as electron donors [49]. Thus, it is expected that for well-crystallised $BaTiO_3$ film, the value of tan $\delta$ should increase with temperature, and this is the case for 0.2 $\mu$ grain sized $BaTiO_3$ (Fig. 36). In the case of the fine grained $BaTiO_3$ films, the grains are separated by a glass phase (See Fig. 33), which is a highly insulated material. Thus, the value of tan $\delta$ for these films was low over a wide temperature region. For higher frequencies, (1 MHz - 100 MHz), the loss is mainly dipole relaxation which is directly linked to the concentration of oxygen vacancies. Thus, oxygen vacancies play a major role for the dielectric loss. The dielectric loss frequency curves shown in Fig. 37 indicate that for the higher temperature fired films (larger grained), the concentration of oxygen vacancies is lower than that for the lower temperature fired films. Thus, the high k, low loss $BaTiO_3$ film should be fired at high temperature and in an oxygen rich atmospheres.

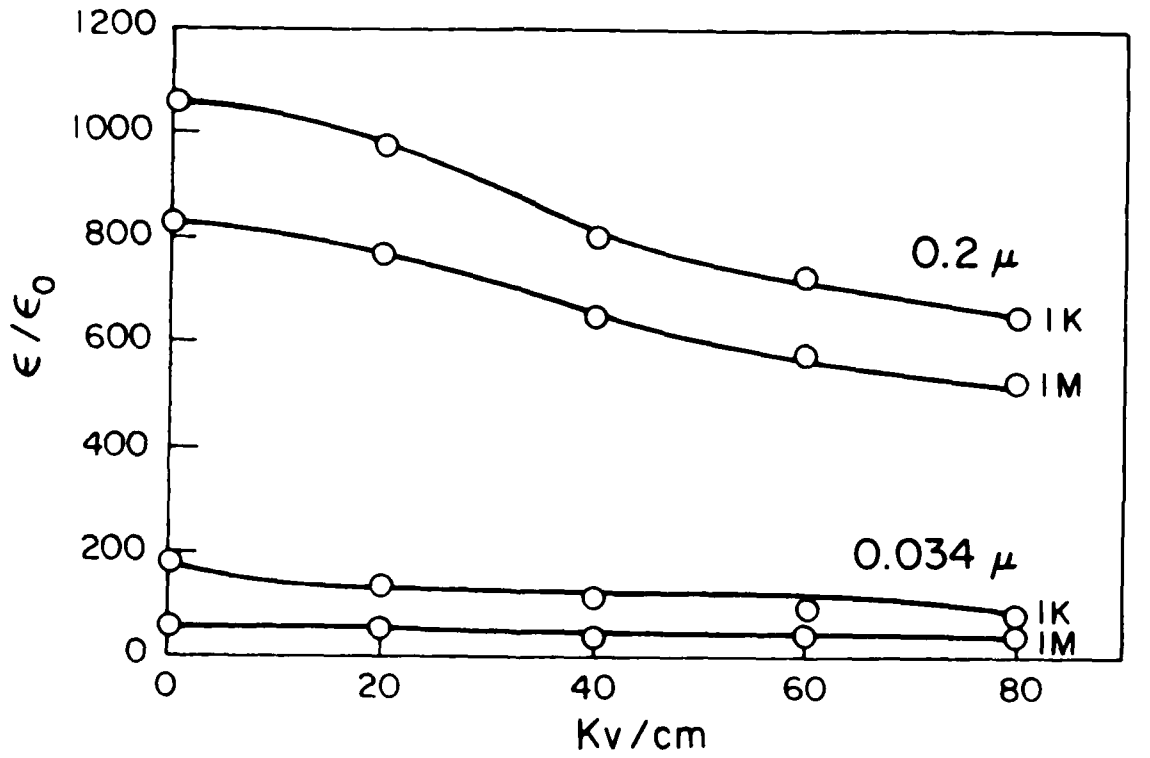


Figure 39. Variation of Dielectric Constant Measured at Various Frequencies of $BaTiO_3$ Films of Varying Grain Size with D.C. Bias Electric Field.

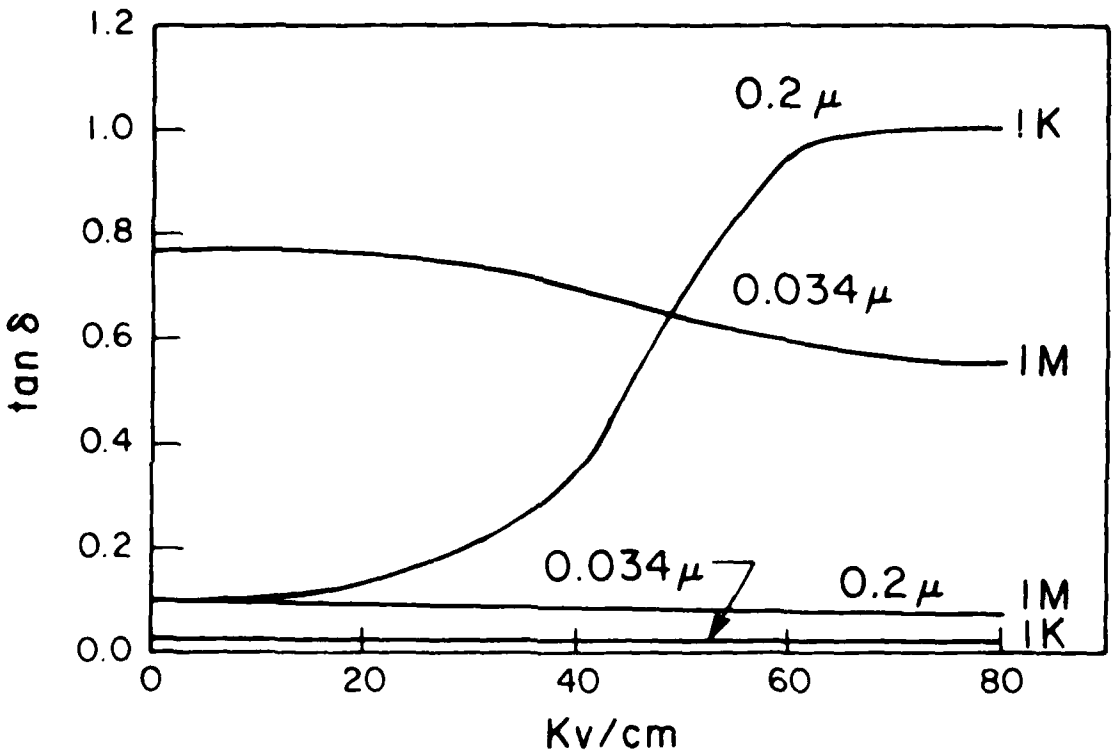


Figure [illegible] Variation of Dissipation Factor Measured at Various Frequencies for Ceramic Bodies of Varying Grain Size as a Function of the Electric Field.

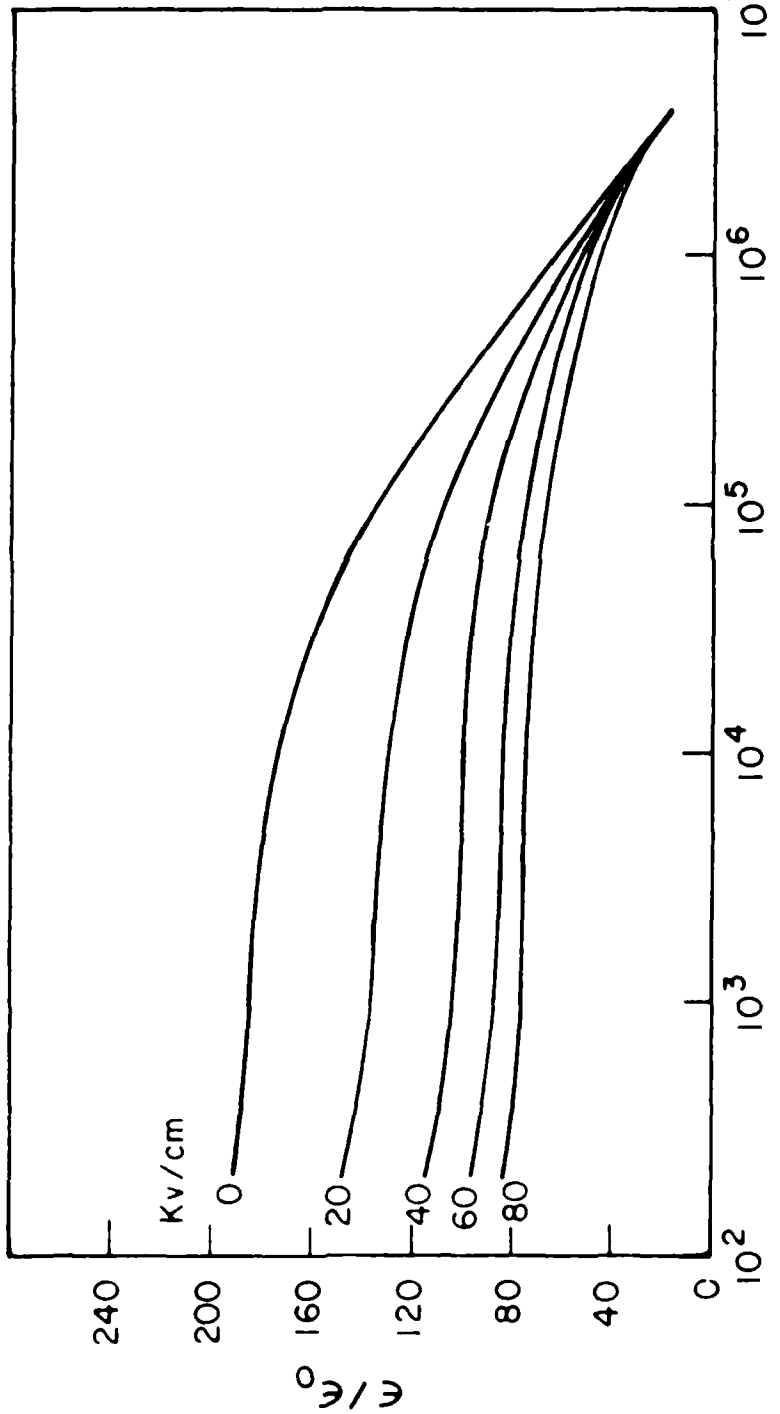


Figure 41. Variation of Dielectric Constant Measured at Variation D.C. Bias Electric Field of 0.034 $\mu$ Grain Sized $BaTiO_3$ Film with Frequency.

#### *4.3.2.4 Spontaneous Polarization*

Figure 42 shows a typical hysteresis loop of the polarization of $BaTiO_3$ films which indicates that the $BaTiO_3$ films made by the MOD method are ferroelectric. For the fine grain $BaTiO_3$ film, a very narrow hysteresis loop was observed, indicating that only a very small portion of the film had a domain structure. As the grain size increased to 0.1 $\mu$, a normal hysteresis loop was observed. The grain size dependence of the spontaneous polarization is shown in Fig. 43. This result is very similar to that reported for $BaTiO_3$ in a disc form [22].

#### *4.3.2.5 Dielectric Breakdown*

A dielectric strength larger than 100 kV/cm was observed for all the $BaTiO_3$ films made by the MOD method. A higher value of dielectric strength indicated that the $BaTiO_3$ films prepared by MOD process are pin hole free and dense.

## 4.4 Relaxor Film

### *4.4.1 Thermogravimetric Analysis of MOD Compounds*

The firing temperature for the MOD relaxor ferroelectric films was determined from the decomposition obtained by the TGA analysis.

The information about the solvent removal temperature, organic decomposition, and % wt. yield of the final product was also obtained from the TGA. The solvent, which was xylene for all of the MO compounds, was removed between 25°C and 150°C. As heating was continued, the compounds decomposed to a series of complex metallo-organics, and finally, to the metal oxides. In some cases (e.g. magnesium neodecanoate) carbonates were formed by the decomposition of metallo-organic compounds, which decomposed to oxides. Figure 44 is a thermogram for Mg neodecanoate. Below 100°C, the xylene was removed from

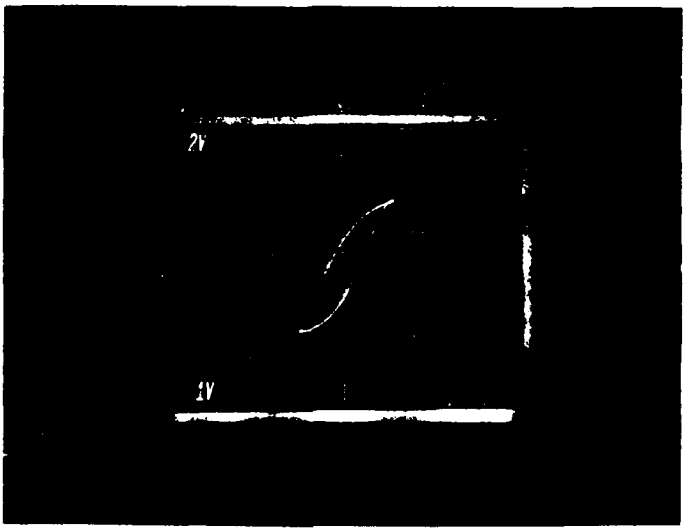


a) v: 2.55 $\mu c/cm^2/div$

Figure 42. Hysteresis loop of $BaTiO_3$ Films of Varying Grain Sizes. a) 0.2 $\mu$ Grained $BaTiO_3$ Film; $P_s$ = 3.06 $\mu c/cm^2$.

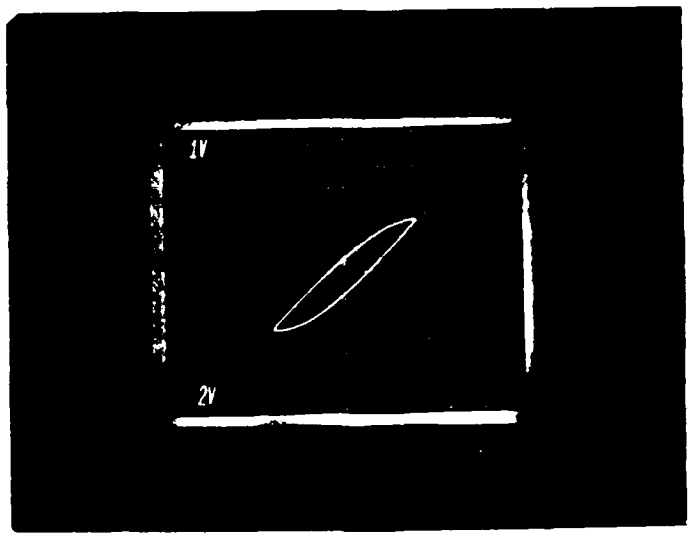


b) y: 1.27 μc/cm$^2$/div

b) 0.1 μ Grained Film $P_s$ = 1.27 μc/cm$^2$.

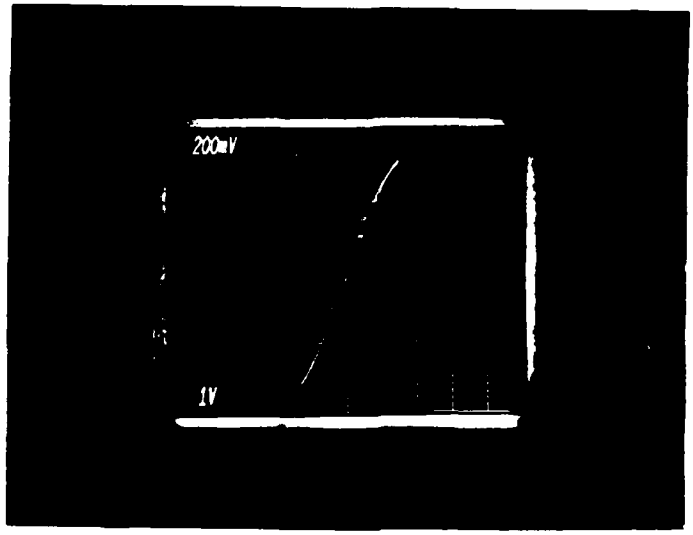


c) v: 0.028 ;c/cm$^2$/div.

c) 0.034 :: Grained Film $P_s$ = 0.025 ;c/cm$^2$.

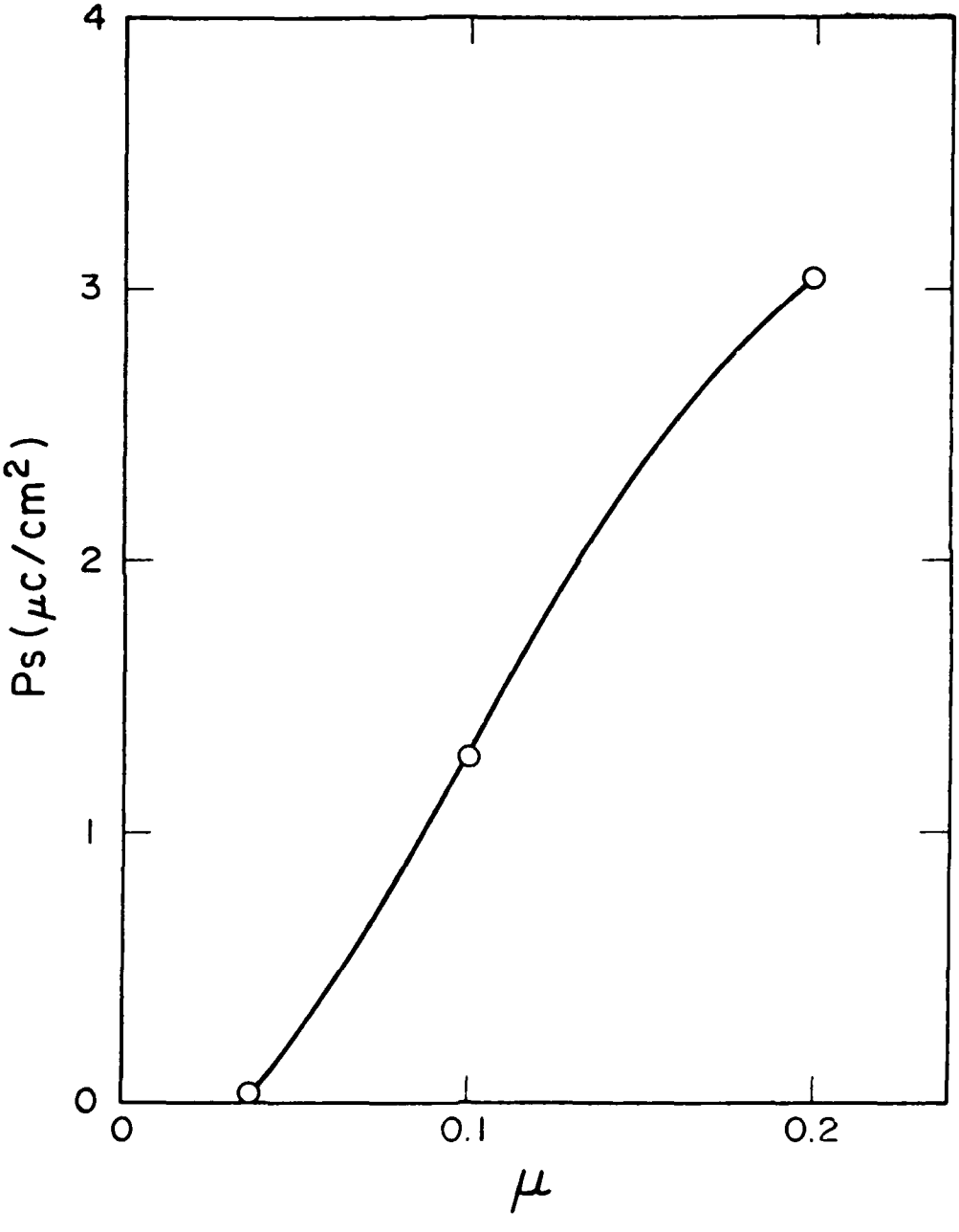


Figure 43. Variation of Spontaneous Polarization of $BaTiO_3$ Fired at Room Temperature with Grain Size.

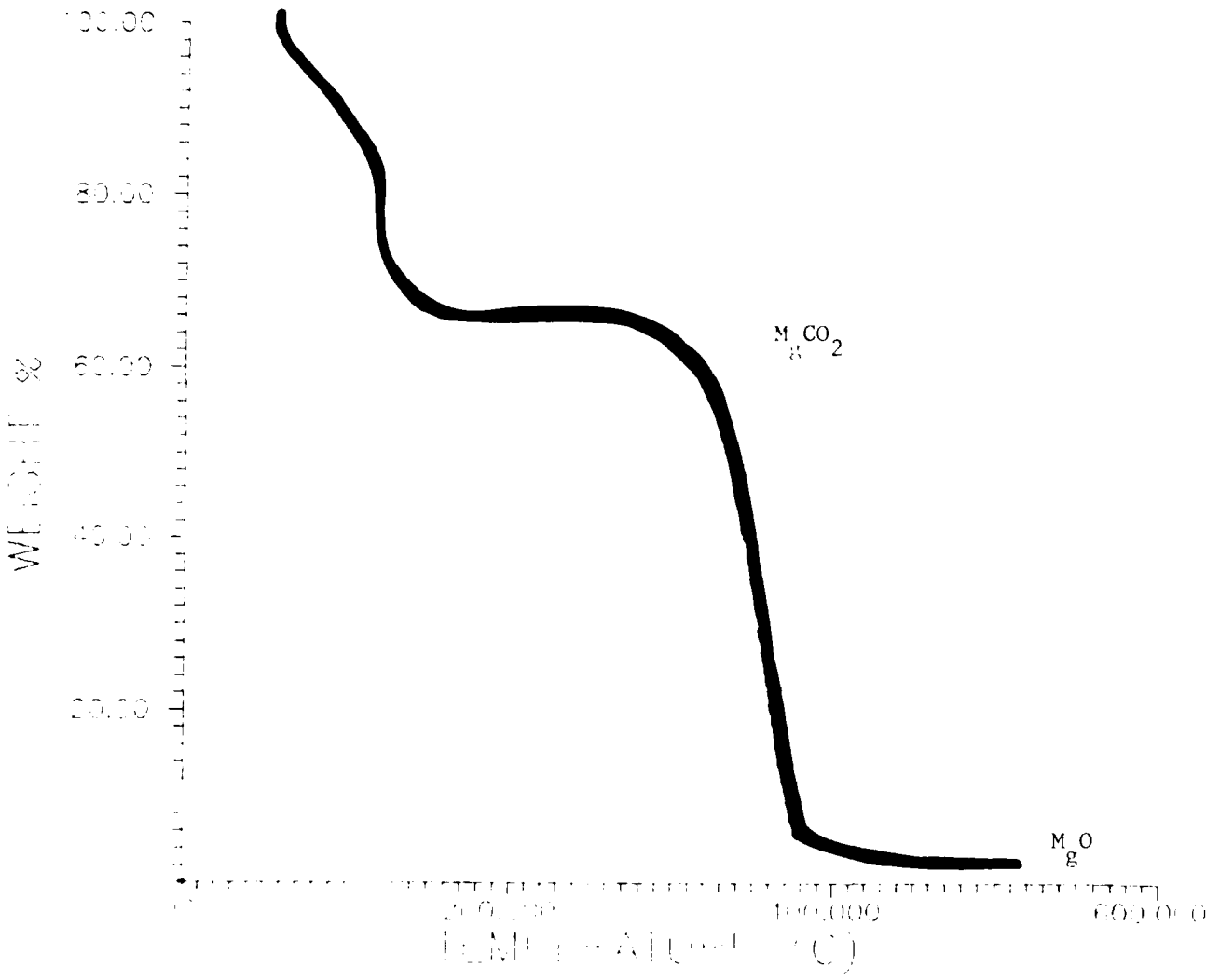


Figure 44. TGA Curve for Magnesium Neodecanoate.

$Mg(C_9H_{19}COO)_2$. Between 100° and 375°C, the neodecanoate groups were removed, leaving $MgCO_3$. By 425°C, the $MgCO_3$ had decomposed to the final metal oxide, MgO.

The thermal decomposition of the lead neodecanoate solution at lower temperatures (350°C - 500°C) lead to the formation of several lead oxides ($Pb_2O_3$, $Pb_3O_4$ and PbO). This was attributed to the different oxidation states of Pb at different temperatures. A larger weight loss was observed when the heating rate from room temperature to 600°C was changed from 1°C/min. to 5-10°C/min. This was due to the evaporation of lead neodecanoate before its decomposition. By firing the Pb neodecanoate at 600°C, essentially single phase PbO material was obtained according to the x-ray diffraction analysis.

The thermal decomposition of nickel neodecanoate and niobium trimethoxy dineodecanoate lead to the formation of NiO and $Nb_2O_5$, respectively. However, the locations of the x-ray diffraction peaks of both the oxides were shifted slightly, indicating that they were nonstoichiometric oxides. These powders were annealed in an oxygen rich atmosphere so that the oxygen deficient powders would become stoichiometric and the true yield of oxides from the metallo-organic compound could be determined. Nickel oxide and niobium oxide powders were placed in a small quartz-lined diffusion furnace and annealed at 400°C in a 3:1 $N_2$:$O_2$ atmosphere for one hour. The annealed powders exhibited x-ray diffraction peaks which matched with those of the stoichiometric oxides.

### *4.4.2 Bulk Decomposition of MOD Relaxor Solutions*

Table IX shows the d-spacings of the crystalline phases obtained by the decomposition of PMN and PNN bulk formulations at 800°C, along with the standard d-spacings of the perovskite and pyrochlore phases. As shown in Table IX, a large amount of the perovskite phase was formed for both PMN and PNN, when the PMN and PNN formulations were fired in a crucible. By introducing a stabilization period at 450°C during the first part of the heat treatment, the PbO was able to combine with the other compounds and, thereby, reducing PbO

Table [illegible] Substrate Effect on the Formation of Perovskite $BaTiO_3$ Thin Films.

| Substrate | Firing Temperature of substrate & electrode | Maximum Co-Firing Temp. of Dielectric & Electrode | Max. Grain Size Obtained |
|---|---|---|---|
| $SiO_2$ + Si (Si wafer fired at 1200°C in air for 1 hr.) | 1200°C | ·1050°C, perovskite structure<br>·1050°C unknown phase | ·0.1 |
| Pt (7[illegible] Å) Coated Si wafer | 550°C | 750°C (Pt film destroyed) | very fine grain + amorphous |
| $RuO_2$ (·0.3 μ) Coated Si wafer | 600°C | 850°C ($RuO_2$ film destroyed) | very fine grain + amorphous |
| $MgAlO_4$ (·0.3 μ) Coated Si wafer | 650°C | 1000°C<br>>1000°C, $MgAlO_4$, $SiO_2$ + $BaTiO_3$ interaction | fine grain size |
| ITO coated (0.5 μ) Si | fired at 600°C, annealed at 1200°C in air, 1 hr. | 1100°C<br>>1100°C, interaction ITO + $SiO_2$ + $BaTiO_3$ | 0.1 μ - 0.12 μ grain film can be formed |
| Pt Foil | | 1200°C > thermal stress cracking | 0.2 |
| ITO coated Pt | fired at 600°C, annealed at 1200°C in air, 1 hr. | 1200°C | grain size · that formed on pure Pt foil |

evaporation losses at a higher temperature. A slow ramp rate in the beginning also eliminated a volatilisation of lead neodecanoate before its decomposition.

The solutions of metallo-organic compounds were mixed to obtain a formulation. Thus, the mixing was on a molecular level. Thus, upon decomposition the inorganic species formed are in intimate contact with each other and have very small particle size. This aspect enhances a more rapid formation of the compounds and lowers the firing temperature as compared to the conventional powder methods. For instance, Veitch [24] reported that a PNN sample prepared by milling and calcining stoichiometric amounts of the oxide powders, only 7.0% perovskite at 800°C was achieved. This increased to 68% at 1000°C. By prereacting NiO and $Nb_2O_5$ as described by Shrout and Swartz [23], the samples contained 98% perovskite between 950-1000°C but a negligible amount at 800°C. Similar results have been recorded for PMN [29,31]. For PMN samples fabricated by mixing the oxide powders and firing the mixture at 1000°C for four hours, the percentage of the perovskite phase present was 76.3%. Using the intermediate method, 98.9% perovskite phase was detected after calcining for 4 hours at 800°C and 870°C. In the present study, for PMN 80% of perovskite was observed at 875°C and for the PNN 90% perovskite was observed at 875°C. Thus, the MOD process, gave better results than the conventional technique by increasing the reactivity of the metal oxides involved in the reaction.

### *4.4.3 Film Formation*

Each of the variables studied in the experiments for MOD PMN and PNN films will be discussed in the following section.

### *4.4.4 Formation of the Perovskite Phase in PMN*

Table X summarizes the effects of various processing variables on the amount of perovskite phase in the PMN films.

Table X. X-ray Analysis of the Powders Obtained by Bulk Decomposition of PNN and PMN Formulation.

A. PNN

| d Spacings from Powder | d Spacings from JCPDS File 34-103* | % Perovskite |
|---|---|---|
| 4.02 | 4.03 | 90% |
| 3.03** | 2.85 | |
| 2.85 | 2.33 | |
| 2.31 | 2.01 | |
| 2.01 | 1.80 | |
| 1.80 | 1.65 | |
| 1.64 | | |

* Perovskite Structure Type
** Pyrochlore Phase

B. PMN

| d Spacings from Powder | d Spacings from JCPDS File 33-769* | d Spacings from JCPDS File 27-1199** | % Perovskite |
|---|---|---|---|
| 3.99 | | 4.06 | 80% |
| 3.01 | 3.058 | 2.87 | |
| 2.81 | 2.649 | 2.34 | |
| 2.54 | 2.431 | 2.03 | |
| 2.30 | 2.16 | 1.66 | |
| 2.21 | 2.04 | 1.434 | |
| 1.99 | 1.87 | | |
| 1.81 | | | |
| 1.79 | | | |
| 1.63 | | | |

* Pyrochlore Structure Type
**Perovskite Structure Type

a) Solvent Effects:

The concentrated PMN solution (concentration 16.1 w% PMN) wet the Pt foil and quarts glass electrode surface but not the silicon. To enhance wetting of this solution part of the MOD solution was first diluted with xylene to a 5% solution. Wetting improved but severe cracking was observed after the samples were fired. Subsequently xylene was removed from the 5 w% solution and was replaced with THF. This solution wet the electroded silicon surface much better but did not wet the Pt foil surface at all. The SEM micrograph (Fig. 45) shows the film formed by spinning a 5 w% solution in THF on a Pt-foil and firing at 800°C. The THF is also extremely volatile and thus the concentration of the solution changes very quickly when exposed to air. Since the solution with xylene was more stable and wetted Pt foil well, xylene was selected as the best solvent for PMN as well as PNN and PFN.

b) Substrate-Electrode-Dielectric Interactions

Substrate, dielectric and electrode interaction lead to the formation of pyrochlore phases in the PMN and PNN film processing. Silicon wafer, ITO electrode and thin Pt-MOD film reacted with dielectric to form pyrochlore. Silicon wafer quarters were also used for substrates, however, interaction of Pt film electrode with silicon was a problem. The ITO films coated the silicon wafer well and did not interact with Si. Previous investigations also showed that ITO was more stable at higher temperatures than the Pt electrode material. From Table XI, the sample fired with ITO on Si contained more pyrochlore than one fired under the same conditions on Pt foil. This is due to the interaction of ITO with PMN which is not completely understood at this point. It is proposed that there is some interaction between magnesium in PMN Platinum foil, either 50 mils thick or 25 mils thick, was the best candidate for an inert substrate as well as inert electrode material. It was noted that the films tended to crack on the 25 mil thick Pt foil especially when multiple layers were applied. This was due to the substrate being held down on the spinner chuck by a small vacuum. This vacuum was sufficient to depress the

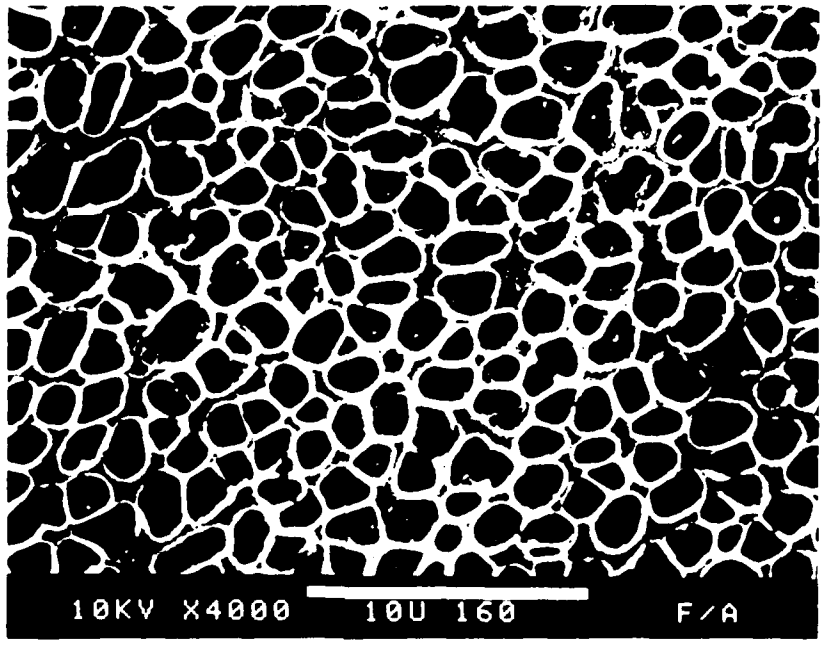


Figure 45. PMN Fired on Pt Foil at 800$^{O}$C (5% PMN Solution in THF).

Table XI. Results of Processing Experiments for MOD Films.

A. PMN

| Solvent | Conc. (%) | Substrate | Electrode | # of Layers | Heating Cycle | Temp. °C | % Perovskite |
|---|---|---|---|---|---|---|---|
| THF | 5 | Si | Pt* | 1 | II | 500 | 0.0+ |
| Xylene | 16.1 | Pt Foil | Pt Foil | 1 | II | 600 | 0.0+ |
| Xylene | 16.1 | Pt Foil | Pt Foil | 3 | II | 600 | 0.0+ |
| THF | 5.0 | Si | Pt | 1 | II | 600 | 0.0+ |
| THF | 1.0 | Pt Foil | ITO* | 1 | II | 700 | 0.0+ |
| Xylene | 16.1 | Pt Foil | Pt | 1 | II | 750 | 0.0+ |
| THF | 5.0 | Si | ITO | 1 | III | 800 | 0.0+ |
| Xylene | 16.1 | Si | ITO | 1 | II | 800 | 20.0 |
| THF | 5.0 | Si | Pt | 1 | II | 800 | 4.13 |
| Xylene | 16.1 | Pt Foil | Pt Foil | 1 | IV | 800 | 41.9 |
| Xylene | 16.1 | Quartz | ITO | 3 | II | 800 | 9.33 |
| Xylene | 16.1 | Quartz | ITO | 4 | II | 800 | 2.30 |
| Xylene | 16.1 | Quartz | ITO | 5 | II | 800 | 0.0+ |
| Xylene | 16.1 | Pt Foil | Pt Foil | 1 | II | 800 | 38.7 |
| Xylene | 16.1 | Pt Foil | Pt Foil | 3 | II | 800 | 80.4 |
| Xylene | 16.1 | Pt Foil | Pt Foil | 4 | II | 800 | 82.0 |
| Xylene | 16.1 | Pt Foil** | Pt Foil | 8 | II | 800 | 80.1 |
| THF | 5.0 | Si | Pt | 1 | II | 875 | 0.0+ |
| Xylene | 5.0 | Si | Pt | 1 | I | 875 | 0.0+ |
| Xylene | 16.1 | Pt Foil | Pt Foil | 1 | II | 875 | 0.0+ |

+ 100% Pyrochlore peak at 29.1° 2θ (Peak intensity: $\frac{I}{I_o}$ = 37).
* 1-3 Layers thick
**50 mils thick

Table XI. Results of Processing Experiments for MOD Films.

B. PNN

| Solvent | Conc. (%) | Substrate | Electrode | # of Layers | Heating Cycle | Temp. °C | % Perovskite |
|---|---|---|---|---|---|---|---|
| THF | 5.0 | Pt Foil | ITO | 1 | II | 700 | 0.0+ |
| THF | 5.0 | Si | Pt | 1 | II | 800 | 33.3 |
| THF | 5.0 | Si | ITO | 1 | II | 800 | 0.0+ |
| THF | 5.0 | Pt Foil | Pt Foil | 1 | II | 800 | 0.0* |
| THF | 5.0 | Si | ITO | 1 | III | 800 | 0.0 |
| Xylene | 11.8 | Pt Foil | Pt Foil | 1 | IV | 800 | 23.7 |
| Xylene | 11.8 | Pt Foil | Pt Foil | 1 | I | 875 | 0.0+ |
| Xylene | 11.8 | Si | Pt | 1 | I | 875 | 0.0+ |
| THF | 5.0 | Si | ITO | 1 | III | 875 | 0.0+ |

[illegible] of major pyrochlore peak: 52

[illegible] after 3 months

| [illegible] | Substrate | Electrode | # of Layers | Heating Cycle | Temp. °C | % Perovskite |
|---|---|---|---|---|---|---|
| [illegible] | [illegible] Foil | Pt Foil | 1 | IV | 800 | 72.0 |
| [illegible] | [illegible] | Pt Foil | 1 | II | 800 | 0.0 |

AD-A182 395 MULTILAYER CAPACITOR DIELECTRICS PRODUCED FROM METALLO-ORGANIC PRECURSORS(U) PURDUE UNIV LAFAYETTE IN R W VEST ET AL 15 MAY 87 N00014-83-K-0321 2/2

UNCLASSIFIED F/G 9/1 NL

END
8-87
DTIC


1.0
1.1
1.25
1.4
1.6
1.8
2.0
2.2
2.5
2.8
3.2
3.6
4.0
4.5
5.0
5.6
6.3
7.1
8.0
9.0
MICROCOPY RESOLUTION TEST CHART
NATIONAL BUREAU OF STANDARDS-1963-A

center of the film and cause longitudinal microcracks. This was not observed with the 50 mil thick Pt foil.

The amount of perovskite in the multi-layered PMN film on Pt foil was more at 800°C than at 600°C. No film cracking was observed at both temperatures. The thickness of all of the films were measured on a Tencor* profilometer. The stylus was started on a bare region on the substrate and moved across the surface. One layer of PMN film prepared from the 5 % THF solution had fired thickness of 0.1 $\mu$m, while the fired film thickness of one layer of PMN from the 16.1% solution in xylene averaged 0.3 $\mu$m. The 8 layered PMN film prepared from the 16.1% solution was 2.4 $\mu$m thick. Also, it contained 80.1% perovskite.

Finally, the heating cycles used throughout the investigations also influenced the amount of perovskite formed. For one layer film, the optimum temperature for producing the lowest amount of pyrochlore in PMN was 800°C. Little or zero perovskite was present at temperatures above or below 800°C. Heating cycles II and III differed by ramp rates to 800°C. The results from these two experiments confirm that faster heating rates lead to excessive lead loss and enhanced pyrochlore formation. Heating cycles II and IV differed in atmosphere conditions and the temperature at which the samples are placed in the furnace, (see Figs. 12 and 14 for details). It was noted that a small amount of oxygen introduced during the firing increased the amount of perovskite phase in PMN film from 38.7% to 41.9%. Future work will be done with multiple layer samples fired in $O_2$.

### *4.4.5 Formation of the Perovskite Phase in PNN and PFN*

The substrate and the electrode material interaction with PNN was very severe particularly with silicon as the substrate material. Nickel is a "fast" diffusing species in silicon and it is

---

* Alpha-Step 200, Tencor Instruments, Mountain View, CA 94043

known that nickel can create holes and other defects in silicon. Nickel can also react with platinum at ~600°C and over a period of time, the platinum forms an alloy with nickel. In one experiment, where the silicon was used as the substrate at a firing temperature of 800°C holes were observed in the substrate. In this experiment the electrode material was Pt. An SEM micrograph of this sample is shown in Fig. 46. A similar tunneling effect had been observed on silicon wafers contaminated with heavy metals, particularly by nickel. Other problems described in the previous section were also encountered with PNN.

The most perovskite formed was with a 5% PNN solution in THF at 800°C on Pt-electroded silicon. However, the results were not reproducible. Work is continuing to find the optimum conditions for producing pyrochlore-free PNN and understanding the kinetics of this particular ferroelectric.

Only two experiments were performed with PFN. The perovskite formation was favored with the oxygen rich environment. Additional experiments will be performed to study the effects of film thickness as well as temperature and atmosphere.

### *4.4.6 Electrical Properties of PMN*

The PMN films containing the highest percentage (80.2% - 82%) of the perovskite phase were selected to determine the electrical properties of PMN. Many of the gold dots probed on the 4-layer PMN film deposited on a thin Pt foil were shorted. It was believed that due to the lack of rigidity of the substrate, the pressure of the spinner's vacuum lead to microcrack. Therefore, the thicker 8-layer or 2.4 $\mu$m PMN film on 50 mil thick Pt foil was used to study the electrical properties. Figure 47 shows variation of the dielectric constant of PMN film as a function of temperature at frequencies ranging from 200 Hz to 2 MHz. The Curie temperature of the PMN film was -16°C at 200 Hz and increased with increase in frequency. The dielectric constant of 1500 was observed at 200 Hz. This was much lower than the previously cited literature values of ~15000. Freancombe [50] observed a lower dielectric constant for $BaTiO_3$

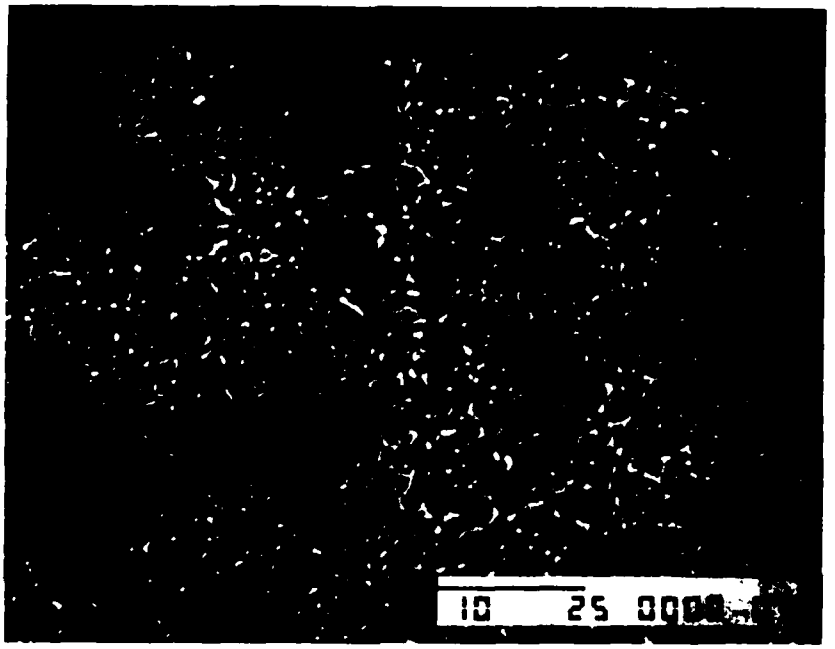


Figure 46. Silicon Surface with PNN Film Fired at 800°C (3500X).

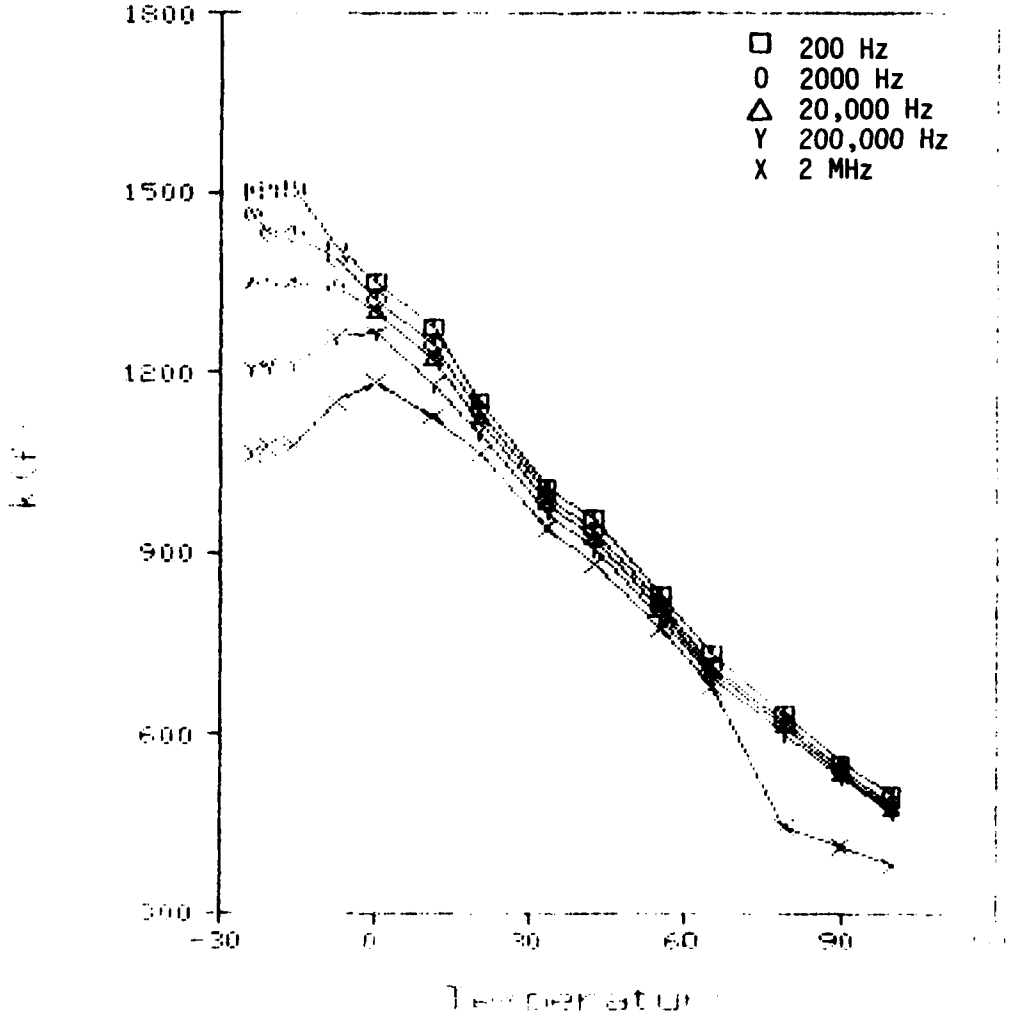


Figure 47. Dielectric Constant as a Function of Temperature at 200 Hz, 2000 Hz, 20,000 Hz, 200,000 Hz, 2 NHz.

films as compared to bulk samples and attributed this to the grain size and layer thickness. Furthermore, Swartz, et.al. [32] demonstrated that grain size does affect the dielectric constant of PMN materials. It was noted for the 2.4 $\mu$m PMN film that the peak width of the x-ray diffraction patterns indicated a very fine grain size. Also, the existence of the pyrochlore has also been known to decrease the dielectric constant [29,31]. From this preliminary data, efforts will be focused to eliminate the pyrochlore phase and increase the grain size by changing heating cycles and increasing the number of layers.

The dissipation factor over a range of frequencies as a function of temperature ranged from 0.02 - 0.18 (Fig. 48). These values for the dissipation factor for PMN are much lower than what has been recorded in the literature [32]. This is a highly desirable property, for device application. The effect of bias on the room temperature dielectric constant is shown in Fig. 49 as a smooth curve for different frequencies. The curve becomes linear and never saturates as the bias increases. The dissipation factor under a D.C. bias electric field measured at higher frequencies (>1.0 kHz) showed maximum at lower dc bias electric field (Fig. 50). However no maximum was observed at lower frequencies. From both Figs. 49 and 50, though, it should be noted that PMN has a dielectric strength greater than 150 kV/cm. This is very favorable for application in capacitors. Finally, a hysteresis loop was observed for the PMN film at room temperature at 60 Hz (Fig. 51). This indicated that ferroelectric domains were present in the PMN films above their Curie temperature. The hysteresis loop did not saturate.

All of the electrical properties observed for PMN were very good except for the dielectric constant. However, since the films are very thin (2.4 $\mu$m) the capacitance/area is still very high. As stated earlier, work will be focused on eliminating the pyrochlore phase by increasing thickness and processing under oxygen atmosphere.

## 5. SUMMARY

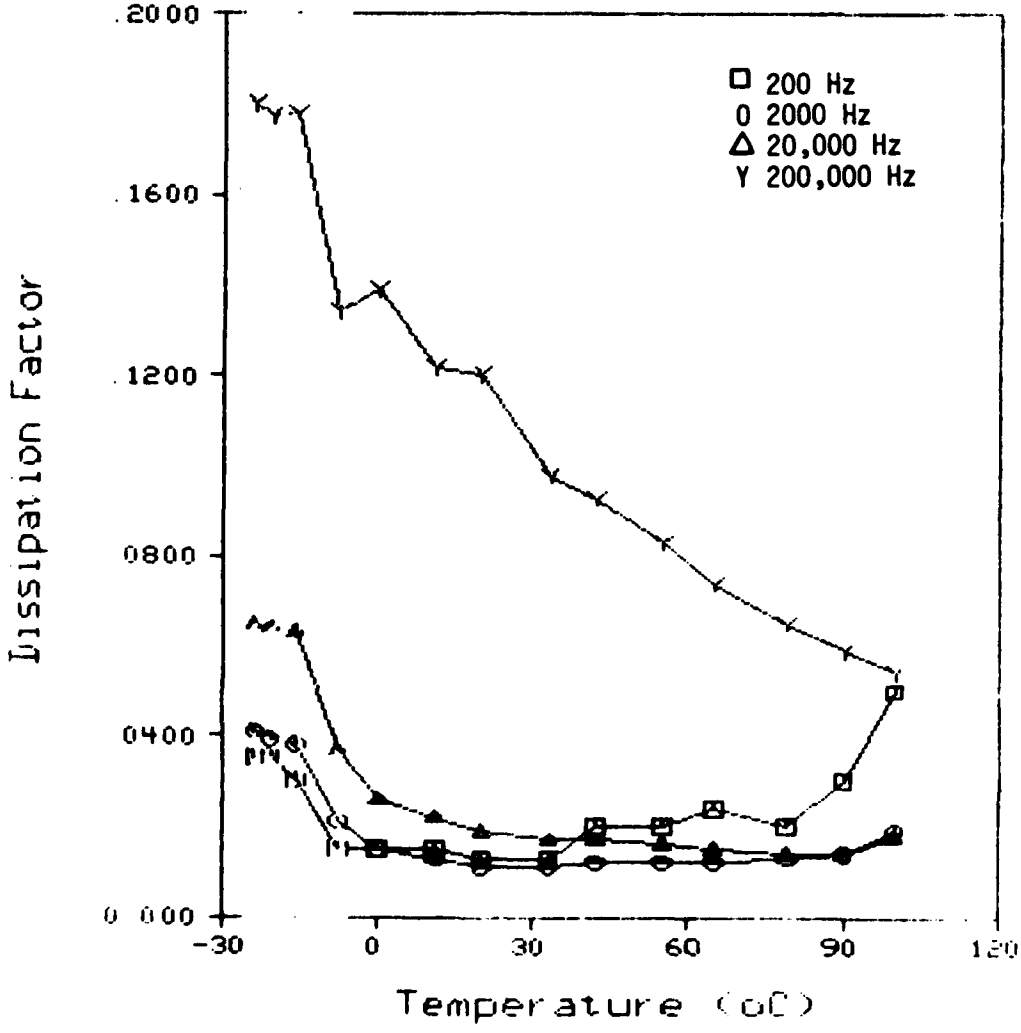


Figure 48. Dissipation Factor vs. Temperature at 200 Hz, 2000 Hz, 20,000 Hz, and 200,000 Hz.

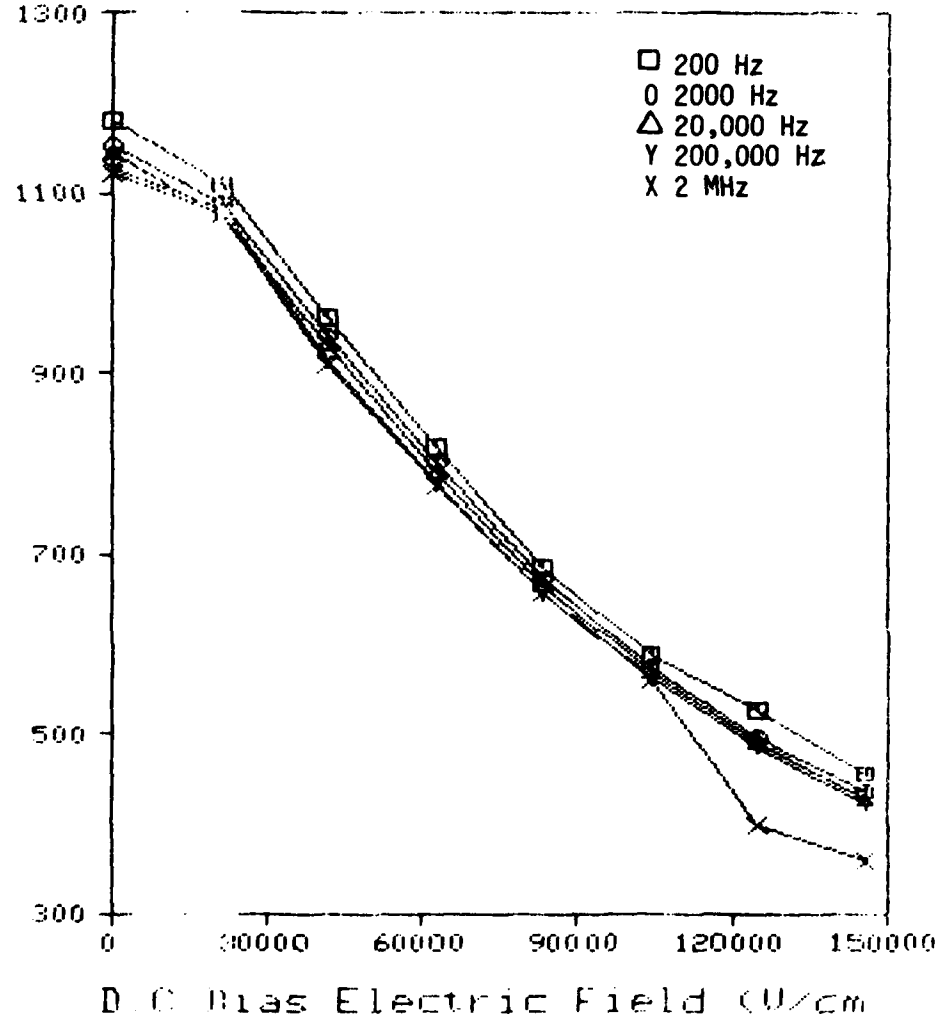


Figure 49. Dielectric Constant vs. Electric Field at 200 Hz, 2,000 Hz, 20,000 Hz, 200,000 Hz, 2 MHz.

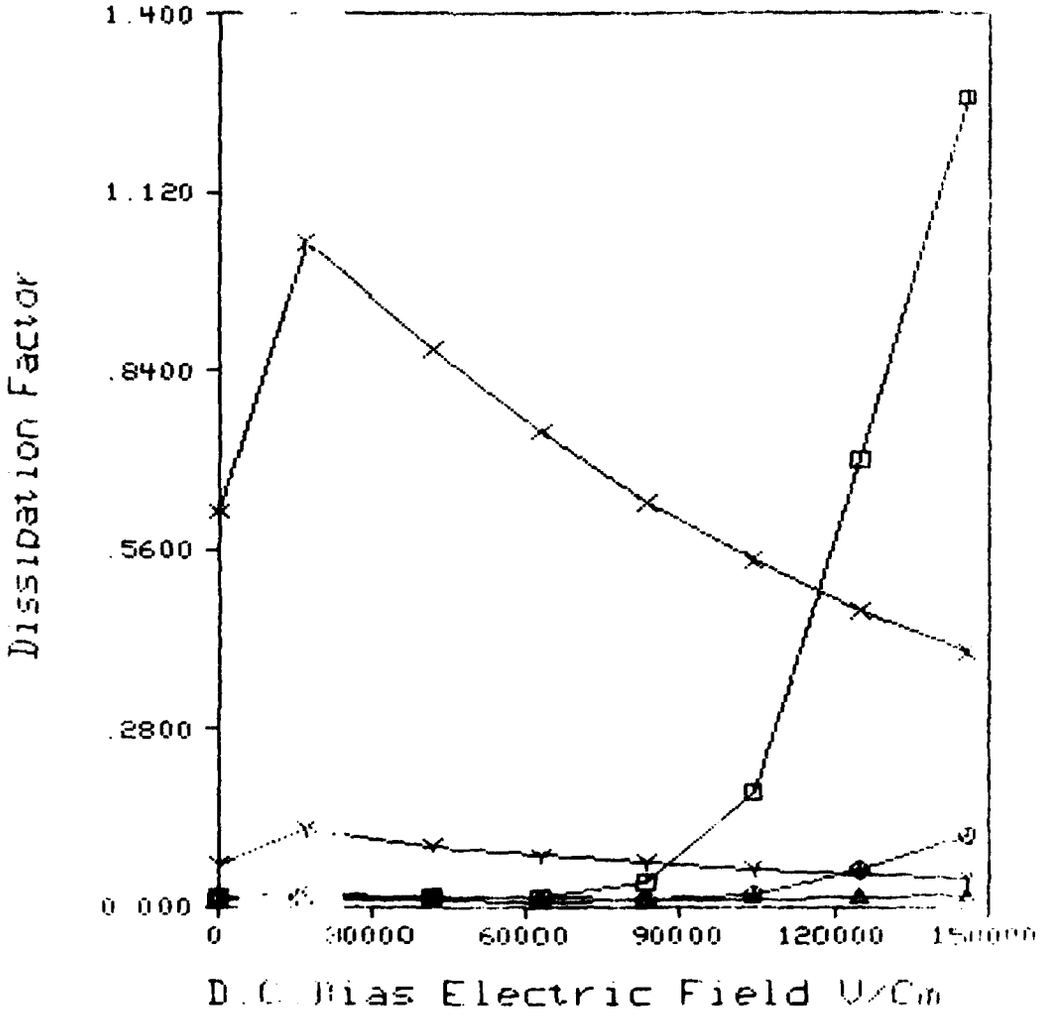


Figure 50. Dissipation Factor as a Function of D.C. Bias Electrical Field Measured at:

- □ 200 Hz
- 0 2000 Hz
- △ 20,000 Hz
- Y 200,000 Hz
- X 2 MHz

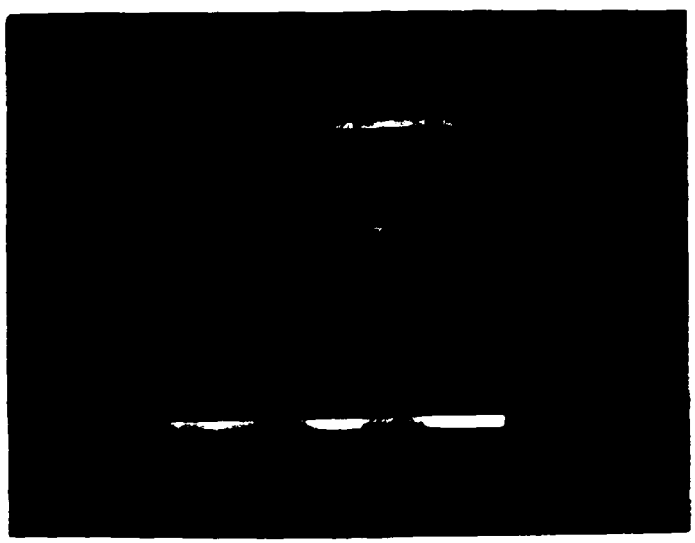

Figure 51. Hysteresis Observed for PMN Film.

1. High k (room temperature k>1000), low loss (room temperature, tan $\delta$ <0.1) $BaTiO_3$ films of thickness 4 $\mu$ to 8 $\mu$ were made from metallo-organic precursors by spinning MOD solutions on a substrate and the pyrolysis of the wet film. The dielectric properties of the films can be controlled by firing temperature and atmosphere.
2. Ferroelectric $BaTiO_3$ films from metallo-organic precursors takes place at lower temperature and at fast rates as compared to that from solid state reaction. The low activation energy (120 kJ/mole) for grain growth in $BaTiO_3$ films is probably due to an interface controlled reaction.
3. Dielectric loss-frequency and dielectric loss-temperature studies indicate the possible role of oxygen vacancies [51-52]. These facts need further investigation.

Metallo-organic decomposition techniques were used to fabricate the relaxor ferroelectric films, PMN and PNN. The MOD precursors were analysed using TGA and x-ray analysis then, mixed in stoichiometric proportions to form PMN and PNN. From the bulk decomposition of the ferroelectric films, PMN was 80% perovskite, and PNN was 90% perovskite. Several variables were studied in the PMN and PNN film processing. These included solvent, substrate and electrode material, heating cycles and temperatures, and film thickness. The optimum conditions found for forming nearly pyrochlore-free PMN (80.1% perovskite) were the following:

1. Temperature: 800°C
2. Heating cycle: samples placed in furnace at 500°C, slow ramp and soak at 800°C.
3. Substrate and electrode - Pt foil
4. Film thickness - 8 layers or 2.4 $\mu$m thick
5. MOD solution solvent - xylene.

The dielectric constant and dissipation factor for the PMN film processed under these

conditions was tested. The dielectric constant was 1500 at 200 Hz and the dissipation factor ranged from .02 - .18. A hysteresis loop of polarisation was observed at room temperature indicating that it was a ferroelectric material. The dielectric strength was greater than 1 X $10^5$ V/cm. The dependence room temperature dielectric constant on a dc bias electric field remained approximately linear over 0-150 kV/cm and had little effect of frequency. An increase in the amount of perovskite phase formed in an $O_2$ atmosphere was observed for 0.3 $\mu$m PMN film. Additional layers fired under these conditions will be studied. Work will continue to fabricate pyrochlore-free PMN in order to increase the dielectric constant and maintain a low dissipation factor.

Problems were encountered with processing PNN films. The best results were obtained with the following conditions:

1. Substrate and electrode: Pt foil
2. Solvent of MOD solution: xylene
3. Temperature - 800°C
4. Heating cycle - samples placed in furnace at room temperature, slow ramp to 500°C moderate ramp to 800°C in $O_2$ atmosphere
5. Film thickness: 1.3 $\mu$m.

The PNN sample processed under these conditions was only 27.3% perovskite.

Perovskite formation was also enhanced under the optimum conditions described for PNN as for PFN. The PFN film was 72.0% perovskite. Work will also be continuing in the area of firing thicker films in $O_2$.

## 6. REFERENCES

1. R.W. Vest and G.M. Vest, "Multilayer Capacitor Dielectrics Produced from Metallo-Organic Precursors," ONR Contract No. N0014-83-K-0821, Annual Report, June 1985,

Purdue University, W. Lafayette, IN.

2. E.H. Gillery, J. Vac. Sci. Tech., 15, 306 (1978).

3. P.J. Clarke, J. Vac. Sci. Tech., 14, 141 (1977).

4. R. Groth, Phys. Status Solidi, 14, 69 (1966).

5. G. Heartling and C. Land, J. Am. Ceram. Soc., 54, 1 (1971).

6. H. Roberts, Appl. Opt., 11, 397 (1972).

7. H. Adachi, et.al., J. Appl. Phys., 60, 736-741 (1986).

8. M. Ishida, et.al., J. Appl. Phys., 48, 951 (1977).

9. A. Okada, J. Appl. Phys., 49, 4494 (1978).

10. R. Castellano, Ferroelectrics, 28, 387-390 (1980).

11. M. Oikawa and K. Toda, Appl. Phys. Lett., 29, 491 (1976).

12. Y. Shintani and O. Tada, J. Appl. Phys., 41, 2376 (1970).

13. T. Putner, Thin Solid Films, 1, 165 (1967).

14. R.Vu Huy Dat and C. Baumberger, Phys. Status. Solidi, 22, k67 (1967).

15. Jamda K.G. Panits and Cheng Cheng Hu, Ferroelectrics, 27, 161 (1980).

16. C. Feldman, Rev. Sci. Instrum., 26, 463 (1955).

17. E. Sekine and H. Toyoda, Rev. Elec. Commum. Lab., 10, 457, (1962).

18. Yu Ya Tomashpolskiiams, M.A. Sevostyanov, Soviet Physics, Solid State, 14, 2319 (1973).

19. H. Pratt and C. Firestone, The J. of Vaccu. Sci. and Tech., 8, 256 (1971).

20. J. Park and W. Graunemarm, Ferroelectrics, 10, 217 (1976).

21. G. Arlt, D. Hennings and G. deWith, J. Appl. Phys., 58, 1619 (1985).

22. A.S. Shaikh, Ph.D. Thesis, Purdue University (1986).

23. T.R. Shrout and A. Halliyal, Am. Ceram. Soc. Bull., 66, (4) 704 (1978)

24. L.C. Veitch, "Dielectric Properties of $Pb(Ni_{1/3}Nb_{2/3})O_3$," B.S. Thesis, Pennsylvania State University, University Park, PA (1983).

25. G.A. Smolenskii and A.I. Agranovskaya, Soviet Physics - Solid State, 1, 1429 (1959).

26. V.A. Bokov and I.E. Myl'nikova, Soviet Physics - Solid State, 3, (3), 613 (1961).

27. I.G. Ismailsade, Soviet Physics - Crystallography, 5, 292 (1960).

28. M. Inada, Japanese National Technical Report, 27, (1), 95 (1977).

29. S.M. Swarts and T.R. Shrout, Materials Research Bulletin, 17, 1245 (1982).

30. M. Lejuene and J.P. Boilot, Ceramics International, 8, (3), 99 (1982).

31. M. Lejuene and J.P. Boilot, Am. Ceram. Soc. Bull., 64, (4), 679 (1985).

32. S.L. Swartz, T.R. Shrout, W.A. Schulze, L.E. Cross, J. Am. Ceram. Soc., 69, (8), C-188 (1986).

33. E. Goo and G. Thomas, J. Am. Ceram. Soc., 69 (8), C-188 (1986).

34. J.P. Guha and H.U. Anderson, J. Am. Ceram. Soc., 69, (11), C-287 (1986).

35. R.W. Vest and G.M. Vest, "Metallo-Organic for Improved Thick Film Reliability," Final Technical Report 4/7/85, Naval Avionics Center, Indianapolis, IN, Contract No. N00163-83-C-0167.

36. G.M. Vest and S. Singaram, "Synthesis of Metallo-Organic Compounds for MOD Powders and Films," MRS Proceedings, Symposium L: Defect Properties and Processing of High Technology Nonmetallic Materials, Boston, MA, December 1985.

37. R. Langman and R. Runk, J. Am. Ceram. Soc., 56, 486 (1973).

38. G. Snow, J. Am. Ceram. Soc., 56, 479 (1973).

39. A.S. Shaikh and G.M. Vest, J. Am. Ceram. Soc., 69, (3), 682 (1986).

40. H. Diamant et.al., Rev. Sci. Instrum., 28 (1), 30-33 (1957).

41. K.D. Christian and S.R. Shatynsky, Appl. Surf. Sci., 15, 179 (1983).

42. H.W. Lehmnn and R.Widmer, Thin Solid Films. 27, 359 (1975).

43. J. Bhattacharyya, Thin Solid Films, 128, 231 (1985).

44. W. Seifert, Thin Solid Films, 121, 275 (1984).

45. B. Banerjee, Solar Energy Materials, 13, 11 (1986).

46. S. Nishikawa, Thin Solid Films, 135, 219 (1986).

47. H.B. Saim, Solar Energy Materials, 13, 85 (1986).

48. A. Amin, et.al., J. Am. Ceram., Soc., 66, 733-38 (1983).

49. J.S. Lack, et.al., J. Phys. C., Solid St. Phys., 4, 898-909 (1971).

50. M.H. Freancombe, Ferroelectrics, 3, 199 (1972).

51. O. Prokopalo, et.al., Ferroelectrics, 5, 99 (1973).

52. S. Ikegami and J. Ueda, J. Phys. Soc. Japan, 19, 159 (1964).

END

8-87

DTIC